Personalized Cancer Vaccine Development for Brain and Colon Cancers Using Synthetic HDL Nanoparticles

by

Lindsay Scheetz

A dissertation submitted in partial fulfillment
of the requirements for the degree of
Doctor of Philosophy
(Pharmaceutical Sciences)
in The University of Michigan
2020

Doctoral Committee

Associate Professor James J. Moon, Co-Chair
Associate Professor Anna Schwendeman, Co-Chair
Professor Maria Castro
Professor David Smith

Lindsay Scheetz

scheetzl@umich.edu

ORCID iD: 0000-0002-3201-367X

Dedication

To my paternal grandfather, Robert Scheetz, an alumnus of the University of Michigan whose spirit made Ann Arbor a new home for me.

To my maternal grandfather, Lawrence Fantechi, whose strength and struggle with cancer inspired the research documented within.

To my Uncle Brett, Aunt Alison, and cousin Jimmy, all of whom provided a light to guide me through these past ten years.

I live to make the world a healthier place in honor of you all.

Acknowledgments

First, I would like to thank my parents, Brian and Barbara Scheetz, for their constant support and curiosity about my research despite their expertise in non-biological disciplines. Thank you for inspiring me to keep learning and stay positive no matter how well or poorly my experiments were going. To my siblings, Garrett and Rachel Scheetz, thank you for making mouse jokes with me and being a great source of stress relief when I needed to talk about anything other than science.

Second, I would like to thank my extremely supportive advisors, Dr. Anna Schwendeman and Dr. James Moon. You welcomed me into your labs without question after I made the difficult decision to leave my previous project. I would not have achieved this degree without you. I truly appreciate your confidence in me as you've allowed me to present my research so many times at both domestic and international meetings. Your feedback and investment in me over the last couple of years has been extremely valuable—thank you.

Third, I would like to thank all of my lab members and managers, core facility scientists, veterinary staff, and the COP administrators, staff, and faculty. I received so much help from all of you. My experiments would not have succeeded without you. Karl, Rose, Yao, Anne Marie, and Joel—I appreciate the time you took to train me, advise me, and develop assays with me. Cherie, Antoinette, Dean Dalton, Dean Mason, Dean Mueller, Mark, Regina, Dr. Sun, Dr. Smith, and Dr. Carlson—you have supported me in

ways that I did not expect. Transitioning from one lab to another right in the middle of my program was very difficult but was made much easier with your help.

Finally, I need to thank all of the wonderful people with whom I've developed friendships both in Ann Arbor and before I even thought about going to grad school. To Christina, Candice, Marilyn, Lindsay, and Lauren—thank you for listening to me for hours over the phone when I needed you most. We've been through countless hardships and adventures together, and I treasure your friendship. To Job—I'll never forget how we first met at the Ohio State interview and decided, despite our disgusting colds during interview weekend at Michigan, to choose the better school. Thanks for all of the drop-in lab chats and happy hours, my first Michigan friend. To Al, Morgan, Emily, Waltz, Phil, Ryan, Jason, Brian, Katie, Laura, and Amanda—I wouldn't have preserved my sanity without all of you. Thank you for celebrating with me my love of Justin Bieber, wine, food, and tailgates. And to Jesse—I'm still in disbelief that we have both lived in Ann Arbor for the last 5.5 years and only met last June, but I think you came into my life at exactly the right time. You have magically managed to reduce my stress and put things in perspective for me. Thank you for helping me let go of the things I can't control and to focus on the positives (which is really, really hard in oncology research). I love you so much.

Table of Contents

List of Figures

List of Tables

Abstract

Immunotherapy is an increasingly attractive treatment option for many cancers because it has the potential to reverse the immunosuppressive tumor microenvironment, target tumor antigens, and maintain a long-lasting anti-tumor response. Brain cancers are top candidates for such innovative therapies because current standard-of-care is limited to surgery, radiation, and chemotherapy; surgery often fails to resect 100% of the tumor, and delivery of chemotherapeutic drugs to the brain is very inefficient due to the blood-brain barrier's tightly regulated microenvironment. New immunotherapies for colon cancers are also being explored because of the difficulties of resection surgery and the plethora of adverse effects associated with current targeted therapies and immune checkpoint blockade due to systemic or oral administration. Thus, drug delivery vehicles are being designed to carry antigens and other immunostimulatory molecules directly to tumors or tumor-draining lymph nodes for site-specific treatment that is minimally invasive and reduces off-target side effects.

Within this dissertation, we explored (1) the therapeutic ability of synthetic high density lipoprotein (sHDL) nanodiscs to deliver neoantigens for glioblastoma multiforme (GBM) to exert specific anti-tumor effects, (2) whether immunogenicity of colon adenocarcinoma neoantigen-loaded sHDL nanodiscs following formulation simplification

is retained, and (3) the ability of sHDL nanodiscs to co-deliver chemo- and immuno-therapeutic entities to colon adenocarcinoma tumors.

In the first project, we found that delivery of neoantigens by sHDL nanodisc was significantly more effective compared to delivery of soluble neoantigens in neoantigen-specific CD8+ T cell production, tumor growth reduction, and survival prolongation in murine GBM models. These anti-tumor effects were augmented by the addition of immune checkpoint blockade anti-programmed death receptor ligand 1 (PD-L1), and neoantigen-loaded sHDLs in combination with anti-PD-L1 reversed immunosuppression within the tumor microenvironment by significantly increasing CD8+ T cells and decreasing their PD-1 expression along with regulatory T cell (Treg) frequencies within the tumor.

In the second project, we showed that we were able to simplify our formulation process for neoantigen-loaded sHDL through chemical modification of two neoantigen peptides using short chain poly(ethylene glycol) (PEG) and pre-made lipoprotein films. We verified that the simplified PEGylated formulations induced neoantigen-specific CD8+ T cell expansion similar to our traditional formulations. Although prophylactic vaccination did not slow MC38 colon adenocarcinoma tumor growth or extend overall survival equally between the two neoantigens Reps1 and Adpgk, we did see that PEGylated formulations and traditional formulations exhibited anti-tumor efficacy similar to each other. Together, these results indicated that nanovaccine synthesis could be streamlined for clinical translation.

In the third project, we demonstrated the therapeutic advantage of co-delivering chemo- and immune-therapeutic entities on sHDL nanodiscs in a murine colon

adenocarcinoma model. *In vivo* evaluation of docetaxel-loaded sHDL (DTX-sHDL) co-loaded with CpG oligonucleotide revealed that CpG significantly improved the antitumor efficacy of DTX, suppressing tumor growth and prolonging survival in mice treated with DTX-sHDL/CpG as compared to mice treated with DTX-sHDL or DTX alone. Complete responses were achieved in two of the seven mice treated with DTX-sHDL/CpG without inducing any systemic toxicities, supporting the hypothesis that combination therapy with an immuno-stimulatory component would augment the antitumor efficacy of chemotherapy alone.

In full, this dissertation (1) exposed a highly efficacious, tumor-specific, and personalized nanovaccine design for improving treatment of patients with Glioblastoma multiforme (GBM), (2) streamlined the neoantigen-sHDL nanovaccine formulation process for clinical translation, and (3) proposed an efficient method for co-delivery of chemo- and immuno-therapeutic entities for site-specific, non-toxic cancer treatment using sHDL nanodiscs. We believe that sHDL nanodiscs are versatile drug delivery vehicles and could set the stage for personalized and combinatorial cancer nanovaccine design.

Chapter 1. Introduction

Cancer immunotherapy aims to harness the body's immune system to target and kill tumor cells. A wide variety of cancer immunotherapies have been explored over the years, including immune checkpoint blockade antibodies, cellular therapies based on dendritic cells (DCs) and T lymphocytes, and therapeutic vaccines. In the clinic, antibodies against immune checkpoints cytotoxic T lymphocyte-associated antigen-4 (CTLA-4) and programmed cell death receptor-1 (PD-1) have been game-changers[1-5].

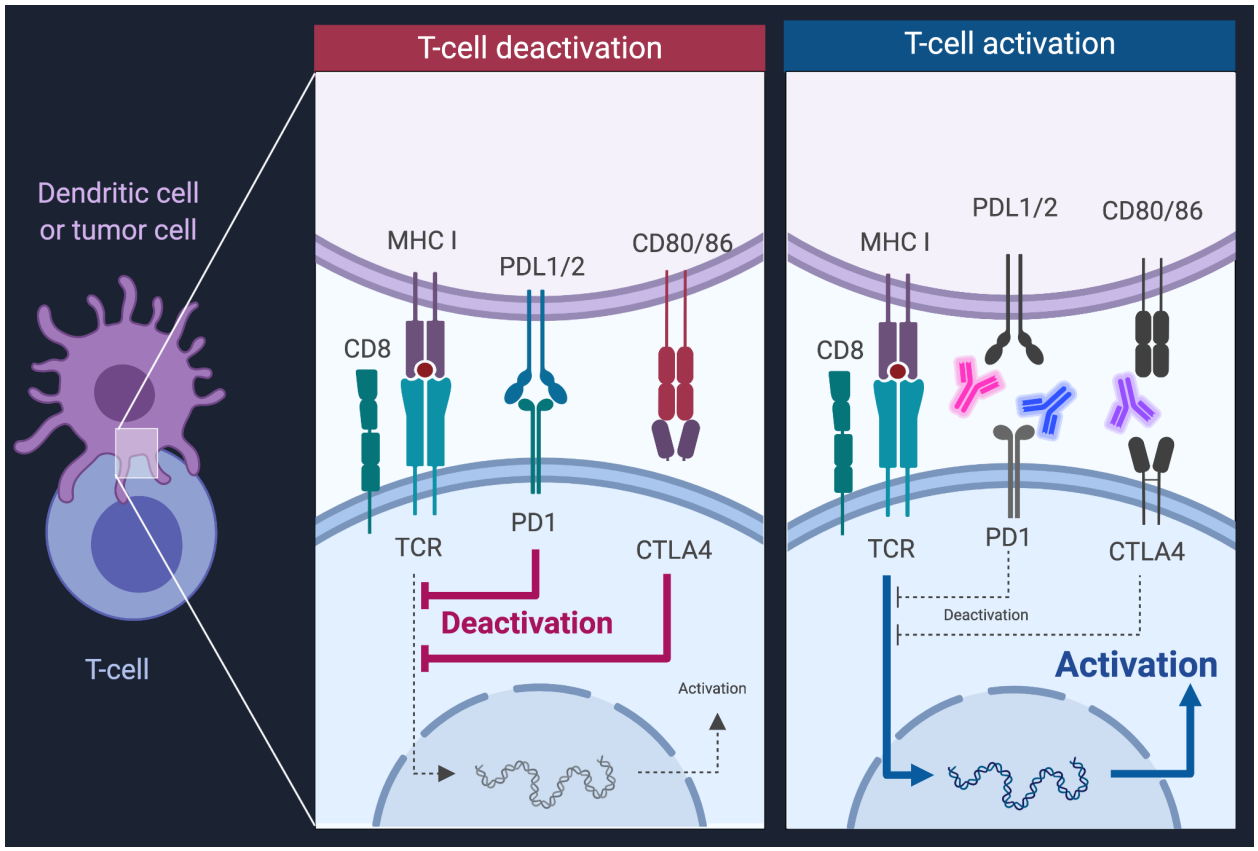

Figure 1-1. Immune checkpoint inhibitors can block tumor cell or dendritic cell ligation with PD-1 on T cells, thereby preventing T cell death and preserving anti-tumor immunity via major histocompatibility complex (MHC)-tumor antigen interaction with T cell receptors (TCRs). Created with BioRender.com.

These antibodies are designed to liberate T cells from immunosuppression mediated by the CTLA-4 and PD-1 pathways, promoting potent and durable T cell responses that can eliminate tumors and put patients in remission[3,6]. However, only a subset of patients (generally 10-40%) currently benefits from immune checkpoint blockade in the clinic[3,6]. While co-administration of both anti-CTLA-4 and anti-PD-1 antibodies can synergistically exert anti-tumor effects, serious immune-related toxicities have been observed. One clinical study reported that 53% of patients treated with the dual anti-CTLA-4/PD-1 immunotherapy experienced grade 3 or 4 adverse events, including hepatic, gastrointestinal, and renal disorders[7]. Thus, there is strong interest to improve patient response rates to cancer immunotherapy in a safe and effective manner. One

potential avenue for achieving these goals would be combining immune checkpoint blockers with emerging treatment modalities, such as cellular therapies and therapeutic vaccines[8-17]. Cellular therapies with patient-derived DCs involve *ex vivo* differentiation of peripheral blood monocytes into DCs, followed by pulsing with tumor-associated antigens (TAAs) to create a rich population of mature DCs presenting TAA peptides on major histocompatibility complexes (MHC). These DCs can then be infused back into the patient for T cell activation and tumor cell killing[18,19]. Alternatively, T cells can be isolated from the patient's blood, and specific T cell populations can be enriched or genetically modified to promote anti-tumor efficacy. Unfortunately, production of MHC-peptide-presenting DCs and tumor-specific T cells are quite labor-intensive, and their yield and quality are variable. Thus, the field is moving towards acellular cancer vaccines and combination immunotherapies.

1.1. The roles of antigens in developing cancer immunotherapies

A major trigger for T cell activation is antigen cross-presentation by antigen-presenting cells (APCs) upon pathogen processing. This mechanism involves the endocytosis and breakdown of pathogens or pathogen products by APCs, which can be macrophages or dendritic cells. Once antigen peptide products are released within the cell and coupled to MHC molecules, the MHC-peptide pair moves to the cell surface for antigen presentation. Different T cells respond to antigen presentation with T cell receptors (TCRs) specific for MHC-I (CD8+) or MHC-II (CD4+) molecules. Historically, it was believed that APCs could process only endogenous antigens by the MHC-I pathway and only exogenous antigens by the MHC-II pathway. They discovered that this peptide processing was not so black-and-white after collecting data over the last 40

years that showed the effective cross-presentation of an MHC-I-associated peptide, OVA257-264, derived from the chicken egg protein Ovalbumin by dendritic cells [20]. Today, ovalbumin and its immunogenic peptide, commonly referred to by its amino acid sequence SIINFEKL, are used extensively in immunological studies involving CD8+ T cell activation. This is important because it has given scientists a model for APC cross-present exogenous antigens, such as tumor antigens, to and subsequent activation of antigen-specific CD8+ T cells.

This enhanced understanding of cross-presentation and T cell activation has been fundamental in developing cancer immunotherapies. Because CD8+ T cells are cytolytic and anti-neoplastic and rely on APCs to activate and cross-present antigens to them, researchers have focused on activating and recruiting antigen-specific CD8+ T cells to the tumor microenvironment to eradicate malignant cells expressing the antigens that the T cells recognize. To this end, adoptive T cell therapy (ACT), the process of manipulating T cells *ex vivo* for subsequent transfer back into patients, has recently gained much attention and become one of the mainstream cancer immunotherapies after immune checkpoint therapy[21]. Three categories of ACT have been established: TIL, TCR, and CAR-T. Tumor infiltrating lymphocytes (TILs) from patients' own tumor biopsies expanded *ex vivo* by IL-2 stimulation were the first type of therapeutic T cells to be studied. However, TILs have shown limited efficacy, prompting the development of other categories of ACT. The other two strategies, TCR and CAR-T, use peripheral T cells transfected with either a specific gene encoding T cell receptor (TCR) of a target antigen or a recombinant chimeric antigen receptor (CAR) (Figure 1-2).

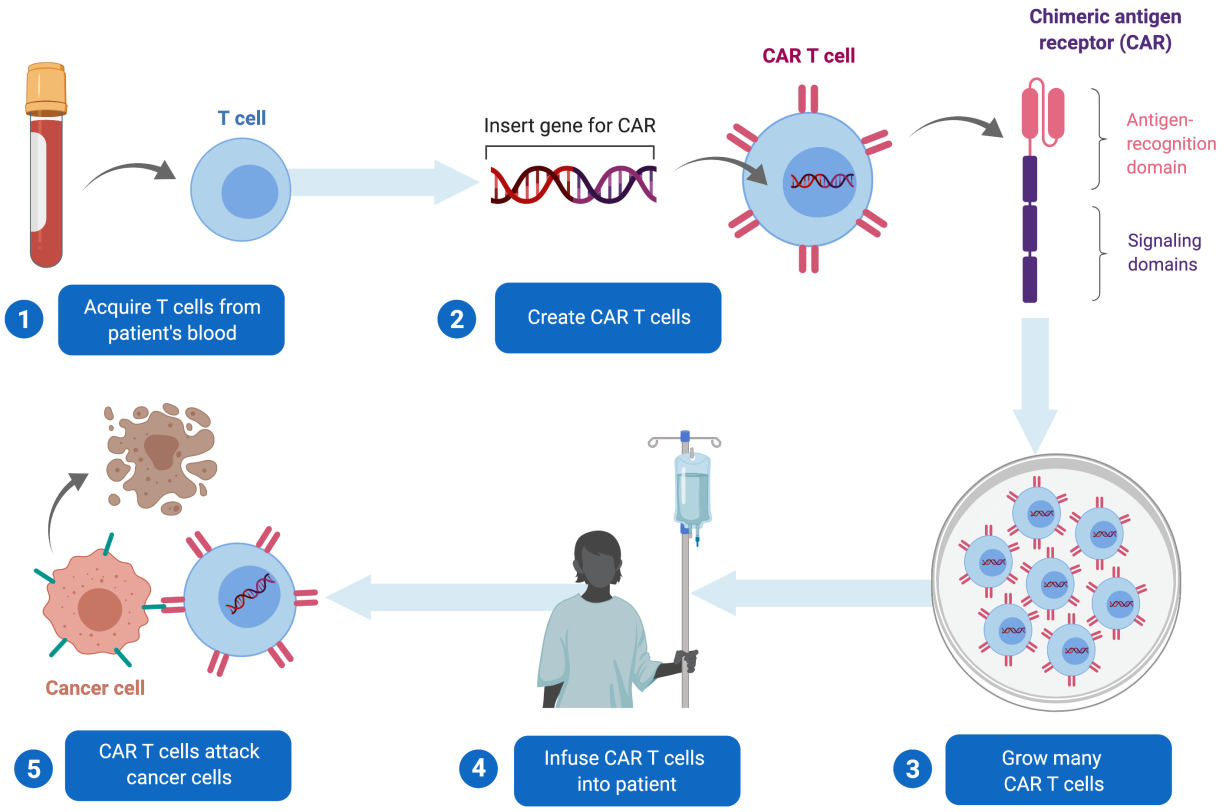

Figure 1-2. General process for generating CAR-T cells. Created with BioRender.com.

In contrast to TCR transgenic T cells, the extracellular single chain variable fragment (scFv) of CAR-T cells binds to antigens independent of MHC, enabling CAR-T cells to target a wider range of tumor-associated antigens. The efficacy of CAR-T therapies in treating hematological malignancies has resulted in two FDA-approved CAR-T cell therapeutics, Tisagenlecleucel and Axicabtagene ciloleucel, for the treatment of acute lymphoblastic leukemia (ALL) and large B-cell lymphoma, respectively[22]. However, when a target antigen is shared by normal and cancer cells, transferred T cells can cause severe on-target-off-tumor toxicity[21]. Therefore, many groups are working to generate CAR-T cells that are more specific to cancer cells while minimizing side effects and increasing efficacy. One approach is to develop patient-tailored neoantigen-specific T cells via genetic engineering. Indeed, it has been found that a higher number of

putative neoantigens in tumors leads to better prognosis for patients receiving ACT[23], suggesting that ACT could become more efficacious when T cells are targeted against neoantigens. A recent study showed that after T cells were transduced with a gene encoding an HLA- and mutation-specific TCR for a shared neoantigen that harbored a H3.3K27M mutation (amino acid substitution from lysine (K) to methionine (M) at position 27 of H3.3) in diffuse intrinsic pontine gliomas, the TCR therapy was able to inhibit tumor growth in a xenograft mouse model[24].

Another limitation of current ACT is generating a sufficient number of cells *ex vivo* prior to infusing cells to patients. This procedure is labor-intensive and requires specialized skills, thus limiting the availability of ACT to only a few institutions worldwide. One potential engineering solution is *in situ* transfection of CAR genes in peripheral T lymphocytes (Figure 1-3)[25].

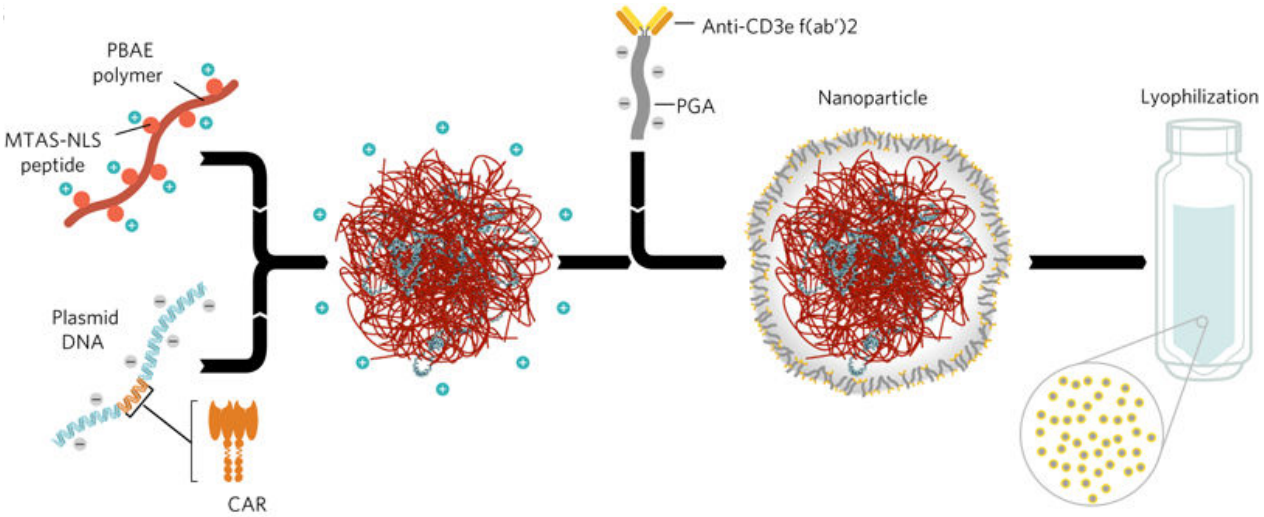

Figure 1-3. Formulation schematic for loading polymeric nanoparticles with CAR genes to enable T cell transfection and subsequent transcription. Figure taken from [25]

Circulating T cells have been targeted by CD3-directed nanoparticles carrying genes for CD19 CAR and piggyBac for sustained transcription, leading to significantly improved survival of mice inoculated with Eμ-ALL01 leukemia cells. This strategy targeted to

circulating T cells may be applicable for generating neoantigen-specific T cells; however, indirect immune activation and biocompatibility of the proposed system should be carefully assessed. Another potential strategy to address the current limitations of ACT is to develop artificial antigen presenting cells (aAPC) for more efficient expansion of functional T cells during *ex vivo* proliferation. Paramagnetic nanoparticles have been designed with agonistic antibodies for providing signals 1 and 2 to enhance T cell activation and proliferation[26]. Interestingly, once magnetic field was applied, these nanoparticles tethered on the cell surface were clustered, mimicking the signal microcluster observed during the activation of T cells. This allows for on-demand control of costimulatory molecules. Similarly, activation and proliferation of CD8+ T cells have been induced with a carbon nanotube-based platform presenting MHC-I molecules and anti-CD28 antibody and PLGA nanoparticles delivering IL-2[27]. Notably, this system required a thousand-fold less amount of soluble IL-2 to obtain comparable number of T cells as commercially available Dynabeads. Alternatively, mesoporous silica micro-rods carrying IL-2, anti-CD3 Ab and peptide-loaded MHC have been developed as an aAPC system (Figure 1-4), which promoted a five-fold greater expansion of antigen specific CAR-T cells, compared with Dynabeads[28]. Interestingly, a slow-release profile of IL-2 from the platform induced less exhausted T cells and consistent CD4:CD8 ratio, enhancing the function and efficacy of adoptively transferred T cells.

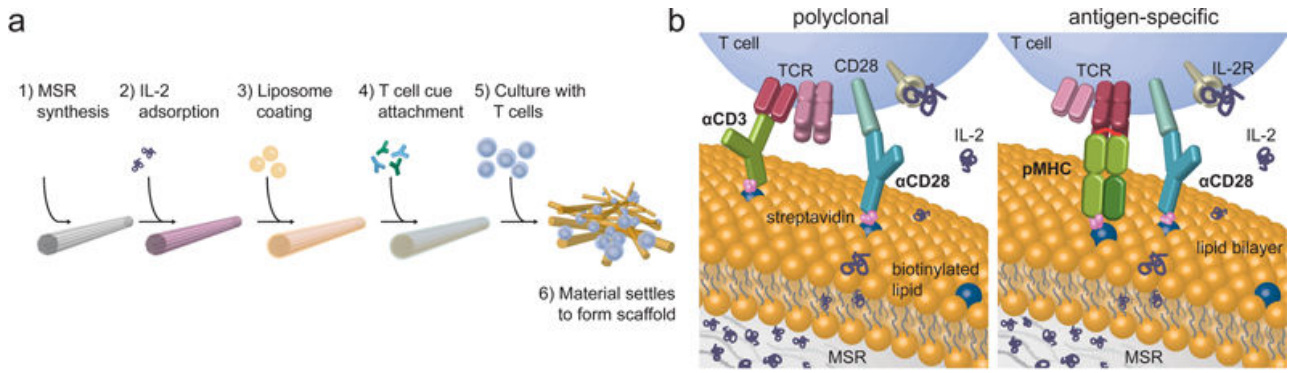

Figure 1-4. (a) Formulation design of mesoporous silica micro-rods carrying IL-2, anti-CD3 Ab and peptide-loaded MHC to form aAPC scaffolds (b) Dynamic simulations of aAPC scaffold interacting with T cells in two different settings depending on which molecules were loaded into the micro-rods. Figure taken from [29].

Maintenance of the viability of adoptively transferred T cells and their tumor infiltration are additional challenges for ACT, especially for improving its efficacy against solid cancers. Due to the immune-suppressive nature of the tumor microenvironment, it is critical that the transferred T cells proliferate sufficiently and home to tumors. To address this, the surfaces of CD8+ T cells have been modified with lipid-based nanoparticles carrying IL-15 super-agonist and IL-21 cytokines for potent proliferation of T cells[30]. Such localized delivery of cytokines enhanced survival and proliferation of T cells after adoptive transfer into cognate antigen-expressing tumor-bearing mice and reduced systemic immunomodulatory effects typically associated with bolus administration of free cytokines. In a similar approach, lipid-based nanoparticles carrying topoisomerase I poison SN-38 have been attached on the surfaces of CD8+ T cells[31]. Notably, these CD8+ T cells were expanded *ex vivo* while maintaining their LN-homing receptors CD62L and CCR7. This strategy allowed efficient homing of transferred T cells to LNs, increasing delivery of SN-38 to LNs by 90-fold as compared with bolus injection of the drug at 10-fold higher dose and extending animal survival in a lymphoma model[31]. Alternatively, adoptively transferred T cells have been targeted *in*

situ with antibody-decorated liposomes carrying IL-2 or TGF-β inhibitor, which promoted proliferation of T cells while reversing immune-suppressive tumor microenvironment[32,33]. Thus, these biomaterial strategies allow specific targeting of drugs to transferred cells and avoiding off-target immunomodulation, thereby safely augmenting T cell therapies.

1.1.1. The promise of neoantigens in personalized cancer immunotherapy

Recent advances in genomics and proteomics are shedding new light on the tumor mutanome, revealing that every tumor has a unique set of driver and passenger mutations[34-36]. Tumor cells expressing mutated proteins present these neoantigens as new epitopes in the context of MHC molecules. Expression of neoantigens is, by definition, restricted to tumor cells as opposed to TAAs with shared expression among healthy and tumor cells. Thus, immunotherapy directed against neoantigens may allow for specific immunological targeting of tumor cells without self-tolerance. As such, neoantigens may hold the key to designing personalized immunotherapy, allowing us to capitalize on rich genomic and proteomic bioinformatics data to customize cancer treatment for patients. The prospect of customizing cancer treatment to individual patients with neoantigen-directed immunotherapy has recently galvanized the field of cancer immunotherapy[34-36]. Identification of neoantigens begins with whole exome DNA and RNA sequencing of tumor cells. Subsequently, a number of filters can be used in the neoantigen identification pipeline to narrow the search, such as predicted proteasome processing, MHC class I and II binding affinities, and confirmation with mass spectrometry analysis of immunoprecipitated peptides. Once top neoantigen candidates are selected, they can be screened further for the presence of neoantigen-specific T cells in patient specimens. First demonstrated in murine models of cancer[37-

[40], the concept of neoantigen-based personalized immunotherapy quickly progressed to where their potency and efficacy have been demonstrated in proof-of-concept Phase I clinical trials with small cohorts of advanced melanoma patients [41,42].

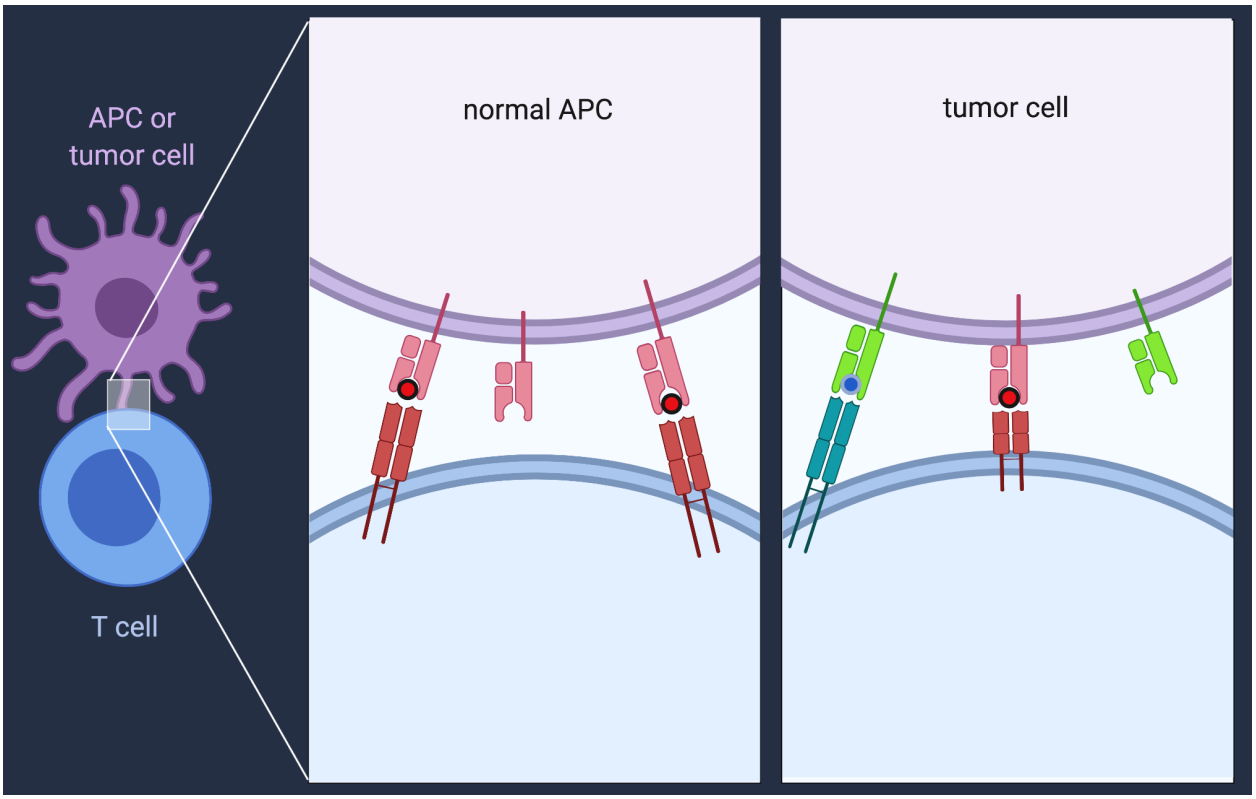

Figure 1-5. Comparative expression of tumor-associated antigens (TAAs, red circle) and tumor-specific antigens (neoantigens, teal). TAAs are expressed by both normal and tumor cells while neoantigens are solely expressed by tumor cells. Created with BioRender.com.

A series of recent papers has showcased striking therapeutic potential of neoantigen-based vaccines. One of the first comprehensive studies that explored vaccination with neoantigen peptides was reported by Castle et al. in 2012[37]. Using next generation exome sequencing, the authors identified over 900 nonsynonymous point mutations in B16F10 murine melanoma cells, over half of which were expressed in tumor cells. Mutated peptide sequences were filtered by MHC-binding prediction tools, and 50 peptides were selected for immunogenicity screening in mice. Subcutaneous

injection of neoantigen or wild type peptides together with polyinosinic:polycytidylic acid (poly(I:C), a Toll-like receptor-3 agonist) adjuvant induced IFN-γ-specific T cell responses with 16 out of 50 peptides, but only 5 of the 16 were specific to neoantigen over wild type stimulation. When tested in a therapeutic setting, neoantigen vaccination slowed the growth of B16F10 tumors, compared with treatment with poly(I:C) alone and no treatment[37]. In 2014, tumor exome sequencing was employed in conjunction with mass spectrometry for the first time to nominate neoantigens. In a hind limb MC38 tumor model, mice vaccinated intraperitoneally with long neoantigen peptides (25-30 amino acid long) together with anti-CD40 and poly(I:C) adjuvant significantly reduced tumor growth and increased tumor-infiltration of neoantigen-specific CD8+ T cells as compared with mice vaccinated with anti-CD40 and poly(I:C) alone[38]. In 2017, results were reported from the first-in-man Phase I clinical in which six advanced melanoma patients were treated with neoantigen peptide vaccines after surgical resection[35]. Briefly, each patient received 7 doses of a mixture of 20 different neoantigen peptides and poly(I:C). Importantly, neoantigen vaccination induced CD4+ and CD8+ T cells targeted against 58 (60%) and 15 (16%) of the 97 unique neoantigens across 6 patients. Four patients had no recurrence at 25 months after vaccination, and two patients had complete tumor regression after treatment with anti-PD-1. This seminal paper showed potential of personalized neoantigen vaccination, especially in combination with immune checkpoint blockade, which can unleash the full cytotoxic potential of neoantigen-specific T cells. In contrast to vaccination with shared tumor antigens, neoantigen vaccinations can reduce the likelihood of immune tolerance as neoantigens are solely and uniquely expressed by individual patients' tumor cells.

These papers have underscored the clinical applicability of personalized neoantigen vaccines as a new therapeutic strategy for long-term protection against tumor relapse and metastasis. In this dissertation, neoantigens were pursued as a tool for cancer immunotherapy in the context of Glioblastoma multiforme (GBM), a stage IV brain cancer, and Colon adenocarcinoma due to the lack of truly effective therapies for these cancers currently available in the clinic. Before discussing the current state of these cancers and the design of our neoantigen immunotherapies, the current and potential delivery options for neoantigens must be reviewed.

1.1.2. Acellular neoantigen delivery systems

As highlighted in the section 1.1.1, these tantalizing results generated with neoantigen vaccines have galvanized the field for personalized immunotherapy; however, there are numerous challenges to overcome to produce potent anti-tumor efficacy with neoantigens in a safe, effective, and personalized manner. In particular, new delivery strategies are needed to enhance transport of neoantigens together with adjuvant molecules to LNs. Amino acid composition of neoantigen peptides can have significant effects on their isoelectric points, and administration of a cocktail of soluble peptides can lead to precipitation, deposition in off-target tissues, or dissemination through the systemic circulation without preferential targeting to lymphoid tissues. The end result is that only a minor fraction of the peptide dose reaches the target lymphoid tissues, limiting the overall vaccine efficacy. While several groups have reported enhanced immunogenicity with peptide vaccines when they include oil-based adjuvants, such as Montanide, to create water-in-oil formulations that form depots for slow release of antigen peptides[43,44], these formulations are often associated with adverse effects,

such as abscess formation and sustained inflammation at the injection site, leading to sequestration and deletion of antigen-specific T cells at the injection site[45-47]. Therefore, neoantigen vaccine platforms should be designed to maximize antigen delivery to LNs while considering the aqueous solubility and physicochemical properties of neoantigen peptides. In addition, co-localized delivery of antigens and adjuvant molecules to the same intracellular compartments (i.e. endosomes with TLRs) within APCs is needed to achieve robust T cell responses[48,49]. Moreover, an ideal vaccine platform for neoantigens should be versatile yet easy to manufacture since personalized vaccine products requires rigorous quality control, patient-to-patient consistency, and adaptability to each patient.

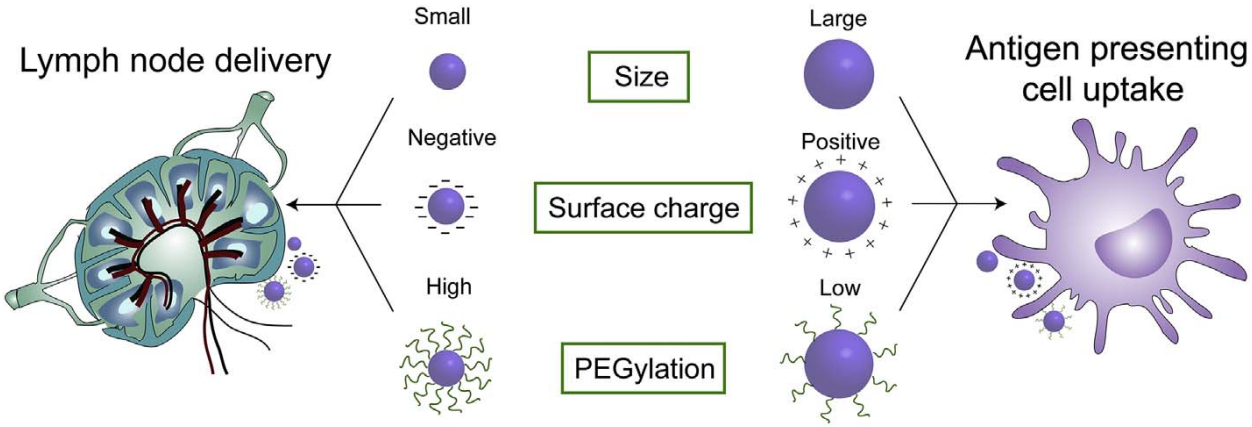

Figure 1-6. Guidelines for drug delivery vehicle design to target lymph node or APC delivery. Particles that are <30 nm in size, negatively charged, and decorated with high densities of polymer are more likely to drain directly through the lymphatic vessels to the lymph node than to be phagocytosed by APCs. Figure taken from [50]

In this respect, nanovaccines are gaining much momentum in the field[51] as nanoparticles with an optimal size (10-100 nm) for lymphatic trafficking (Figure 1-6) are efficient carriers for targeted delivery of antigens to APCs[31,52]. “Albumin-hitchhiking” offers an alternative approach to antigen and adjuvant delivery. Taking advantage of serum albumin’s biophysical properties, cellular interactions, and molecular transport

mechanisms for vaccine design, Liu et al. have shown that TAAs and CpG conjugated to albumin-binding lipid tails generated a 30-fold increase in T cell response and reduced tumor growth in both TC-1 and B16F10 tumor models, compared with free mixtures of TAAs and CpG[53]. Other groups have adopted related albumin-hitchhiking strategies for delivery of chemotherapeutics and antigen/adjuvant combinations. In particular, an Evans blue analog that binds to albumin for effective LN draining has been reported[54]. This analog, termed AlbiVax, tethered to antigens or CpG readily binds to albumin upon injection, allowing for systemic delivery of antigens and adjuvants (Figure 1-7)[54]. Using PET imaging and Cu^{64}-labeled Adpgk neoantigen in the MC38 model, the authors showed that AlbiVax exhibited > 40-fold greater accumulation in LNs as compared to soluble peptide vaccination. Vaccination with AlbiVax-Adpgk plus CpG significantly increased the number of Adpgk-specific CD8+ T cells in peripheral blood, slowed tumor growth, and protected animals against tumor re-challenge. Combination immunotherapy with AlbiVax-Adpgk plus anti-PD-1 therapy further improved therapeutic efficacy[54]. As albumin-bound drug conjugates are already FDA-approved for cancer treatment[55], albumin-mediated vaccine delivery may offer a promising clinical pathway for personalized cancer immunotherapy. Yet, autoimmunity against albumin or albumin-producing hepatocytes as well as off-target toxicity of albumin-hitchhiking therapeutics should be carefully examined for their successful clinical translation.

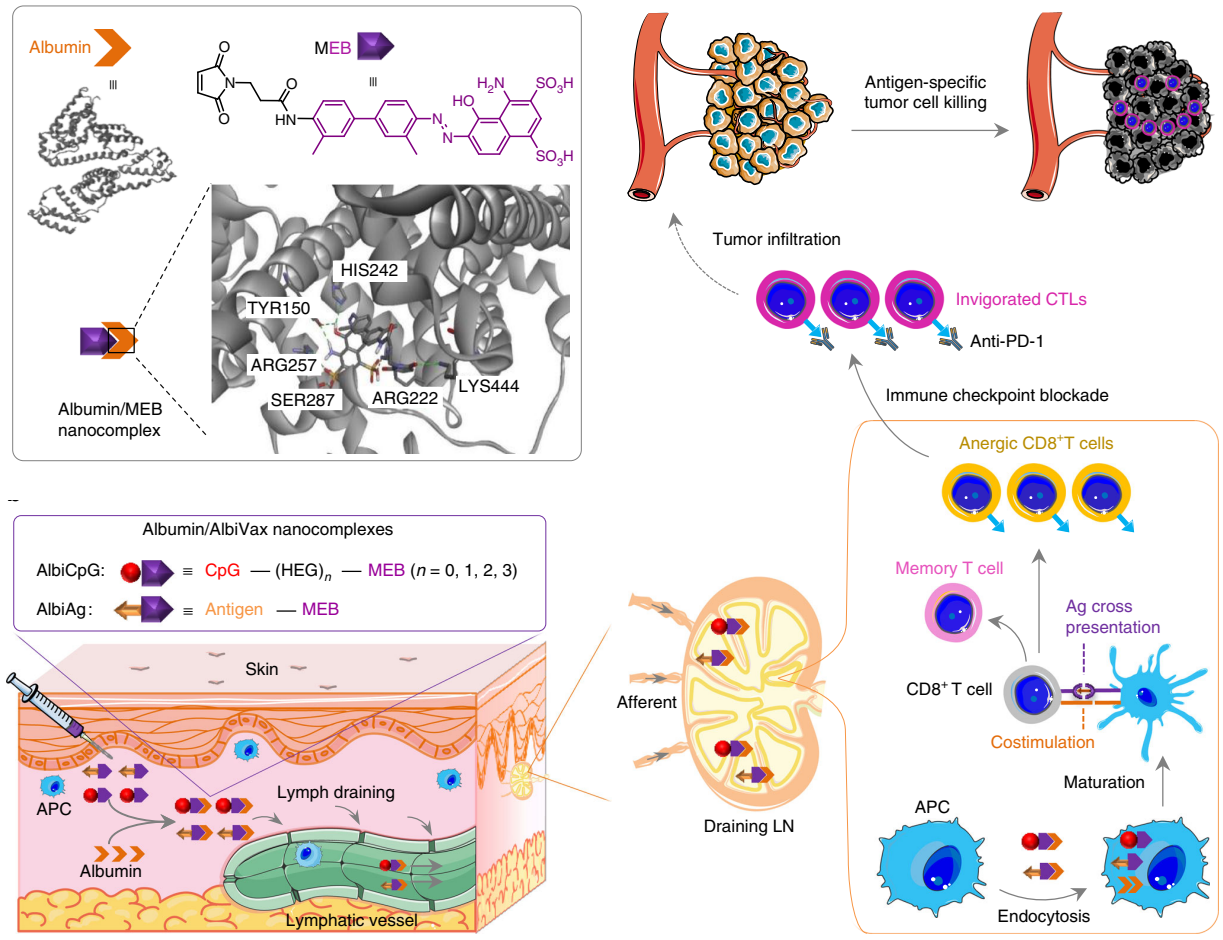

Figure 1-7. Schematic of AlbiVax hypothesis on therapeutic efficacy against tumors. MEB = mimic of Evans blue. Figure taken from [54]

Self-assembled DNA-RNA nanocapsules, termed iDR-NCs, have also been developed for delivery of neoantigen peptides. iDR-NCs were composed of CpG for immune activation, Stat3 shRNA for reversing immunosuppression, and PEG-grafted polypeptides for delivery of neoantigen peptides. After confirming effective internalization of iDR-NCs by bone-marrow-derived dendritic cells (BMDCs), the authors validated synergistic immune-activation of DCs treated with iDR-NCs compared with CpG-containing larger parent particles or CpG alone. In mice, iDR-NCs loaded with MC38 neoantigen Adpgk peptide elicited 8-fold greater level of Adpgk-specific CD8+ T cell responses and exerted stronger anti-tumor efficacy as compared to the soluble

Adpgk + CpG group[56]. In an alternative approach, synthetic polymeric (PC7A) particles with an intrinsic ability to activate the stimulator of interferon genes pathway have been employed for induction of T cell responses against neoantigens[57]. PC7A nanoparticles' small size of ~29 nm facilitated effective lymphatic drainage of antigen and subsequent cellular uptake, cross-presentation, and DC activation. After demonstrating PC7A nanoparticle efficacy in the B16 model of melanoma expressing ovalbumin (OVA), the authors have shown potent anti-tumor effect of PC7A nanoparticles delivering a cocktail of TAAs and neoantigens in murine models of MC38 colon carcinoma and B16F10 melanoma[57]. Recently, mixtures of mesoporous silica microrod scaffolds (MSRs) each separately adsorbed with CpG, GM-CSF, or PEI plus antigens have been used for vaccination[58]. Including the PEI-adsorbed MSRs in the mixture significantly increased the expression of MHC-II and CD86 in BMDCs and production of IL-6 and TNF-alpha *in vitro*. Subcutaneous administration of MSR-PEI-OVA outperformed MSR-OVA in terms of increasing antigen-specific CD8+ T cells, IFN-γ production, and the effector-to-regulatory T cell ratio. Vaccination with mixtures of MSR-CpG, MSR-GM-CSF, and MSR-PEI-neoantigens reduced the number of lung metastases in the model of B16F10 and CT26 and exerted anti-tumor efficacy in synergy with anti-CTLA-4 IgG therapy[58].

Taken together, these innovative nanovaccines have yielded exciting proof-of-concept results for personalized vaccination based on neoantigen peptides. It is notable that nanovaccines' performances were further improved when combined with immune checkpoint blockade therapy, highlighting the importance of addressing immunosuppression in the tumor microenvironment for effective cancer vaccination (Figure 1-8). Moreover, the biomaterials used for these nanovaccines mediated

reduction of off-target toxicities and non-specific immune responses either by improving biotransport of cargo molecules or incorporation of targeting modalities. Toward the goal of making personalized nanovaccines a reality, the remaining engineering challenges include how to promote controlled release of immunomodulatory agents to enhance T cell infiltration into tumors post vaccination and to sustain functionality of T cells within the immunosuppressive tumor microenvironment. It is also necessary to examine and validate LN-draining and APC-targeted delivery of nanovaccines in large animals, as most studies in the field have been performed in murine models; stability of nanomaterials and LN-draining patterns may be entirely different in humans, compared with small murine models. In addition, it is important to streamline GMP-manufacturing of personalized vaccine nanoparticles for robust adaptability to each patient's neoantigens and to establish quality control measures for neoantigens with diverse physicochemical properties.

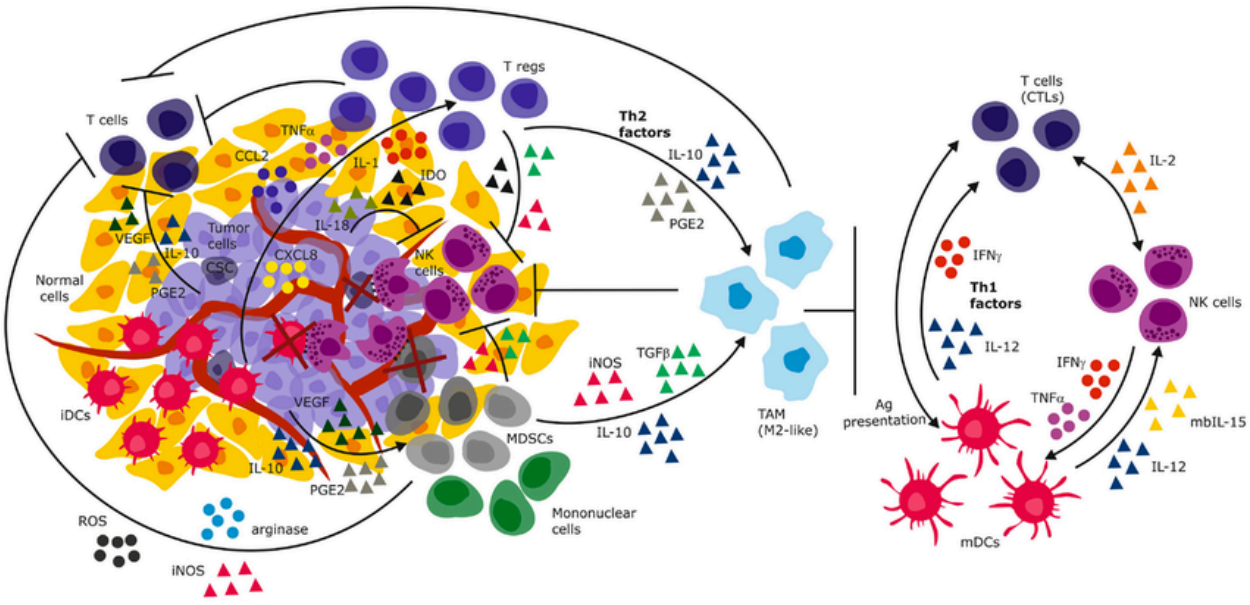

Figure 1-8. Diagram of complex immunosuppressive tumor microenvironment (left) and its inhibition of normal immune activity (right). Figure taken from [37, 59]

1.1.3. Image-guided theranostics for combination immunotherapy

It remains challenging to target nanoparticles to specific tissues and promote their tissue permeation. This poses significant obstacles, especially for applications in immunomodulation because organ inflammation and tissue damage due to drug accumulation in off-target sites can lead to unintended acute or chronic immune responses. Biomaterial-based image-guided methods, including magnetic resonance imaging (MRI) and ultrasound (US), may address these issues by precisely controlling the timing and location of drug release[60-65], potentially limiting off-target toxicity observed with combination immunotherapies. In addition, image-guided delivery technologies may enhance cell permeability and nanoparticle uptake, allowing for better characterization of the tumor microenvironment during and after immunotherapy. Overall, recent innovations and advances in image-guided theranostics for cancer treatment can be directly adapted to combination immunotherapy and may lead to new biomaterial-based treatment options tailored for each cancer patient, opening doors for personalized diagnostics and therapeutics.

For MRI applications, superparamagnetic iron oxide nanoparticles (SPIONs) have been thoroughly investigated as theranostic nanomaterials. SPIONs can be formulated in a variety of sizes and functionalized with different therapeutic moieties using simple chemistry. Several groups have reported the use of SPIONs for early tumor diagnosis and perfusion[66,67], treatment by thermal ablation[68-70], and magnetic guidance of therapeutic entities[71-73]. Importantly, SPIONs and their modified counterparts are generally biocompatible and readily metabolized to iron ions and oxygen molecules. SPIONs decorated with single-chain CD3 antibodies and carrying immunosuppressive

genes have been developed for selective transfection of T cells, leading to significantly downregulated cytokine production and proliferation[60]. Administration of heat shock protein 70-decorated SPIONs carrying C6 glioma antigens have been reported to target DCs and generate anti-tumor T cells, thus inhibiting tumor growth and extending survival of C6 glioma-bearing rats (Figure 1-9) [74]. These two studies have shown the potential of SPION-based theranostics for individualized combination immunotherapy.

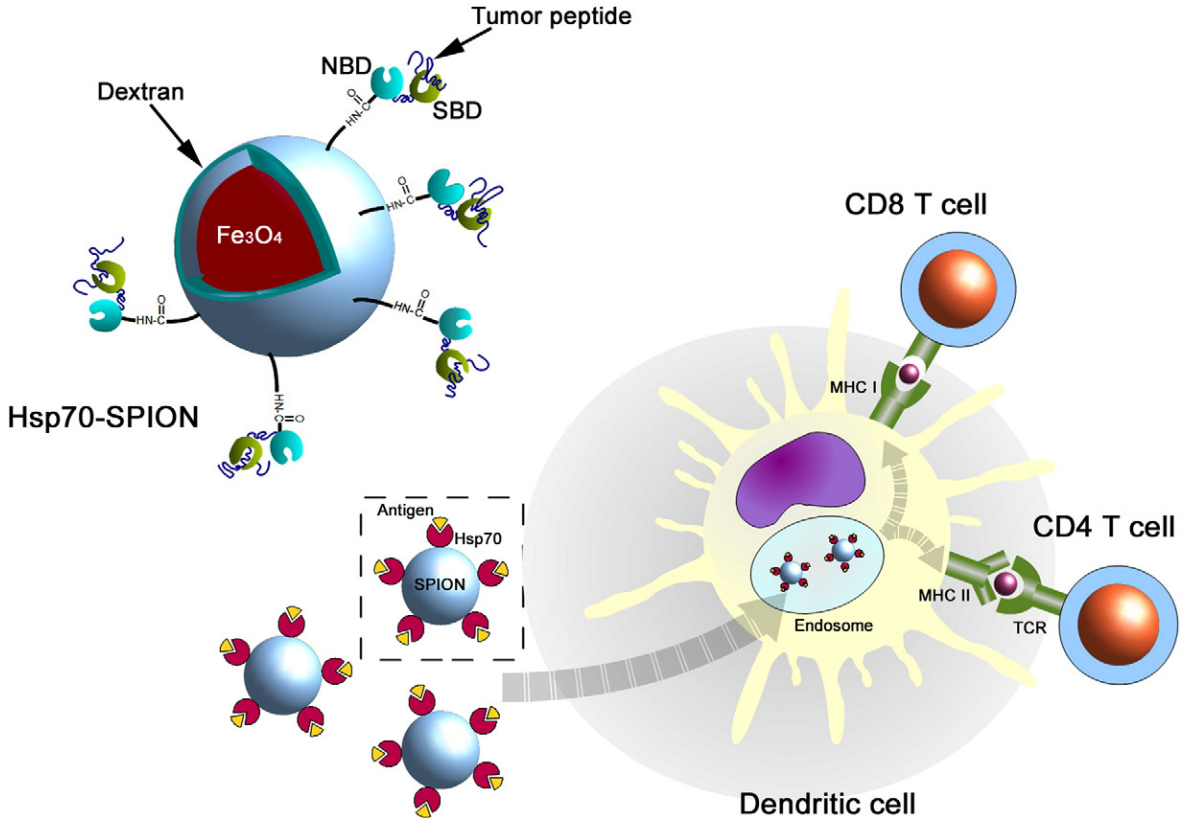

Figure 1-9. Theoretical anti-tumor mechanisms of SPIONs decorated with Heat shock protein 70 (Hsp70, nucleotide-binding domains (NBDs) and substrate-binding domains (SBDs) shown) bound to tumor antigen peptides. Figure taken from [74]

Ultrasound can be applied to a target site in a focused manner with the use of contrast agents to deliver drugs to specific tissues. This could enhance the permeability of tissues for increased drug delivery and also for thermal ablation of tumor tissues while reducing non-specific accumulation of therapeutics. Microbubbles have been used as

ultrasound contrast agents (UCAs) for decades in clinical diagnostics due to their ability to backscatter sound waves with which they come in contact. In the last decade, microbubbles have attracted considerable interest as drug delivery vehicles due to their ability to produce enough shear force during stable oscillations or acoustic collapse to permeabilize cell membranes[75]. Microbubbles, like SPIONs, can be functionalized with a variety of therapeutic molecules. A few groups have shown successful tumor regression using ultrasound-mediated delivery of chemotherapeutics to different solid tumors[76-79]. Others have applied this technology for personalized cancer immunotherapy through the application of ultrasound at the individual's specific tumor site after systemic administration of immunomodulatory agents to maximize delivery to the target site. This strategy has been successfully applied in a number of tumor models, including a rat glioma model using soluble IL-12 (Figure 1-10); a mouse hepatoma model using thymidine kinase; and other murine tumor models, such as lymphoma, neuroblastoma, melanoma, and ovarian cancer[78,80-82].

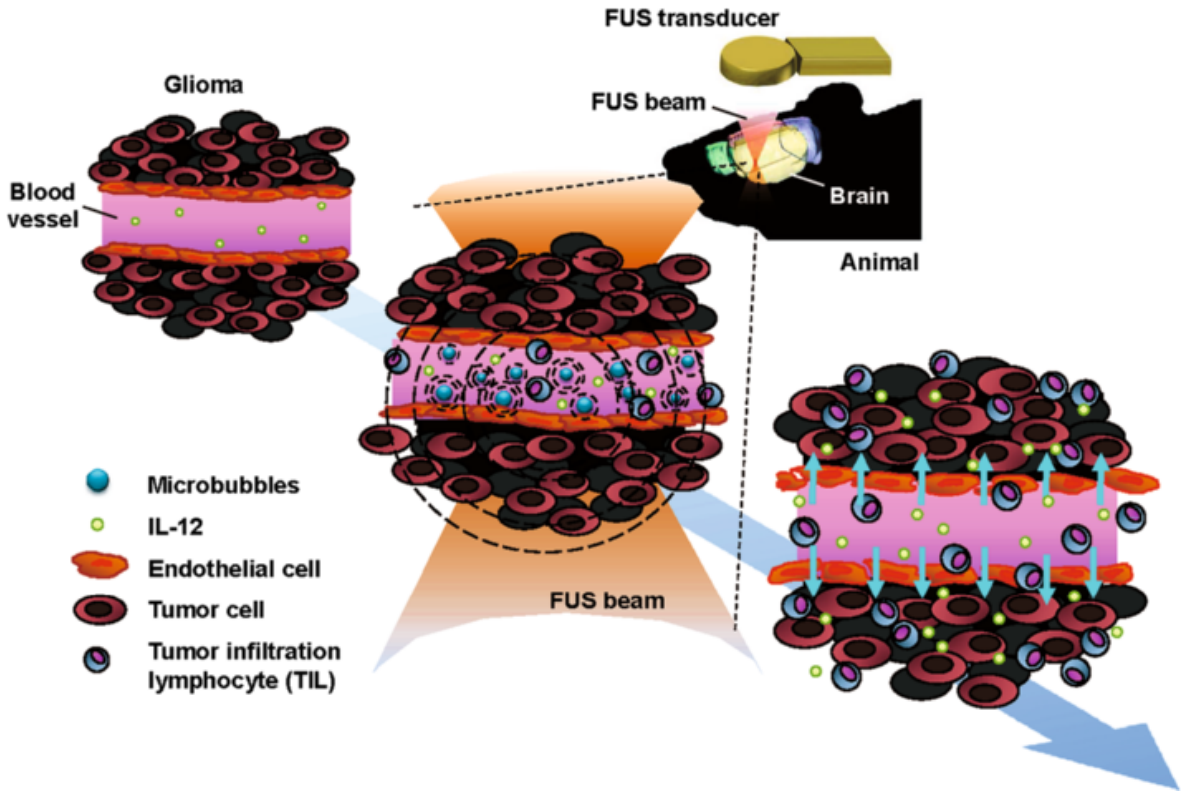

Figure 1-10. Schematic of ultrasound-mediated blood-brain barrier opening following i.v. administration of ultrasound contrast agents (microbubbles) and therapeutic entities (IL-12) with the application of focused ultrasound (FUS) energy. Figure taken from [78]

1.2. Synthetic high density lipoprotein (sHDL) nanoparticles for neoantigen delivery

1.2.1. Composition and physicochemical advantages of sHDL

sHDL nanodiscs are particularly suited for neoantigen vaccination due to their small size (~ 10 nm in diameter), stability, and biocompatibility. In addition, whereas large-scale manufacturability and clinical safety are major hurdles for clinical translation of nanomedicines in general[83], the sHDL vaccine technology builds on cGMP-manufacturability and clinical safety previously demonstrated in clinical trials for cardiovascular applications[84]. sHDL nanodiscs are simply composed of phospholipids and Apolipoprotein-A1 (Apo-A1) mimetic peptides, which spontaneously form nanodiscs upon hydration in aqueous buffer. These nanodiscs are representative of pre-β HDL,

the lipid-poor HDL that readily accumulates other phospholipids and cholesterol that have been effluxed by cells into the blood[85]. As such, the lipid bilayer allows for facile loading of small amounts of lipid-conjugated antigen peptides and adjuvants without increasing the size of the nanodiscs significantly. Furthermore, sHDL nanodiscs can readily bind to lipoprotein cell receptors such as scavenger receptor class B member 1 (SR-B1), which is overexpressed on APCs, allowing for targeted delivery of nanodiscs to APCs in LNs[86-89].

1.2.2. Prior demonstration of neoantigen delivery by sHDL

Earlier studies conducted in our lab evaluated the immunotherapeutic potential of murine colon carcinoma MC38 neoantigen Adpgk in conjunction with toll-like receptor 9 (TLR9) agonist CpG oligonucleotide. Mice vaccinated with Adpgk/CpG-sHDL nanodiscs elicited ~47-fold greater frequency of Adpgk-specific CD8+ T cells, compared with soluble Adpgk and CpG[16]. When neoantigen nanodisc vaccination was combined with immune checkpoint blockade (anti-PD-1 IgG therapy), more than 85% of animals demonstrated tumor eradication in the murine models of MC38 colon adenocarcinoma and B16F10 melanoma. Interestingly, in the murine model of B16F10 melanoma, vaccination with a cocktail of nanodiscs carrying a TAA, TRP2, and two neoantigens, M27 and M30, had a noticeable advantage over vaccination with TRP2 or two neoantigens alone, suggesting the benefits of vaccines targeted against a large set of TAAs and neoantigens[16]. In addition, compared with intramuscular route, subcutaneous administration of nanodiscs enhanced LN-targeted delivery of antigens and adjuvants, leading to an 8-fold increase in the frequency of neoantigen-specific T cells and elimination of large established B16F10 tumors[90]. It remains to be seen whether sHDL

vaccines personalized with neoantigens can achieve significant patient survival benefit in the clinic[16,91,92]. In this dissertation, sHDL nanodiscs were used as carriers for neoantigens derived from GL261 murine GBM tumors to determine the therapeutic potential of the nanovaccine in such a non-targetable cancer (Chapter 2).

1.2.3. Limitations of sHDL as a drug delivery vehicle

Because sHDL is formulated using water-insoluble phospholipids and water-soluble peptides, synthesis of the nanodiscs up until this point has required the use of both organic solvents to create homogeneous mixtures and lyophilization to remove organic solvents from final reaction products. While organic solvent use and removal is common in drug manufacturing, the scale at which these processes would have to occur has not yet been tested for the antigen delivery application. Material loss upon lyophilization and reconstitution would need to be considered in addition to the individualized pH adjustments performed for each antigen peptide formulation. Moreover, the lyophilization process itself can be ridden with inconsistencies leading to instability of the active pharmaceutical ingredients—in this case, peptides and lipids—that could significantly affect therapeutic performance[93]. The complex process of formulating the neoantigen-loaded sHDLs described in Chapter 2 is not entirely compatible with large-scale manufacturing processes. Fortunately, the work described in Chapter 3 potentiates a solution to these limitations.

1.3. Current treatment approaches for GBM

Brain cancers continue to be some of the most deadly and untreatable malignancies around the world, responsible for nearly 17,000 deaths and are diagnosed in over 75,000 people annually. They are the most common forms of childhood cancer with

leukemia being the second most common. Though there are many histologically unique types, brain cancers remain difficult to treat given the delicate complexity of the host tissue [94]. Primary tumors, those that arise in the brain and are not results of metastases, are categorized broadly into meningiomas, gliomas, pituitary tumors, and nerve sheath tumors. These tumors are classified by their original location in the brain but will likely invade neighboring brain tissue with time. Astrocytomas and glioblastomas, both advanced types of gliomas, cannot be fully removed by resection due to their anaplastic nature. Radiation typically follows surgical resection of the tumor to rid the brain of any remaining tumor cells and is also used to treat tumors that cannot be resected. However, the major concern with radiation is that it is quite harmful to normal brain cells and cannot be too specifically focused on the tumor alone. The next level of treatment for brain cancers is chemotherapy, which also has a major obstacle to overcome: the blood-brain barrier (BBB). Most drugs cannot cross the BBB or are effluxed by brain transporters and thus exert no therapeutic effect on the brain tumor but produce unwanted side effects due to systemic administration. Physicians can sometimes circumvent this issue by injecting drug directly into the patient's cerebrospinal fluid (CSF) with a catheter system, but such an approach defeats the purpose of chemotherapy being a noninvasive method of treatment [95]. Increased interest in targeted therapies has led to the development of technologies that can overcome some of these obstacles, but most are either invasive or elicit strong and unfavorable off-target effects. Thus, there remains a need for a minimally invasive yet effective treatment for brain cancers that is limited in action to the tumor site itself.

Gliadel, an FDA-approved wafer implant releasing the anti-neoplastic alkylating agent Carmustine, virtually eliminates treatment-related side effects because it is placed directly into the tumor site. Gliadel was mainly designed for high-grade gliomas that cannot be rid of with surgery and radiation alone. Although the implant is far more tumor site-specific than any other approach, the surgery required for placement of the wafers can result in a variety of complications such as hydrocephalus and brain edema. In fact, physicians predict that almost one out of every four patients receiving the implant will experience brain edemas [96]. In 2009, bevacizumab, an antibody against vascular endothelial growth factor (VEGF) [97], was approved by the FDA for recurrent GBM treatment after having been on the market for several years to treat colorectal, lung, breast, and renal cancers. Bevacizumab showed marked VEGF inhibition in phase 2 clinical trials as evidenced by significant reductions in glucose uptake and cerebral edema but has ultimately provided no survival benefit to patients. Thus, there remains a need for a noninvasive, targeted therapy that will eliminate brain tumors and improve brain cancer patient survival outcomes.

Immunotherapy is an increasingly attractive treatment option for brain cancers because it has the potential to reverse the immunosuppressive tumor microenvironment, target tumor antigens and neoantigens, and maintain a long-lasting anti-tumor response. Enhanced tumor cell expression of programmed death receptor 1 (PD-1) ligands has been shown to increase T cell apoptosis and to suppress anti-tumor immunological efforts in multiple cancers, including the brain [6,98,99]. Anti-PD-1 antibodies effectively block the induction of T cell death by PD-1 ligands to preserve T cell activity, promoting the anti-tumor immune response. Though proven effective in a significant

number of patient cases, the major downfall of these immune checkpoint inhibitors is that they rely on specific cancer cell phenotypes and protein expression profiles in patients with highly heterogenous tumors, including brain cancers.

Thus, the field has shifted focus toward more tumor-specific approaches to immunotherapy. Tumor lysates contain tumor antigens and neoantigens, which can be harnessed to induce a tumor-targeted immune response. Currently, a Phase 3 clinical trial testing DCVax-L, a tumor lysate-pulsed dendritic cell vaccine, against newly diagnosed GBM is underway. DCVax-L has shown promising preclinical and early clinical results, with 50% of treated patients surviving to 32 months as compared to a 16-month 50% survival rate for untreated patients without any dose-limiting toxicities[100]. The vaccine, which is administered intradermally, has also demonstrated significantly enhanced tumor infiltration of CD8+ T cells (Figure 1-11), increasing the probability of antigen-specific cytotoxic T cell-mediated tumor cell killing [101]. However, the manufacturing of DCVax-L requires extensive regulation with respect to culturing the patients' cells for re-injection and preparing tumor lysate, all of which is time-consuming and time-sensitive. Additionally, the tumor-lysate pulsed cells are not guaranteed to express potent antigens due to the variety of components in tumor lysates.

In a more specific approach, Celldex Therapeutics took advantage of the common yet heterogeneous overexpression of EGFRvIII peptide on GBM cells and formulated a tumor-specific antigen vaccine, rindopepimut, which made it into a phase III clinical trial comprised of patients with newly diagnosed EGFRvIII-positive glioblastoma who had undergone tumor resection. On March 7, 2016, Celldex announced that it was halting this phase III trial based on findings from an interim data analysis that showed patients

receiving rindopepimut were unlikely to have an improvement in overall survival compared with patients in the control arm[102]. These lackluster results could be due, in part, to the tumor heterogeneity and also to inefficient peptide delivery to the tumor.

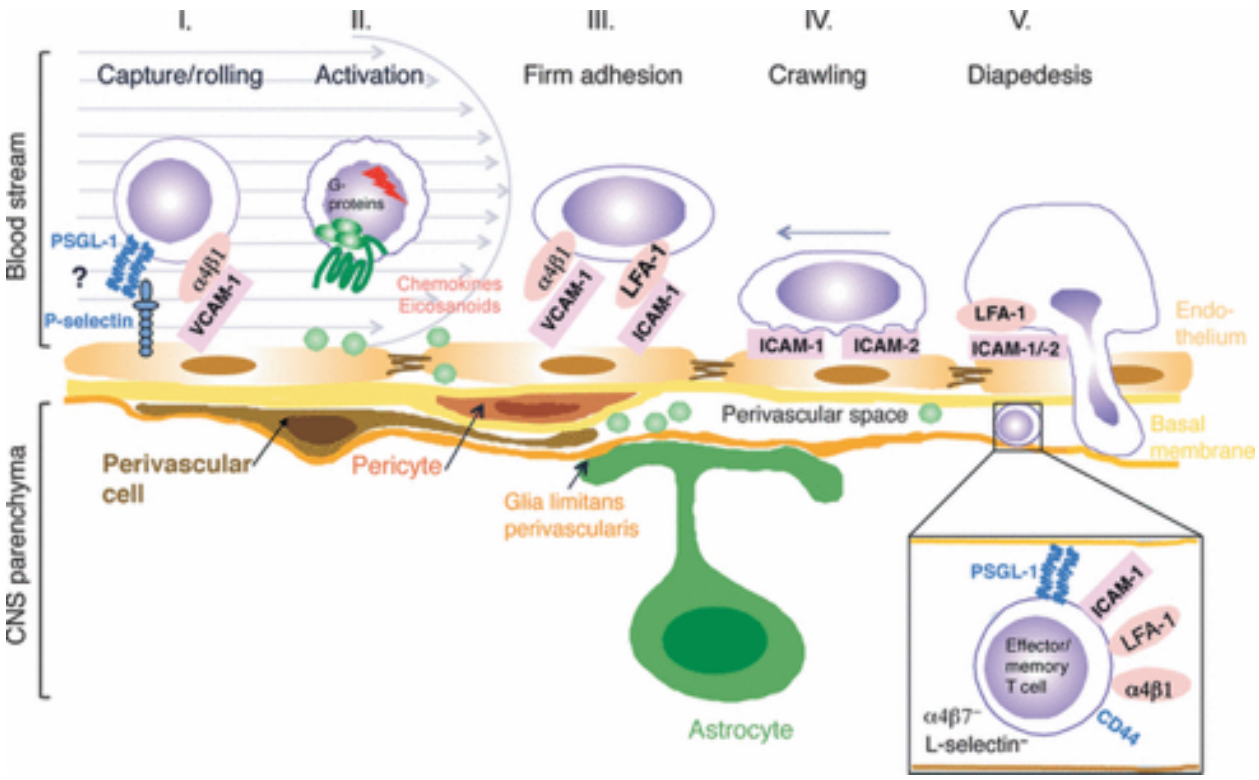

Figure 1-11. Proposed mechanisms of T cell migration across the BBB. Figure taken from [103].

Neoantigens have such a large therapeutic advantage over shared antigens and immune checkpoint antibodies because of their targetability and potential for patient personalization. Neoantigen delivery to dendritic cells can induce highly specific anti-tumor responses through the cross-presentation of neoantigens to cytotoxic CD8+ T cells without any normal cell killing. Interestingly, in 2016, a group out of Washington University in St. Louis published their discovery of several unique neoantigens in GL261 and SMA-560 murine glioblastoma tumors. The investigators used whole exome and RNA sequencing to identify the initial candidate neoepitopes and further narrowed the

candidate pool using enzyme-linked immunosorbent spot (ELISPOT) and tetramer analyses. The most promising results from this study were the detectable frequencies of neoantigen-specific T cells in both brain tumors and the draining cervical lymph nodes in tumor-bearing mice that had not been vaccinated or treated with any other agents[104]. Unfortunately, effective lymphatic delivery methods for neoantigens do not currently exist, and there remains a need for a simple and efficient delivery system for neoantigens to bring a highly effective immunotherapy for GBM to market. In this dissertation, a potential solution for this need was developed using the GL261 neoantigen sequences identified in 2016 and will be described thoroughly in Chapter 2.

1.4. Current treatment approaches for Colon carcinoma

Colon carcinomas are a subset of colorectal cancers, the third most common cancer diagnosed across both sexes. Colon carcinomas themselves comprise over two-thirds of all colorectal cancers with an overall 5-year survival rate of 64%, which rapidly decreases to 14% when the cancer becomes distant or metastatic, usually progressing into the liver. Depending on the stage of colon carcinoma at diagnosis, patients can undergo surgery to attempt tumor resection. These patients are still given chemotherapy following surgery to eliminate any tumor cells that may have been left behind. Patients who do not have the option of surgery usually receive chemotherapy as the first line of therapy with one or a combination of the following drugs: thymidylate synthase inhibitor 5-fluorouracil (5-FU) or its prodrug capecitabine, topoisomerase I inhibitor irinotecan, DNA intercalator oxaliplatin, or a combination drug composed of DNA intercalator trifluridine plus thymidine phosphorylase inhibitor tipiracil. As with most cancers, colon carcinomas do not always respond to chemotherapies, and patients

often discontinue treatment due to unmanageable side effects. Fortunately, regional chemotherapy can be given to patients with localized cancer through the hepatic artery, but many patients do not have this luxury. Thus, targeted therapies and immunotherapies have been developed to aid chemotherapy.

Approved targeted therapies for colon carcinoma are limited to VEGF inhibitors, including bevacizumab used in treatment regimens for aforementioned GBM patients, epidermal growth factor receptor (EGFR) inhibitors, and kinase inhibitors. All of these inhibitors aim to prevent new blood vessel formation around the tumor or to interrupt tumor cell proliferation so that tumor growth can be slowed. Because they do not directly induce tumor cell killing, they are usually given in combination with chemotherapy for maximum therapeutic effect. Immunotherapies also induce indirect tumor cell killing; anti-CTLA-4 and anti-PD-1 prevent T cell death, allowing for increased T cell activation, tumor recognition, and tumor cell killing[105]. Unfortunately, these targeted therapies and immunotherapies are associated with several adverse events due to their systemic or oral administration.

To overcome the limitations of current colon carcinoma therapies, much research is focusing on developing therapeutic vaccines similar to those discussed for GBM. Shared tumor antigen peptide vaccines targeting commonly overexpressed proteins in cancer such as EGFR and Mucin-1 have been developed and studied in combination with chemotherapy but have shown no overall survival benefit when compared to chemotherapy alone[106]. In 2014, Hazama et al. reported the use of a five peptide cocktail comprised of three tumor-associated antigens restricted by HLA-A*2402, a human leukocyte antigen (HLA) allele expressed by a significant proportion of

Southeast Asian people, and two VEGF antigens in combination with oxaliplatin chemotherapy as a potential frontline therapy for Japanese colorectal cancer patients in a phase II study. The peptide cocktail was mixed with Freund's adjuvant for administration. Unfortunately, no differences in survival benefits were observed between patients with and without HLA-A*2402 expression[107]. Around the same time, Okuno et al. reported the use of a seven-peptide cocktail comprised of five tumor-associated antigens restricted by HLA-A*2402 and two VEGF antigens in combination with tegafur-uracil plus leucovorin (UFT/LV) chemotherapy in Japanese colorectal cancer patients. Out of 30 patients, 15 exhibited stable disease while 3 showed partial responses to therapy. The investigators calculated that patients who showed positive antigen-specific T cell responses to all seven antigen peptides were more likely to experience a significant improvement in overall survival[108]. However, a much greater sample size is needed to confirm these results, and the requirement of a response to all seven peptides to increase survival odds is quite lofty. Neoantigen vaccination has also been investigated in colorectal cancer patients. Tumor-specific KRAS mutations have been identified and formulated into vaccines using either the peptide itself or activated cytotoxic T cells that recognize the mutated peptide. Both of these vaccines increased the immune response against neoantigens, but only the T cell vaccine resulted in significant disease regression[109,110]. A major limitation of these therapeutic strategies is the poor delivery system of the therapeutic entities; peptides dissolved in emulsions often have difficulty trafficking to the lymph nodes while vaccination of peptide-presenting dendritic cells or peptide-recognizing T cells requires very particular, time-consuming, and low-yield autologous cell culture. Thus, many researchers have begun

developing delivery systems for tumor-associated antigens and neoantigens using liposomes, viral vectors, and polymeric nanoparticles as well as combinatorial treatment regimens using a mix of chemotherapies, targeted therapies, and immunotherapies. In Chapter 4, a potential solution to improving treatment for colon carcinoma is described, encompassing a couple of the strategies aforementioned through co-delivery of chemotherapy and immunotherapy using sHDLs.

1.5. Research Scope

Thus far, this introduction has highlighted the current state of cancer immunotherapy and the promise of neoantigens as immunotherapeutic agents in brain and colon cancer treatment. Synthetic HDLs have also been discussed as clinically translatable drug delivery platforms given their prior demonstration as biocompatible nanoparticles in both cardiovascular and oncologic applications. Here, we aim to harness the excitement surrounding neoantigens for cancer immunotherapy and the clinical potential of sHDL as a drug delivery vehicle to create novel combinatorial immunotherapies for patients suffering from Glioblastoma multiforme and Colon adenocarcinoma.

1.6. Thesis Overview

The overall goal of this thesis is to develop a clinically translatable and scalable platform for co-delivery of neoantigens or chemotherapeutic molecules and adjuvants directly to tumors or tumor-draining lymph nodes for site-specific treatment that is minimally invasive and reduces off-target side effects. To achieve this goal, we studied the anti-tumor effects elicited by neoantigen or chemotherapy-loaded sHDL in two

different tumor models and simplified the complex formulation process for neoantigen-loaded sHDL to streamline development of personalized cancer vaccines.

In Chapter 2, we explore the ability of murine Glioblastoma multiforme neoantigens co-delivered with adjuvant on sHDL nanodiscs to generate neoantigen-specific CD8+ T cells, slow tumor growth, and prolong overall survival in tumor-bearing mice. We also incorporate immune checkpoint blockade anti-PD-L1 to treatment regimens to study further the anti-tumor effects of combination immunotherapy. Moreover, we evaluate the tumor microenvironment of mice vaccinated with neoantigen-loaded sHDL nanodiscs to determine whether immunosuppression within the tumor could be reversed. In all studies, we compare the pharmacodynamic effects of the nanovaccine with soluble neoantigen vaccination to test the hypothesis that neoantigen delivery by sHDL improves immune processing and anti-tumor immunity of neoantigen peptides.

In Chapter 3, we aim to simplify our formulation process for neoantigen-loaded sHDL through chemical modification of two Colon adenocarcinoma neoantigen peptides using short chain PEG. We study whether the simplified PEGylated formulations retain the anti-tumor immunity of traditional formulations through assaying neoantigen-specific CD8+ T cell expansion and protection from tumor challenge. Through these studies, we can draw conclusions on the clinical translatability of the newly simplified neoantigen-loaded sHDL personalized vaccine platform.

In Chapter 4, we evaluate the therapeutic advantage of co-delivering chemo- and immune-therapeutic entities on sHDL nanodiscs in a murine Colon adenocarcinoma model. We use *in vitro* assays to determine whether docetaxel-loaded sHDL is comparable to free docetaxel regarding tumor cell killing to justify sHDL as a drug

delivery vehicle. We then evaluate the anti-tumor efficacy of docetaxel-sHDL co-loaded with CpG oligonucleotide compared to single therapy docetaxel-sHDL to determine whether combination therapy with an immuno-stimulatory component augments the antitumor efficacy of chemotherapy alone.

Chapter 5 summarizes the findings of all three chapters and provides suggestions for future studies to deepen the knowledge gained. Chapters 2 and 4 have been submitted for publication, and additional studies related to Chapter 3 are ongoing in an effort to publish.

Chapter 2. Personalized vaccination against Glioblastoma multiforme using synthetic high-density lipoprotein nanodiscs

2.1. Abstract

Glioblastoma multiforme (GBM) continues to be the most deadly and untreatable brain malignancy. Cancer immunotherapy is an increasingly attractive treatment option for patients who have been through the trifecta of surgery, radiation, and chemotherapy only to experience tumor recurrence. A precise and sustainable approach to cancer immunotherapy is the delivery of tumor-specific antigens, also known as neoantigens (NeoAgs). However, efficient delivery of NeoAgs to immune activation sites remains a major challenge in this therapeutic approach.

We have developed a synthetic high-density lipoprotein (sHDL) platform for delivery of NeoAgs. sHDL's small size (< 15 nm) and high biocompatibility make sHDL an ideal candidate for lymphatic trafficking[16,111]. Here, we have tailored NeoAg peptide-sHDL vaccine formulations to treat GBM. We show that vaccinating GL261 tumor-bearing mice with sHDL nanodiscs co-loaded with GL261 NeoAg peptides and CpG (a Toll-like receptor 9 agonist) elicits robust NeoAg-specific T cell responses and delays tumor growth. We also show that anti-tumor effects were significantly enhanced when combined with anti-PD-L1 immune checkpoint blockade therapy.

Briefly, blank sHDL nanodiscs were made using DMPC and apo-A1 mimetic peptide 22A[16]. GBM NeoAg peptides were conjugated to DOPE via PDP thiol chemistry and incorporated into sHDL nanodiscs by simple mixing, and cholesterol-modified CpG was added to GBM NeoAg peptide-sHDL. To study therapeutic effect, C57BL/6 mice were inoculated with GL261 cells and vaccinated once weekly via subcutaneous (s.c.) injection at the tail base with NeoAg peptide-sHDL/cho-CpG cocktail, NeoAg peptide + CpG cocktail, or PBS. anti-PD-L1 checkpoint blockade therapy was administered intraperitoneally (i.p.).

We successfully formulated sHDL co-loaded with GBM NeoAgs and cholesterol-CpG with loading efficiencies > 90% for NeoAg peptides and cholesterol-CpG. In our s.c. GL261 tumor model, we found that mice vaccinated with NeoAg peptide-sHDL/cho-CpG cocktail + anti-PD-L1 exhibited significantly slowed tumor growth when compared to the control tumor-bearing mice administered with PBS (day 18, $p < 0.01$). Mice vaccinated with NeoAg peptide-sHDL/cho-CpG cocktail + anti-PD-L1 survived significantly longer than mice treated with NeoAg peptide-sHDL/cho-CpG and NeoAg peptide + CpG +/- anti-PD-L1 and PBS in both flank and orthotopic GL261 tumor models. Both PBMCs and splenocytes isolated from s.c. tumor-bearing mice and PBMCs isolated from orthotopic tumor-bearing mice immunized with NeoAg peptide-sHDL/cho-CpG cocktail group exhibited stronger NeoAg-specific IFN-γ responses compared to mice immunized with NeoAg peptide + CpG + anti-PD-L1 or PBS. Moreover, vaccination with NeoAg peptide-sHDL/cho-CpG cocktail + anti-PD-L1 was able to reverse immunosuppression within the tumor microenvironment in both s.c. and orthotopic GL261 models.

We conclude that NeoAg peptides delivered via sHDL nanodiscs elicit strong T cell responses against GBM NeoAgs and exhibit significant anti-tumor efficacy against GL261 tumors in both s.c. and orthotopic tumor models. Future work will include further optimization of treatment regimens for orthotopic models and in-depth analysis of tumor-infiltrating neoantigen-specific T cells.

2.2. Introduction

Glioblastoma multiforme (GBM) is a devastating stage IV brain cancer that affects less than 5 per 100,000 people each year but has a median survival rate of only 15 months[112]. Currently, the standard-of-care for patients diagnosed with GBM is limited to surgery, radiation, and chemotherapy. This care is likely ineffective due to failure to resect 100% of the tumor and inefficient delivery of chemotherapeutic drugs to the brain. GBM spreads quickly throughout the brain, and the blood-brain barrier is difficult to penetrate given the plethora of transporters policing the brain and forcing foreign molecules back out into the systemic circulation, leading to off-target toxicities. To address these issues, the controlled release implant Gliadel, launched in 1995, can be placed at the site of tumor resection for sustained, long-term release of Carmustine, an alkylating agent, into the brain to attack any residual tumor cells or recurring malignancy. Unfortunately, Gliadel has not significantly improved patients' prognoses, warranting a need for new therapeutic approaches. Immune checkpoint blockade has been employed in several types of cancer as an immunotherapy to reinvigorate the immunogenic response against tumor cells but has not yet been clinically approved for GBM. Clinical trials studying anti-PD-1 and anti-CTLA4 therapies in patients with both primary and recurring GBM are ongoing but have no conclusive results yet[113].

A more specific approach to immunotherapy is to vaccinate patients against their own tumor cells using tumor-specific antigens, or neoantigens. Current neoantigen delivery methods, such as direct injection and oil emulsions, often result in precipitation, accumulation, and sustained inflammation at the injection site with minimal lymphatic drainage and consequential tolerance and deletion of antigen-specific T cells at the injection site. Thus, there is a need for better delivery methods to ensure neoantigen get to the antigen presenting cells [56] in the lymph nodes to elicit the anti-tumor immune response. An ideal neoantigen vaccine system should promote stable and efficient transport of neoantigen peptides to APCs in lymphoid tissues while allowing co-localized delivery of both antigens and adjuvant molecules to the same APCs without causing an unwanted inflammatory response. These “nanovaccines” are gaining momentum in cancer immunotherapy as nanoparticles with an optimal size (10-100 nm) for lymphatic trafficking and targeted delivery of antigens to APCs[52].

Endogenous HDL is known to be endocytosed by dendritic cells through the scavenger receptor-B1 (SR-B1) pathway, making the nanostructure a good candidate for carrying neoantigen peptides to target cells. Our lab has previously demonstrated that lipid-conjugated peptides can be successfully inserted into sHDL nanodiscs along with toll-like receptor 9 (TLR9) agonist CpG as an adjuvant and that these nanoformulations traffic effectively to draining lymph nodes. Here, we tailored previous methods for peptide loading into sHDL to newly discovered murine GBM neoantigen peptides in order to develop a nanoformulation for vaccinating against GBM in tumor-bearing mice.

2.3. Materials & Methods

2.3.1. Selection of neoantigen peptides

Neoantigen peptide sequences chosen from an immunogenomics study on murine glioblastoma models published in 2016 were computationally screened for predicted MHC reactivity using the artificial neural network (ANN) method tool before selection for formulation [104]. Six out of ten neoantigen peptides identified in the study were synthesized (RS Synthesis) and screened for *in vivo* immunogenicity according to the results from predicted MHC binding affinities produced by the Immune Epitope Database and Analysis Resource (Table 2-1).

2.3.2. Design of screening study

Female C57BL/6 mice, aged 6-7 weeks, were shaved and inoculated with 1.2 x 10^6 GL261 cells subcutaneously (s.c.) in the flank. On days 4 and 11 after inoculation, 50 μg of each neoantigen peptide (n = 4) was co-administered with two strong adjuvants, anti-CD40 (50 μg) and toll-like receptor 3 (TLR3) agonist Polyinosine-polycytidylic acid (polyIC) (100 μg), intraperitoneally (i.p.) to amplify the immune responses to highly immunogenic peptides. Anti-CD40 is an agonistic monoclonal antibody for CD40 present on DCs and promotes ligation with CD40 ligand [114] on T cells. The interaction between CD40 and CD40L enhances DC survival, cytokine release, and upregulation of costimulatory receptors like CD80 and CD86 as well as MHC class I and II molecules to induce DC maturation. The interaction also stimulates CD4+ T cells themselves and can prime cytotoxic T lymphocytes via DCs[114]. PolyIC is an agonist for TLR3 present on DCs to promote immunostimulatory cytokine release. The top peptide candidate was also incorporated into sHDL nanodiscs to test the

immunogenicity of the complete nanovaccine. The formulation details are explained in the next section. On day 26, all mice were euthanized for spleen extraction and Interferon-γ (IFN-γ) ELISPOT analysis to evaluate and compare the immunogenicity of the neoantigen peptide candidates.

2.3.3. Formulation and characterization of neoantigen peptide-loaded sHDL nanodiscs

sHDL nanodiscs were prepared by dissolving 1,2-dimyristoyl-sn-glycero-3-phosphocholine (DMPC, NOF America Corporation) and 22A Apolipoprotein-A1 mimetic peptide (GenScript) in acetic acid, lyophilizing the mixture, and rehydrating the mixture in 10 mM sodium phosphate buffer followed by thermocycling to form ~10 nm nanodiscs spontaneously. The DMPC phospholipid enabled formation of a lipid bilayer while the 22A peptide wrapped itself around the bilayer to mimic an endogenous HDL particle. Nanodisc size was confirmed by dynamic light scattering (DLS) analysis. For neoantigen peptide incorporation, the peptides were modified with a cysteine-serine-serine sequence at the N-terminus for facile conjugation to thiol-modified lipids. Modified peptides were mixed with a pyridiyl disulfide-modified neutral lipid, 1,2-dioleoyl-sn-glycero-3-phosphoethanolamine-N-[3-(2-pyridyldithio)propionate] (DOPE-PDP, Avanti Polar Lipids), in dimethylformamide (DMF) for 2-3 hours on an orbital shaker to form a lipid-peptide conjugate through thiol chemistry. The conjugate was lyophilized to remove DMF and rehydrated in dimethylsulfoxide (DMSO). Before adding the conjugate to the sHDL solution, the sHDL solution's pH was adjusted according to the peptide's predicted isoelectric point (pI) with either hydrochloric acid (HCl) or ammonium hydroxide (NH4OH) to ensure complete peptide solubility. The full mixture was

incubated on an orbital shaker at 200 rpm for 1 hour. Cholesterol-modified CpG1826 (cho-CpG, Integrated DNA Technologies), a TLR9 agonist, was incorporated into peptide-loaded nanodiscs as an adjuvant by simple mixing at a DMPC:cho-CpG weight ratio of 50:1. All formulations were analyzed by DLS for size, by UPLC/MS and HPLC to confirm lipid-peptide conjugation and conjugate incorporation into nanodiscs, and by GPC to confirm cho-CpG loading. A Malvern Zetasizer was used for size and zeta potential analysis (Nanotechnicum, University of Michigan). HPLC was performed using a Thermo Scientific™ BioBasic™ Phenyl HPLC Column. UPLC/MS was performed using either an Acquity UPLC® BEH HILIC 1.7 μm 2.1 x 50 mm column or an Acquity UPLC® BEH300 C4 1.7 μm 2.1 x 150 mm column. GPC was performed using a TSKgel G3000SWxl column from Tosoh Bioscience.

2.3.4. Treatment regimens for *in vivo* studies using subcutaneous GL261 tumor models

For the screening study, female C57BL/6 mice, aged 6-7 weeks, were shaved and inoculated with 1 x 10^6 GL261 cells subcutaneously (s.c.) in the flank. On days 4 and 11 after inoculation, 50 μg of each neoantigen peptide (n = 4) was co-administered with two strong adjuvants, anti-CD40 (50 μg) and toll-like receptor 3 (TLR3) agonist Polyinosine-polycytidylic acid (polyIC) (100 μg), intraperitoneally (i.p.) to amplify the immune responses to highly immunogenic peptides. The predicted top peptide candidate, AALLNKYLA, was also incorporated into sHDL nanodiscs to test the immunogenicity of the complete nanovaccine. On day 26, all mice were euthanized for spleen extraction and Interferon-γ (IFN-γ) ELISPOT analysis to evaluate and compare the immunogenicity of the neoantigen peptide candidates.

For therapeutic vaccination studies, immunocompetent female C57BL/6 mice were inoculated with 1.2 x 10^6 GL261 cells s.c. in the flank. When tumors were palpable 8 days after inoculation, mice were administered s.c. at the tail base with neoantigen peptide-sHDL/CpG cocktail, soluble neoantigen peptide cocktail + CpG, or PBS. Half of the mice received anti-PD-L1 i.p. at days 1 and 4 after vaccination. A prime-boost regimen was followed with vaccinations 7 days apart. Peptides were dosed at 15 μg each, CpG was dosed at 15 μg, and anti-PD-L1 was dosed at 100 μg (Figure 2-5). Five treatment groups were analyzed (n = 14), two of which represented combination immunotherapy regimens with checkpoint inhibitor anti-PD-L1: neoantigen peptide-sHDL/CpG cocktail (+/-) anti-PD-L1, soluble neoantigen peptide cocktail + CpG (+/-) anti-PD-L1, and PBS. Anti-PD-L1 was chosen as the checkpoint blockade antibody for combination immunotherapy groups because PD-L1 is known to be highly expressed on the majority of glioblastoma cells [115]. Mice were euthanized when tumors reached 1.5 cm in diameter. Long-term survivors that exhibited complete tumor regression were rechallenged on the contralateral flank with 1 x 10^6 GL261 cells.

2.3.5. IFN-γ ELISPOT assay of splenocytes and PBMCs

For analysis of splenocytes, mice were euthanized 15 days after the boost vaccination in the neoantigen screening study and 6 days after the prime vaccination for the therapeutic study. Spleens were excised and processed with ACK lysis buffer (Invitrogen) to remove red blood cells. Splenocytes were washed with PBS, resuspended in RPMI media (Invitrogen) + 10% FBS + 1% Penicillin/Streptomycin, and counted using a hemocytometer. Splenocytes were plated on a 96-well ImmunoSpot plate (Fisher Scientific) that was pre-coated with anti-IFN-γ capture antibody at a cell

density of 0.5 x 10^6 cells per well. Neoantigen peptides were dissolved in water and incubated with PBMCs for 18 hours at 37°C. Culture solutions were then discarded, and spots were enumerated using a mouse IFN-γ ELISPOT reagent kit (Fisher Scientific). An ImmunoSpot analyzer was used to count the number of spots per well (Cancer Center Immunology Core, University of Michigan).

For analysis of PBMCs, blood was taken from the submandibular veins of mice 6 or 7 days after each vaccination and processed with ACK lysis buffer to remove red blood cells. PBMCs were washed with PBS, resuspended in RPMI media (Invitrogen) + 10% FBS + 1% Penicillin/Streptomycin, and counted using a hemocytometer. Neoantigen peptides were dissolved in water and incubated with PBMCs for 18 hours at 37°C. Culture solutions were then discarded, and spots were enumerated using a mouse IFN-γ ELISPOT reagent kit (Fisher Scientific). An ImmunoSpot analyzer was used to count the number of spots per well (Cancer Center Immunology Core, University of Michigan).

2.3.6. Tumor microenvironment analysis of GL261 tumors in s.c. GBM model

Immunocompetent C57BL/6 mice were inoculated with 1.2 x 10^6 GL261 cells s.c. in the flank. Three treatment groups were analyzed, two of which represented combination immunotherapy regimens with checkpoint inhibitor anti-PD-L1: neoantigen peptide-sHDL/CpG cocktail + anti-PD-L1 (n=4) and soluble neoantigen peptide cocktail + CpG + anti-PD-L1 (n=4), and PBS (n=6). Mice were vaccinated when tumor reached 7-9 mm in diameter so that tumors would be large enough to harvest sufficient cells at the point of analysis, and they were given anti-PD-L1 on days 1 and 4 after vaccination as in other studies outlined above. On day 8 after vaccination, mice were euthanized so that tumors could be harvested for fluorescence-activated cell sorting (FACS) analysis

(BioRad Ze5, Flow Cytometry Core, University of Michigan) (Figure 2-13). Tumors were digested into single cell suspensions using a cocktail of DNase I and collagenase. Three different panels were assessed: regulatory T cells, CD8 T cells, and dendritic cells. Both CD8 and dendritic cells were further analyzed for activation markers and phenotypes. Antibodies used for FACS analysis were rat anti-mouse CD16/32 (Fisher Scientific), rat anti-mouse CD8a Brilliant Violet 605 (BD Biosciences), rat anti-mouse CD4 Brilliant Violet 605 (BioLegend), rat anti-mouse FoxP3 PE (BD Biosciences), anti-mouse CD279/PD-1 (BioLegend), rat anti-mouse CD107a APC (BD Biosciences), anti-mouse CD103 APC (BioLegend), rat anti-mouse CD86 PE-Cy7 (BioLegend), anti-mouse CD3 FITC (BioLegend), anti-mouse MHC Class II/I-A/I-E PE (ThermoFisher Scientific), hamster anti-mouse CD69 PE (BD Biosciences), anti-mouse CD11c FITC (BioLegend), and rat anti-mouse CD25 PE-Cy7 (BD Biosciences).

2.3.7. Treatment regimens for *in vivo* studies using orthotopic GL261 tumor models

Immunocompetent female C57BL/6 mice were stereotactically injected with 20,000 GL261 cells into the right striatum using a 22-gauge Hamilton syringe (1 μL over 1 minute) with the following coordinates: +1.00 mm anterior, 2.5 mm lateral, and 3.00 mm deep to establish brain tumors[116]. Three treatment groups were analyzed: neoantigen peptide-sHDL/CpG cocktail + anti-PD-L1, soluble neoantigen peptide cocktail + CpG + anti-PD-L1, and PBS. For the pilot therapeutic study, mice were vaccinated s.c. at the tail base with the nanodisc vaccine or free neoantigen peptides and given anti-PD-L1 i.p. on the same day for 3 vaccinations each one week apart. For the second therapeutic study, mice were vaccinated s.c. at the tail base with the nanodisc vaccine

or free neoantigen peptides for 4 vaccinations each one week apart and given anti-PD-L1 i.p. on the same day as each vaccination plus 1 and 4 days after each vaccination for 12 total doses (Figure 2-17). Long-term survivors in the nanovaccine treatment group were rechallenged by inoculating mice with GL261 cells in the left hemisphere.

2.3.8. Tumor microenvironment analysis of GL261 tumors in orthotopic GBM model

To assess the immune cell population within the GL261 tumor microenvironment in the brain, mice were euthanized two days after the third vaccination, and brains were extracted. Tumor mass was dissected and homogenized using Tenbroeck (Corning) homogenizer in DMEM media containing 10% FBS. Immune cell populations in the tumor microenvironment were enriched with 30%-70% Percoll (GE Lifesciences) density gradient. Live/dead staining was carried out using fixable viability dye (eBioscience). Non-specific antibody binding was blocked with CD16/CD32. Dendritic cells were labeled with CD45, CD11c, and B220 antibodies. Plasmacytoid dendritic cells (pDCs) were identified as $CD45^+/CD11c^+/B220^+$ and conventional dendritic (cDCs) cells were identified as $CD45^+/CD11c^+/B220^-$. Macrophages were labeled with CD45, F4/80, and CD206 antibodies. T cells were labeled with CD45, CD3, CD8 and CD4 antibodies. All antibodies were purchased from BioLegend. M1 macrophages were identified as $CD45^+/ F4/80^+/ CD206^{low}$ and M2 macrophages were identified as $CD45^+/ F4/80^+/ CD206^{high}$. Effector T cells were identified as $CD45^+/ CD3^+/ CD8^+$ and helper T cells were identified as $CD45^+/ CD3^+/ CD4^+$. T cell exhaustion was assessed by staining for anti-PD1. Regulatory T cells (Tregs) were identified as $CD45^+/ CD3^+/ CD4^+/CD25^+$. All stains were carried out for 30min at 4°C with 3X flow buffer washes between live/dead

staining, blocking, surface staining, cell fixation, intracellular staining and data measurement. All flow measurements have been made utilizing with FACSAria flow cytometer (BD Biosciences) and analyzed using Flow Jo version 10 (Treestar).

2.3.9. Statistical analysis

Analyses of ELISPOT, FACS, and tumor growth were executed using one-way ANOVA tests with Tukey's post-hoc analyses for multiple comparisons and two-tailed t-tests for individual group comparisons, all at an alpha level of 0.05. Analyses of survival differences were executed using Kaplan-Meier survival analyses with Log-rank Mantel-Cox tests at an alpha level of 0.05.

2.4. Results & Discussion

2.4.1. Three neoantigens were identified as highly immunogenic through *in vivo* screening.

Three out of six peptides, including the peptide in the sHDL formulation, elicited very strong CD8+ T cell responses as evidenced by high IFN-γ spot counts (**Error! Reference source not found.**). Two H2-D^b-restricted neoantigens, GAIFNGFTL and AALLNKYLA, and one H2-K^b-restricted neoantigen, MSLQFMTL, were so immunogenic that, when incubated with splenocytes, produced enough IFN-γ to reach the maximum readable spots per well (3000). Compared to the remaining three peptides, GAIFNGFTL, AALLNKYLA, and MSLQFMTL were significantly more immunogenic ($p<0.001$). We proceeded with these three peptides for optimization of sHDL formulations.

Table 2-1. GL261 neoantigens identified by Johanns et al.[117] that were screened by us in vivo *to evaluate the immunogenicity of each neoantigen by ELISPOT.*

Amino acid mutation	Neoantigen sequence	Epitope restriction	Predicted MHC affinity [6]	#IFN-γ spots/0.5 x 10^6 splenocytes
mTmem2 K1042N	VMLENGYTI	H-2D^b	4.71	42.875
mRtn2 L405F	GAIFNGFTL	H-2D^b	7.76	3000
mImp3 D81N	AALLNKLYA	H-2D^b	42.8	3000
mNtrk1 H470Q	MSLQFMTL	H-2K^b	4.69	2266.5
mPcdh18 Q1012R	MSSVFRRL	H-2K^b	15.22	36.625
mTtbk1 C450R	RSLRYRRV	H-2K^b	10.44	92.25

2.4.2. Three neoantigens were successfully incorporated into sHDL nanodiscs with optimal size for lymphatic delivery.

Following incorporation of neoantigens AALLNKYLA (GBM1, NeoAg-1), MSLQFMTL (GBM2, NeoAg-2), and GAIFNGFTL (GBM3, NeoAg-3) into sHDL nanodiscs, each formulation was analyzed by DLS to confirm particle size. Indeed, all three neoantigen-loaded sHDL nanodiscs had particle sizes between 9 and 13 nm (Figure 2-2), ideal for lymphatic trafficking following administration. GBM1-sHDL had an overall positive charge of 3.1 mV while GBM2-sHDL and GBM3-sHDL had overall negative charges of -1.81 mV and -3.43 mV, respectively. These zeta potentials reflect the slightly positive and negative charges of the neoantigens alone at neutral pH as

predicted by Innovagen's peptide property calculator[118]. We also analyzed a mixture, or cocktail, of all three neoantigen-loaded sHDL formulations to determine whether the formulations would aggregate—they did not. All three formulations mixed well together with an average particle size of 12.2 nm and zeta potential of -2.33 mV. This simple test allowed us to test the anti-tumor potential of all three neoantigens in one vaccine rather than multiple separate vaccines.

Next, we analyzed each of the three formulations by UPLC/MS and HPLC for conjugation efficiency of peptide to lipid and incorporation of peptide-lipid conjugate into sHDLs. We found that NeoAg-1, NeoAg-2, and NeoAg-3 were all successfully conjugated to DOPE lipid with >99% efficiency as determined by detection of remaining DOPE-PDP and its correlation with a standard curve of DOPE-PDP. For incorporation of the neoantigens, we found that all three peptide-lipid conjugates were successfully inserted into sHDL nanodiscs with >90% incorporation efficiency as determined by remaining conjugate in the formulation after purification and removal of free peptide (Figure 2-3). Finally, we used GPC to assess the incorporation efficiency of cho-CpG into the neoantigen-loaded nanodiscs (NeoAg-Nanodisc) and found >99% incorporation as determined by the absence of free cho-CpG peaks and a leftward shift in retention time in the NeoAg-Nanodisc peaks, indicating an increase in molecular weight to form NeoAg-CpG-Nanodiscs (Figure 2-4).

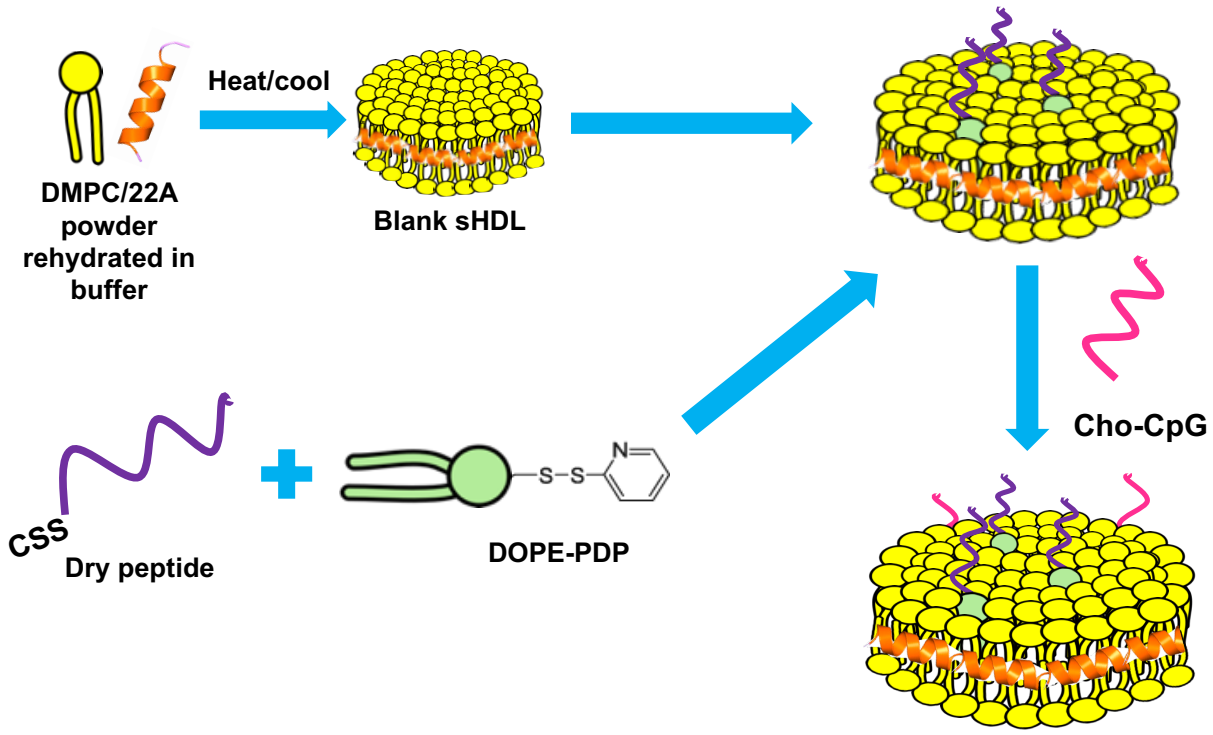

Figure 2-1. Schematic of the formulation process for NeoAg-loaded sHDL nanoparticles.

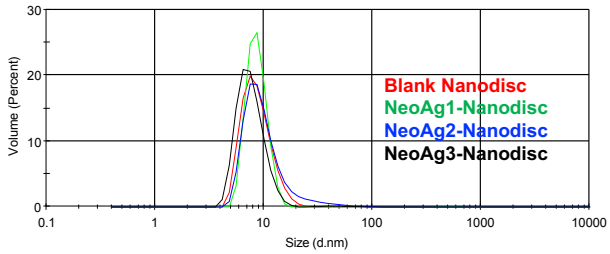

	Size (nm)	Zeta Potential (mV)
Blank Nanodisc	8.9 ± 2.9	-4.8 ± 1.8
NeoAg1-Nanodisc	9.8 ± 1.6	3.1 ± 2.3
NeoAg2-Nanodisc	13.0 ± 4.0	-1.8 ± 3.1
NeoAg3-Nanodisc	13.1 ± 4.1	-3.4 ± 4.2
Mixture of all three	12.2 ± 2.7	-2.3 ± 3.9

Figure 2-2. Representative DLS readings for size of each GBM NeoAg-sHDL formulation and table displaying exact measurements of size and zeta potential for each GBM NeoAg-sHDL formulation.

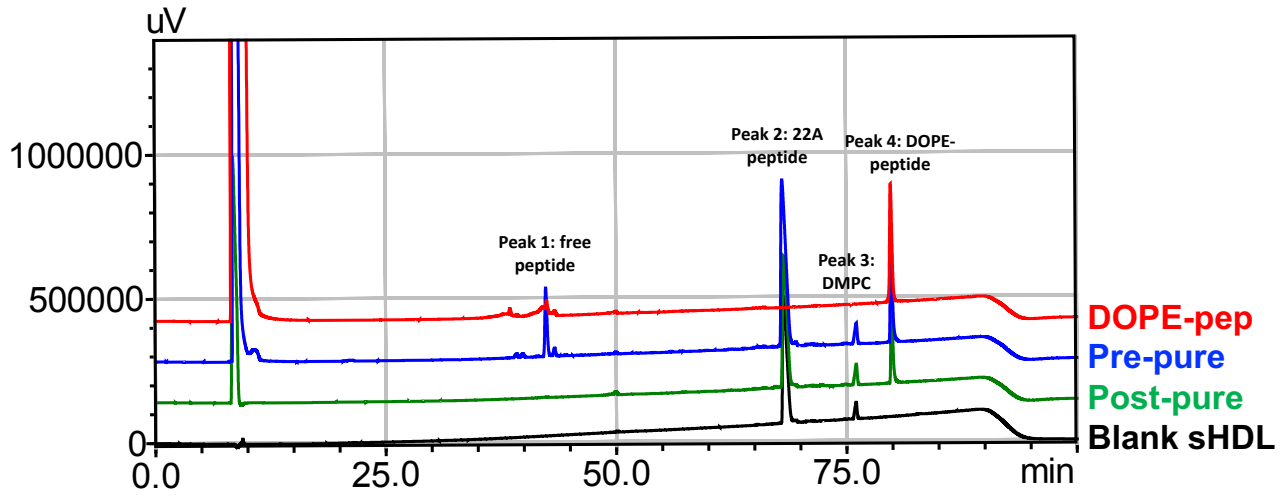

Figure 2-3. Representative HPLC chromatogram set for one GBM NeoAg-sHDL formulation. DOPE-NeoAg lipid-peptide conjugate is shown in red, the pre-purified formulation is shown in blue, the purified formulation is shown in green, and blank sHDL is shown in black.

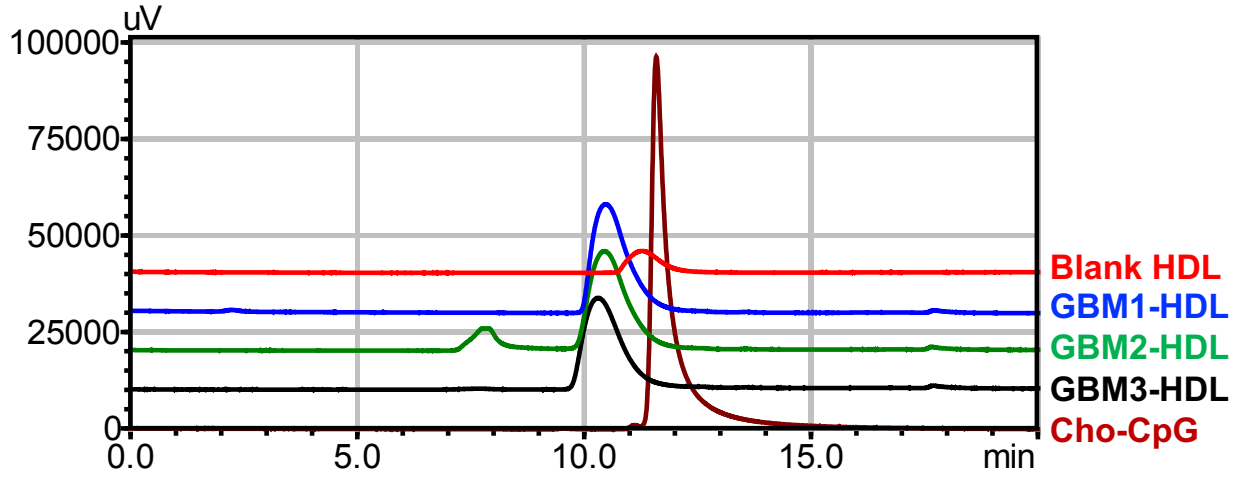

Figure 2-4. GPC chromatogram set for all GBM NeoAg-sHDL formulations after loading adjuvant, cholesterol-modified CpG.

2.4.3. Vaccination with a cocktail of GBM1, GBM2, and GBM3 NeoAgs-CpG-Nanodisc elicits strong anti-tumor effects in s.c. GL261 tumor-bearing mice

2.4.3.1. NeoAg-specific CD8+ T cell frequencies are high in mice vaccinated with NeoAgs-CpG-Nanodiscs

ELISPOT analysis of the peripheral blood showed us that a boost vaccination increased neoantigen-specific CD8+ T cell expansion 2-to-10-fold compared to prime vaccination results in all treatment groups except PBS control, supporting our rationale for using the prime-boost treatment regimen in our initial therapeutic studies (Figure 2-6). Additionally, mice treated with the nanovaccine + anti-PD-L1 exhibited significantly greater frequencies of NeoAg-1- and Neo-Ag-2-specific CD8+ T cells after prime and boost vaccination compared to mice treated with soluble NeoAgs + anti-PD-L1, substantiating the efficacy of sHDL as a nanocarrier for these tumor-specific peptides. While NeoAg-3-specific CD8+ T cell frequencies were objectively greater in mice treated with nanovaccine +/- anti-PD-L1 compared to mice treated with soluble NeoAgs +/- anti-PD-L1, differences were not statistically significant. We believe these results are due to competitive binding to MHC-I between NeoAg-1 and NeoAg-3 because the two neoantigens have the same H-2 restriction, H-2D^{b}, with NeoAg-1 having a higher binding affinity, while NeoAg-2 is H-2K^{b} restricted. H-2, or histocompatibility 2 molecule, is a class I MHC molecule that can be encoded by a variety of genes, including D and K, which have different haplotypes, including haplotype b[119]. This allows for a number of different antigens to be presented on MHC-I molecules, but antigens with the same gene and haplotype restrictions will have to compete for binding to their MHC molecules.

Looking again at the ELISPOT results, we expected the lack of statistically significant differences in neoantigen-specific CD8+ T cell frequencies between mice treated with the nanovaccine + anti-PD-L1 and the nanovaccine alone because anti-PD-L1 only prevents T cell death and does not induce antigen-specific T cells directly. ELISPOT analysis of splenocytes resulted in even more pronounced differences between treatment groups compared to the blood, showing significantly greater frequencies of NeoAg-1-, Neo-Ag-2-, and NeoAg-3-specific CD8+ T cells after just one vaccination in mice treated with the nanovaccine + anti-PD-L1 compared to all other treatment groups except for nanovaccine alone (Figure 2-7). These results indicate that our nanovaccine induces strong systemic anti-tumor immunity, potentiating production of memory T cells and further expansion of neoantigen-specific T cells. Further studies must be done to identify frequencies of memory T cells in mice following treatment with the nanovaccine, but the strong induction of systemic immunity and the resistance of long-term survivors to tumor rechallenge suggest that these memory cells do, in fact, exist.

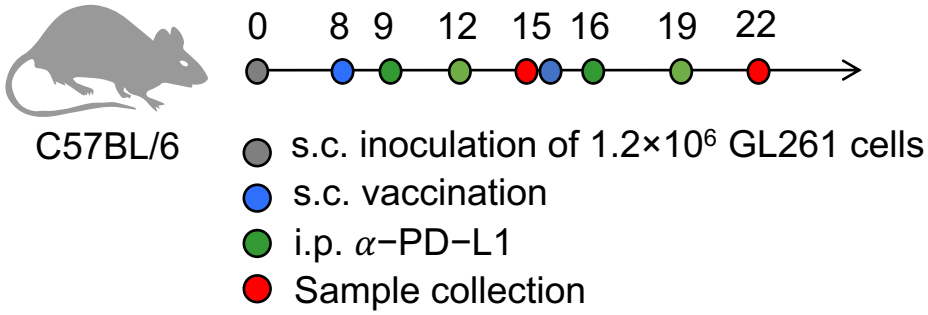

Figure 2-5. Treatment regimen and study timeline for therapeutic vaccination in GL261 s.c. tumor-bearing mice for analysis of vaccine immunogenicity.

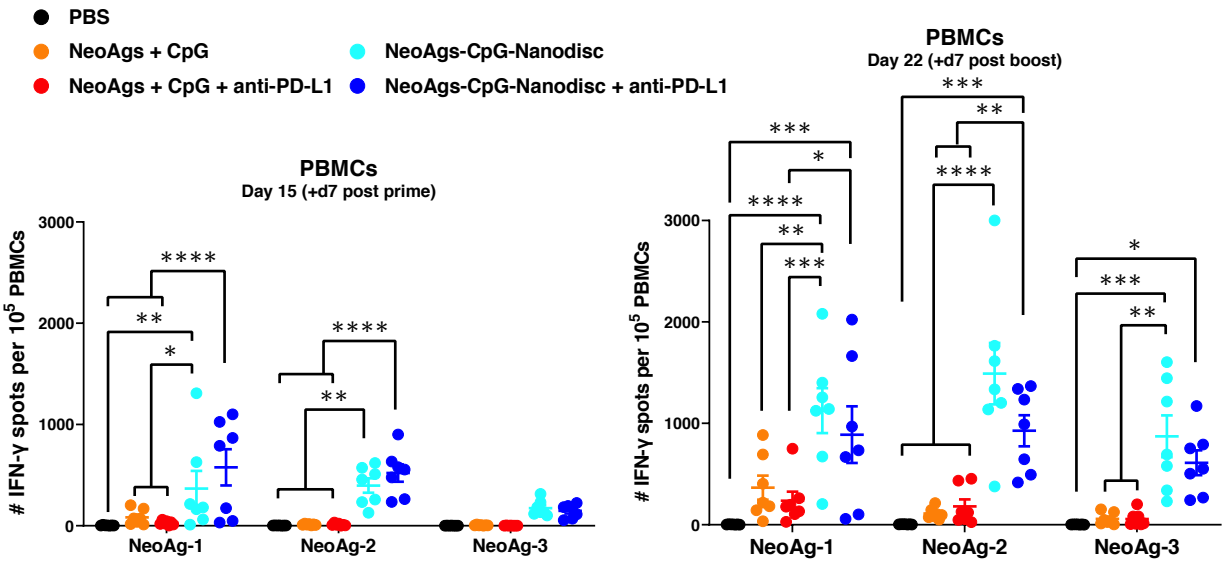

Figure 2-6. IFN-γ ELISPOT of cells in the blood of mice 7 days after prime (left) and boost (right) vaccinations.

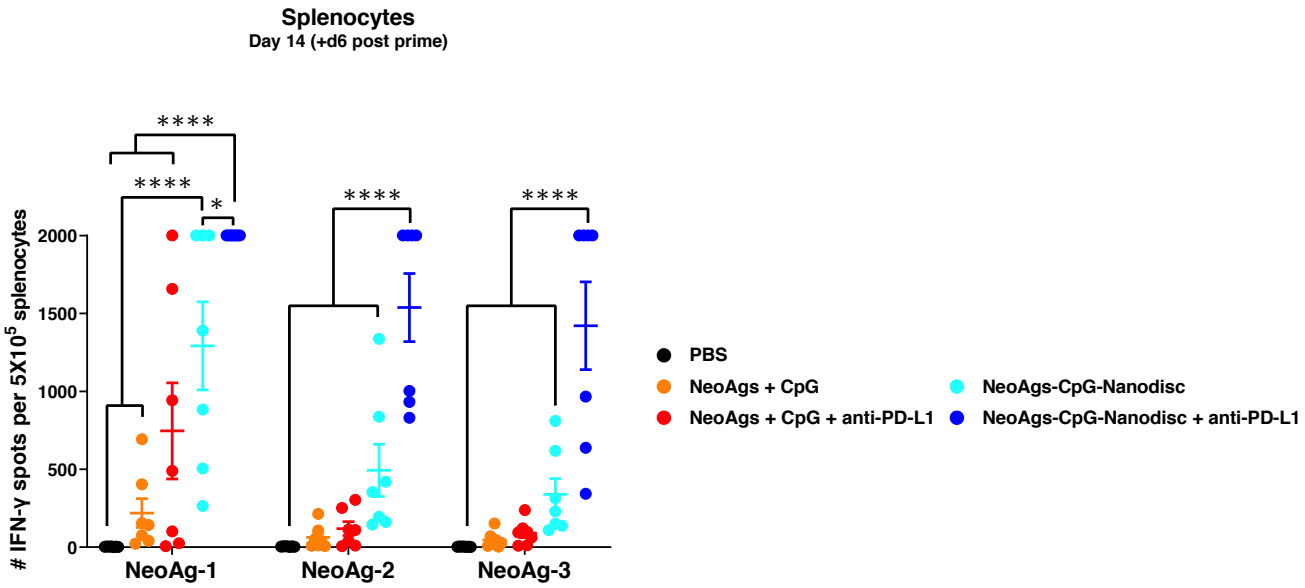

Figure 2-7. IFN-γ ELISPOT of cells in the spleen of mice 6 days after prime vaccinations.

2.4.3.2. NeoAgs-CpG-Nanodiscs + anti-PD-L1 exhibit synergistic tumor growth retardation and survival prolongation

Looking at the effect of each treatment on tumor growth and overall survival, we observed that the nanovaccine in combination with anti-PD-L1 immune checkpoint blockade was superior to all other treatment groups in reducing tumor growth and

prolonging overall survival (Figure 2-9, Figure 2-10, Figure 2-11). At day 18, the day before mice in the PBS control group began reaching the tumor size endpoint, we saw complete tumor regression in all mice treated with the nanovaccine + anti-PD-L1, tumor growth arrest in mice treated with the nanovaccine and soluble neoantigens + anti-PD-L1, and slowed tumor growth in mice treated with soluble neoantigens and anti-PD-L1 alone. As time progressed, one mouse in the nanovaccine + anti-PD-L1 group began regrowing a tumor and eventually reached the tumor size endpoint at day 44 to give the group a complete response rate of 13/14 (Figure 2-10). Mice treated with either nanovaccine alone or anti-PD-L1 alone also experienced impressive tumor regression with 50% complete response rates (7/14), supporting the synergistic anti-tumor potential of combining neoantigen-loaded sHDL with immune checkpoint blockade. Complete response rates for mice treated with the nanovaccine alone (7/14), anti-PD-L1 alone (7/14), soluble neoantigens + anti-PD-L1 (5/14), and soluble neoantigens alone (5/14) were all similar and not significantly different from each other. The Kaplan-Meier analysis of overall survival matches these tumor growth trends, showcasing the synergy between treatment with the nanovaccine and anti-PD-L1 (Figure 2-11).

We observed that combining soluble neoantigen vaccination with immune checkpoint blockade offered no therapeutic advantage over soluble neoantigen vaccination alone. This observation could possibly be explained by antigen-induced tolerance due to substantial antigen deposition at the injection site coupled with poor clearance and prolonged T cell exposure to antigen in the absence of co-stimulation. This may occur because, in the NeoAgs + CpG + anti-PD-L1 treatment group, neoantigens and TLR9 agonist CpG were delivered separately without co-loading on

sHDL. In this setting, CpG could be inefficiently delivered to DCs, resulting in less DC maturation and subsequent stimulation of T cells [16,120-122]. Without DC stimulation via B7 molecular interactions with CD28 in the presence of neoantigen, T cells could become tolerant, downregulating their CD8 expression and converting to an anergic population or undergoing clonal deletion[122]. Treatment with anti-PD-L1 would then be irrelevant without active neoantigen-specific T cell populations to protect from tumor cell-mediated death. Fortunately, co-delivery of neoantigens and CpG adjuvant via sHDL seemed to overcome these potential mechanisms of tolerance as its combination with anti-PD-L1 showed synergistic anti-tumor efficacy.

Of the mice treated with nanovaccine + anti-PD-L1, complete responders were rechallenged with the original dose of tumor cells in the contralateral flank and exhibited no tumor recurrence, suggesting generation of immune memory (Figure 2-12). Researchers have shown that, in mice, memory T cells can be generated as soon as 3 days after initial vaccination and expand dramatically as soon as 1 week after boost vaccination[123,124]. In fact, effector memory T cells, the cells residing in non-lymphoid tissues, are more likely to develop after T cells' second exposure to antigen while central memory T cells residing in lymphoid tissues are more likely develop after T cells' first antigen exposure. Long-term survival of memory T cells, however, is not well understood. Yet, it is clear in our studies that memory cell populations remained active for several weeks after the last vaccination. Additional studies must be done to identify frequencies of memory T cells in mice following treatment with our nanovaccine, but the strong induction of systemic immunity as shown in ELISPOT analyses and the

resistance of long-term survivors to tumor rechallenge suggest that these memory cells do, in fact, exist.

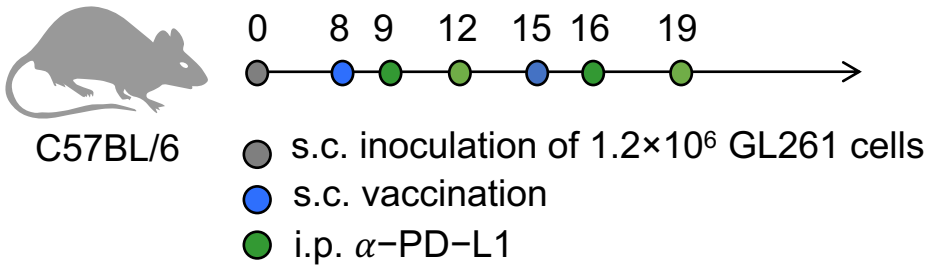

Figure 2-8. Treatment regimen and study timeline for therapeutic vaccination in GL261 s.c. tumor-bearing mice for evaluation of tumor growth and survival.

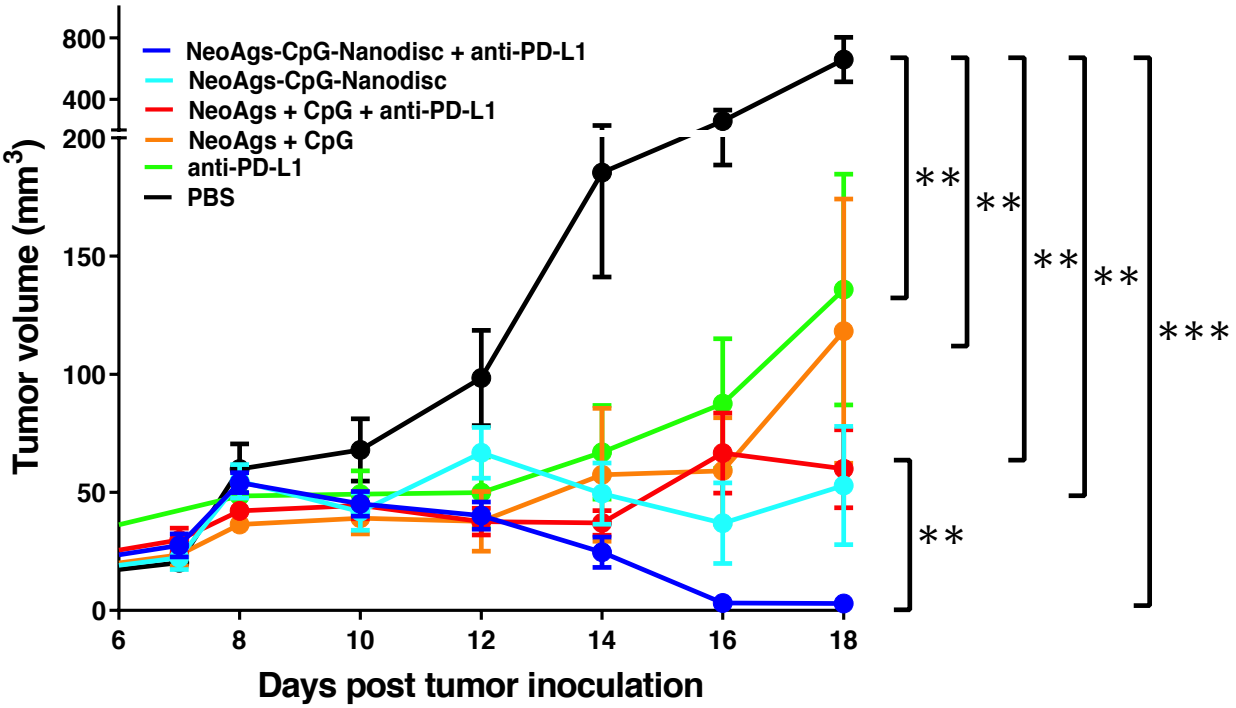

*Figure 2-9. Tumor growth summary for all treatment groups up to day 18. *P<0.05, **P<0.01, ***P<0.001, ****P<0.0001.*

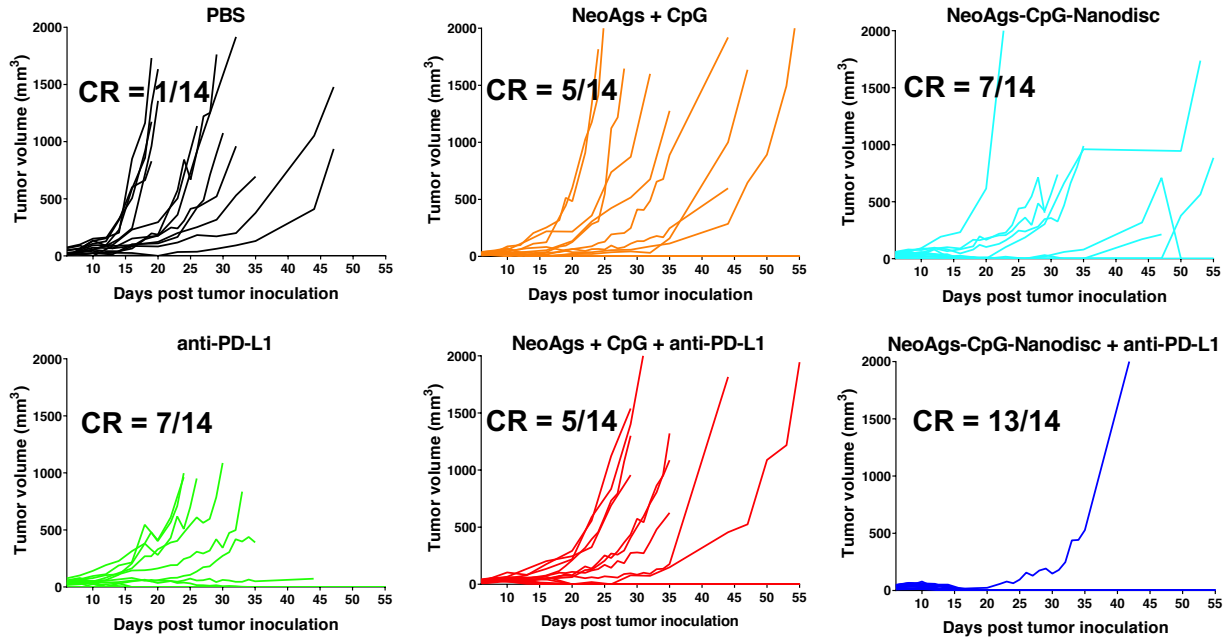

Figure 2-10. Individual tumor growth curves for all animals in the study through the duration of the study.

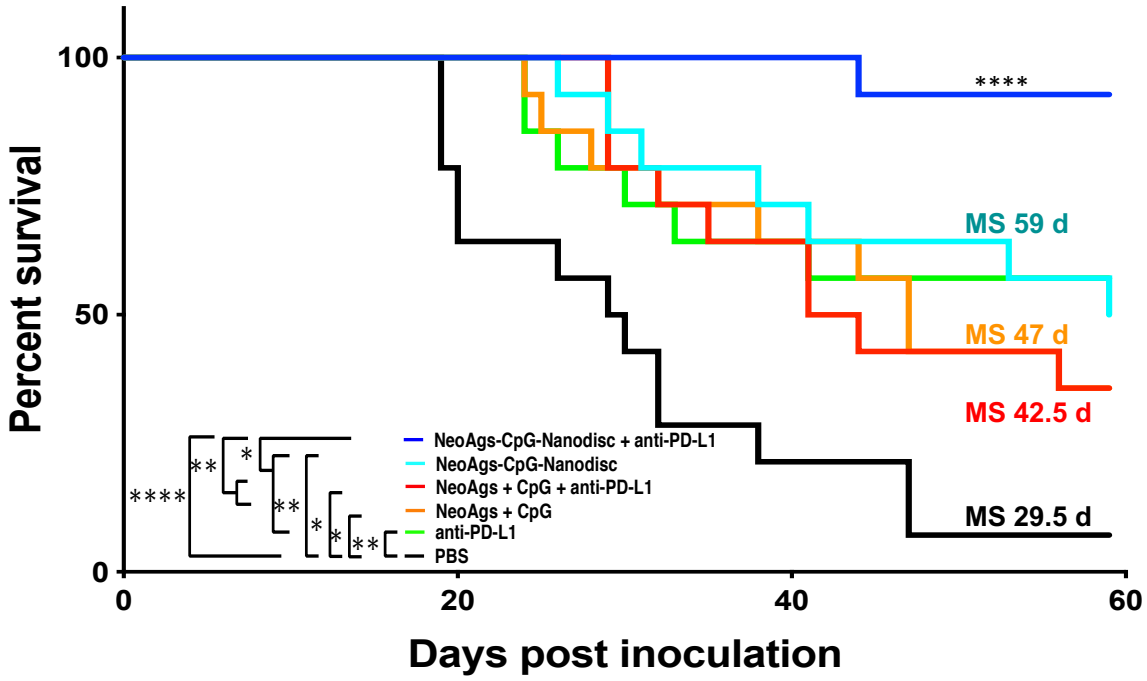

*Figure 2-11. Kaplan-Meier overall survival curve for all treatment groups. *P<0.05, **P<0.01, ***P<0.001, ****P<0.0001. MS = median survival.*

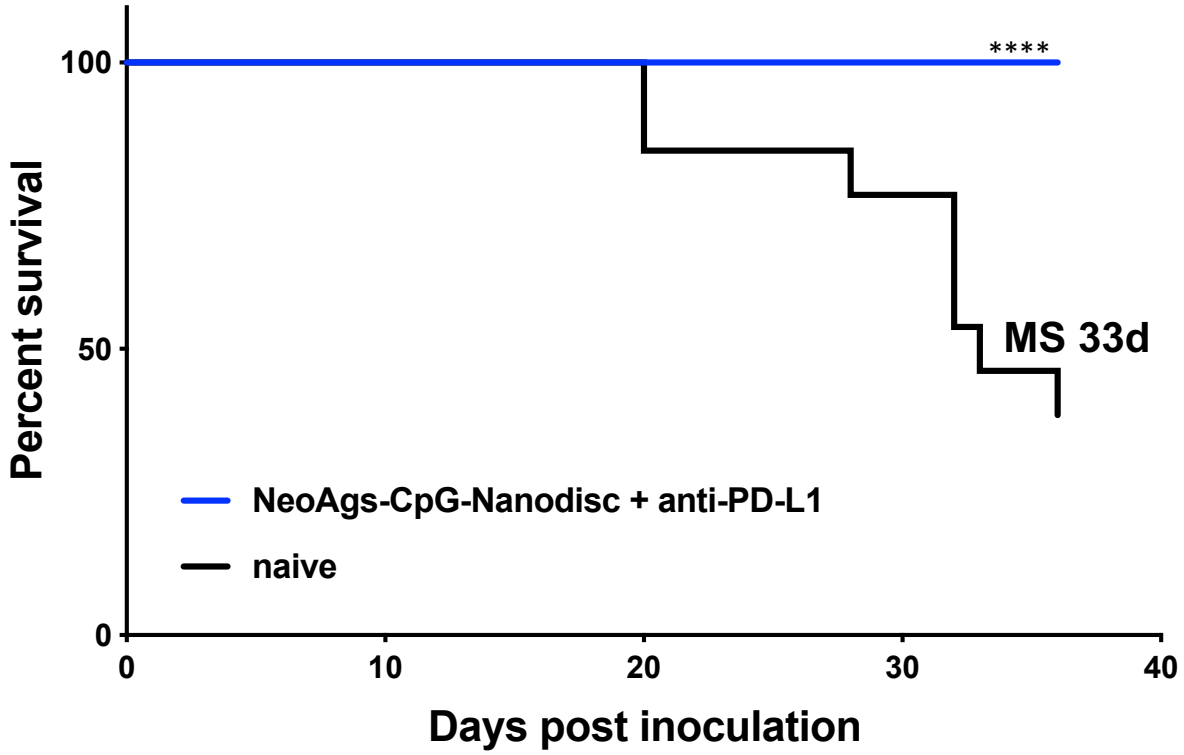

*Figure 2-12. Kaplan-Meier survival curve of rechallenged mice in the NeoAgs-CpG-Nanodisc + anti-PD-L1 treatment group compared to naïve mice inoculated with tumors for the first time. ****P<0.0001. MS = median survival.*

2.4.4. Vaccination with a cocktail of GBM1, GBM2, and GBM3 NeoAgs-CpG-Nanodisc reverses the immunosuppressive tumor microenvironment

We found that the mice treated with neoantigen peptide-loaded nanodiscs recruited significantly more CD8+ T cells ($p < 0.0001$), activated CD107a+ CD8+ T cells ($p < 0.001$), and activated CD86+ dendritic cells ($p < 0.001$) to the tumor site as compared to untreated controls. These mice also exhibited significantly greater intratumoral ratios of CD8+ T cells to FoxP3+ CD4+ Tregs compared to mice vaccinated with soluble neoantigen peptides ($p < 0.05$) and untreated controls ($p < 0.01$). No significant differences in CD4+ T cell or Treg frequencies were observed between groups. PD-1 expression by CD8+ T cells in nanodisc-treated was significantly reduced ($p < 0.01$) compared to untreated control. Though statistically insignificant, soluble

NeoAgs + CpG + anti-PD-L1 vaccination also decreased PD-1 expression by CD8+ T cells compared to untreated control, the difference being about 1.2-fold lower for soluble vaccination versus 1.4-fold lower for nanodisc vaccination. This trend in PD-1 expression could, in part, explain how our nanovaccine in combination with immune checkpoint blockade is so effective. It would also be interesting to evaluate whether CTLA-4 expression by CD8+ T cells, another marker of T cell exhaustion, is also significantly decreased in mice treated with our nanovaccine or whether anti-CTLA-4 vaccination would be needed for such a result[1].

Taken together, these results tell us that treating mice with neoantigen peptide-loaded nanodiscs in combination with anti-PD-L1 significantly shifts the balance between pro-tumor and anti-tumor immunity within the tumor microenvironment away from immunosuppression towards an immunostimulatory environment when compared to treatment with soluble neoantigen peptides in combination with anti-PD-L1. Moreover, the decreased PD-1 expression by CD8+ T cells reduces the probability of tumor-induced T cell death through ligation with PD-L1 on tumor cells, which in turn increases the probability of CD8+ T cell activation and neoantigen-specific tumor cell killing. With one of the cruxes of tumor progression and recurrence being the unchecked immunosuppressive tumor microenvironment, the shift we observed gives our nanovaccine promise for succeeding as a novel, effective treatment that ensures increased tumor-specific CD8+ T cell and activated dendritic cell infiltration and decreased proportions of regulatory T cells. Despite the exciting *in vivo* results we observed in s.c. GL261 tumor models, we know that the model does not serve justice to the complexity of true glioblastomas in the brain. Thus, we proceeded to test our

nanovaccine's efficacy in an orthotopic GBM mouse model to represent a more accurate therapeutic setting.

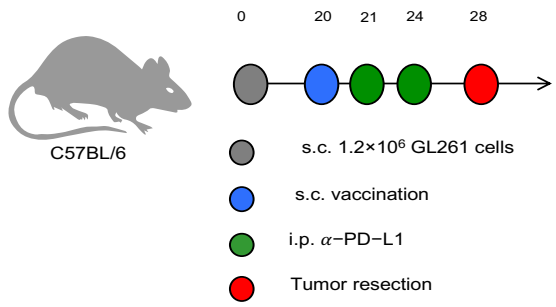

Figure 2-13. Treatment regimen and study timeline for tumor microenvironment analysis of GL261 s.c. tumors.

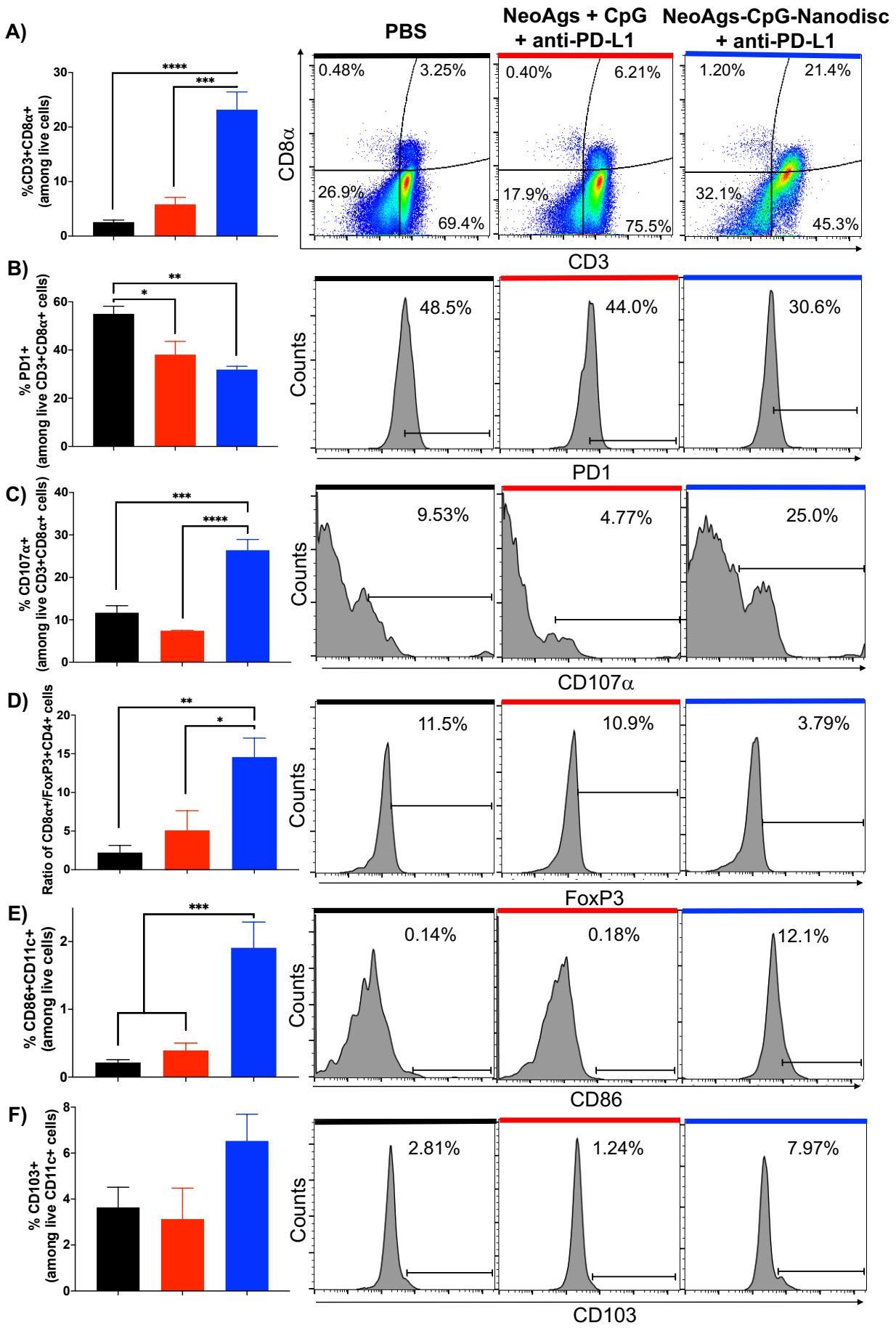
A)
PBS
NeoAgs + CpG + anti-PD-L1
NeoAgs-CpG-Nanodisc + anti-PD-L1
%CD3+CD8α+ (among live cells)
****
***
0.48%
3.25%
26.9%
69.4%
0.40%
6.21%
17.9%
75.5%
1.20%
21.4%
32.1%
45.3%
CD8α
CD3
B)
% PD1+ (among live CD3+CD8α+ cells)
**
*
48.5%
44.0%
30.6%
Counts
PD1
C)
% CD107α+ (among live CD3+CD8α+ cells)
***
****
9.53%
4.77%
25.0%
Counts
CD107α
D)
Ratio of CD8α+/FoxP3+CD4+ cells
**
*
11.5%
10.9%
3.79%
Counts
FoxP3
E)
% CD86+CD11c+ (among live cells)
***
0.14%
0.18%
12.1%
Counts
CD86
F)
% CD103+ (among live CD11c+ cells)
2.81%
1.24%
7.97%
Counts
CD103

*Figure 2-14. Immune activation within the tumor microenvironment after NeoAgs-CpG-Nanodisc plus anti-PD-L1 therapy. A-E) C57BL/6 mice inoculated s.c. with 1.2 X 10^6 GL261 tumor cells were vaccinated on day 20 and administered with anti-PD-L1 on days 21 and 24. Tumor tissues were stained with antibodies and analyzed by flow cytometry for CD8a+ T-cells, Tregs, and DCs.. *P<0.05, **P<0.01, *** P < 0.001, ****P<0.0001.*

2.4.5. Vaccination with a cocktail of GBM1, GBM2, and GBM3 NeoAgs-CpG-Nanodisc prolongs survival in a GL261 orthotopic model

In our pilot study, we observed a significant increase in overall survival in mice treated with our nanovaccine in combination with anti-PD-L1 compared to mice treated with soluble neoantigen peptides in combination with anti-PD-L1 (Figure 2-16) with a ~1.4-fold increase in median survival. We also rechallenged the long-term survivor in the nanovaccine treatment group. After 30 days of observation, the rechallenged mouse did not exhibit any signs of morbidity, suggesting the nanovaccine's elicitation of anti-tumor immune memory. More studies must be done to validate this hypothesis, but we first proceeded to improve overall survival further by adjusting the treatment regimen.

In our second therapeutic study, we observed the same overall survival trends as seen in the pilot study, once again increasing median survival ~1.4-fold when comparing nanovaccine-treated mice to soluble neoantigen-treated mice (Figure 2-18). Also, the long-term survivor was rechallenged as done in the pilot study and again showed no signs of morbidity, suggesting anti-tumor immune memory was induced by our nanovaccine. To investigate the immunogenicity of our nanovaccine in GL261 brain tumor-bearing mice, we also took blood samples from the mice in the survival study to run IFN-$\boldsymbol{\gamma}$ ELISPOT and determine the frequencies of neoantigen-specific CD8+ T cells. We observed 4-to-10-fold higher frequencies of neoantigen-specific CD8+ T cells across all three neoantigens in mice treated with our nanovaccine compared to soluble neoantigen peptides (Figure 2-19), which followed the trends observed in our

subcutaneous GBM mouse model. Significant increases in neoantigen-specific CD8+ T cell frequencies were observed in mice treated with nanodiscs compared to soluble peptides or PBS after the second and third vaccinations (Figure 2-19). Larger differences between groups may be seen if the sample size is increased as the ELISPOT assays included only 4-5 samples per group. Nonetheless, these results mean that our nanovaccine is indeed more effective than soluble neoantigens in the induction of neoantigen-specific CD8+ T cells.

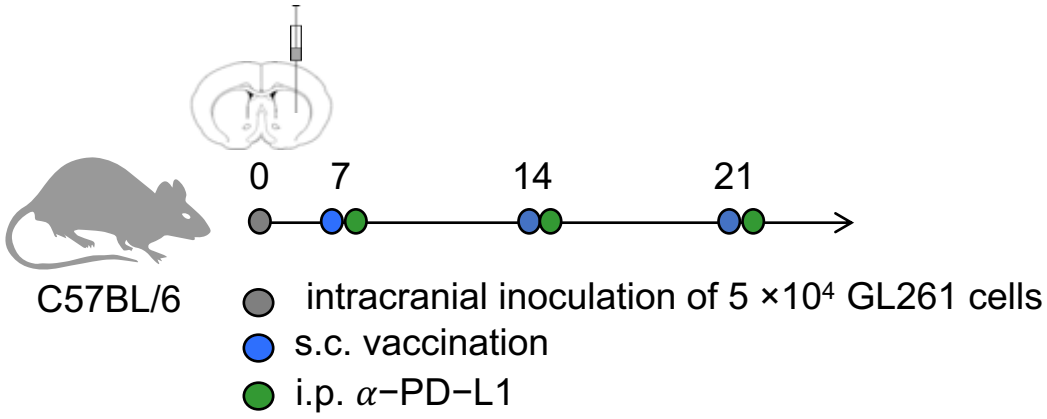

Figure 2-15. Pilot study treatment regimen and study timeline for evaluation of anti-tumor efficacy of GBM NeoAg vaccination on orthotopic GL261 tumor-bearing mice.

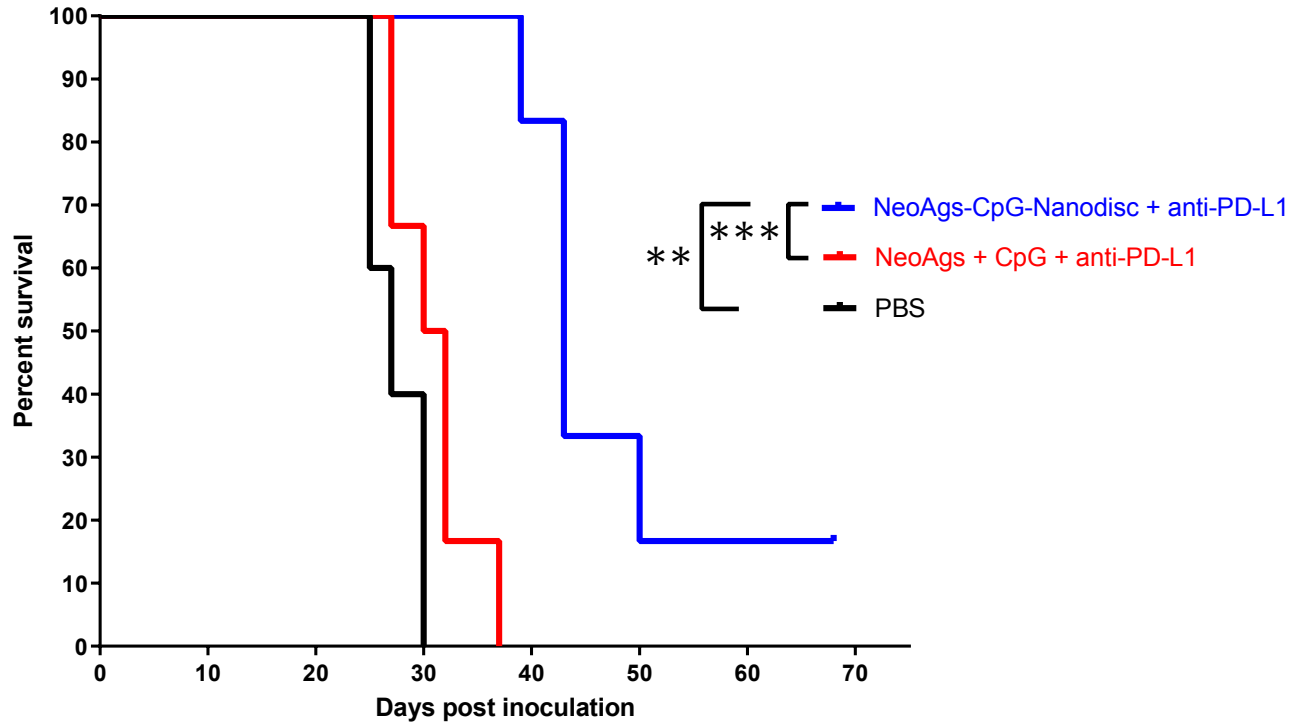

*Figure 2-16. Kaplan-Meier overall survival curve for all treatment groups in pilot therapeutic study. **P<0.01, ***P<0.001.*

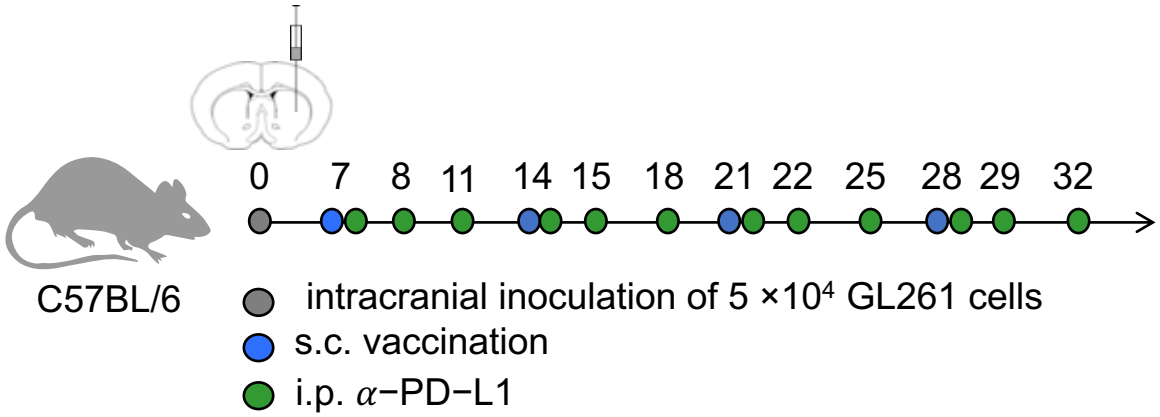

Figure 2-17. Second therapeutic study treatment regimen and study timeline for evaluation of anti-tumor efficacy of GBM NeoAg vaccination on orthotopic GL261 tumor-bearing mice.

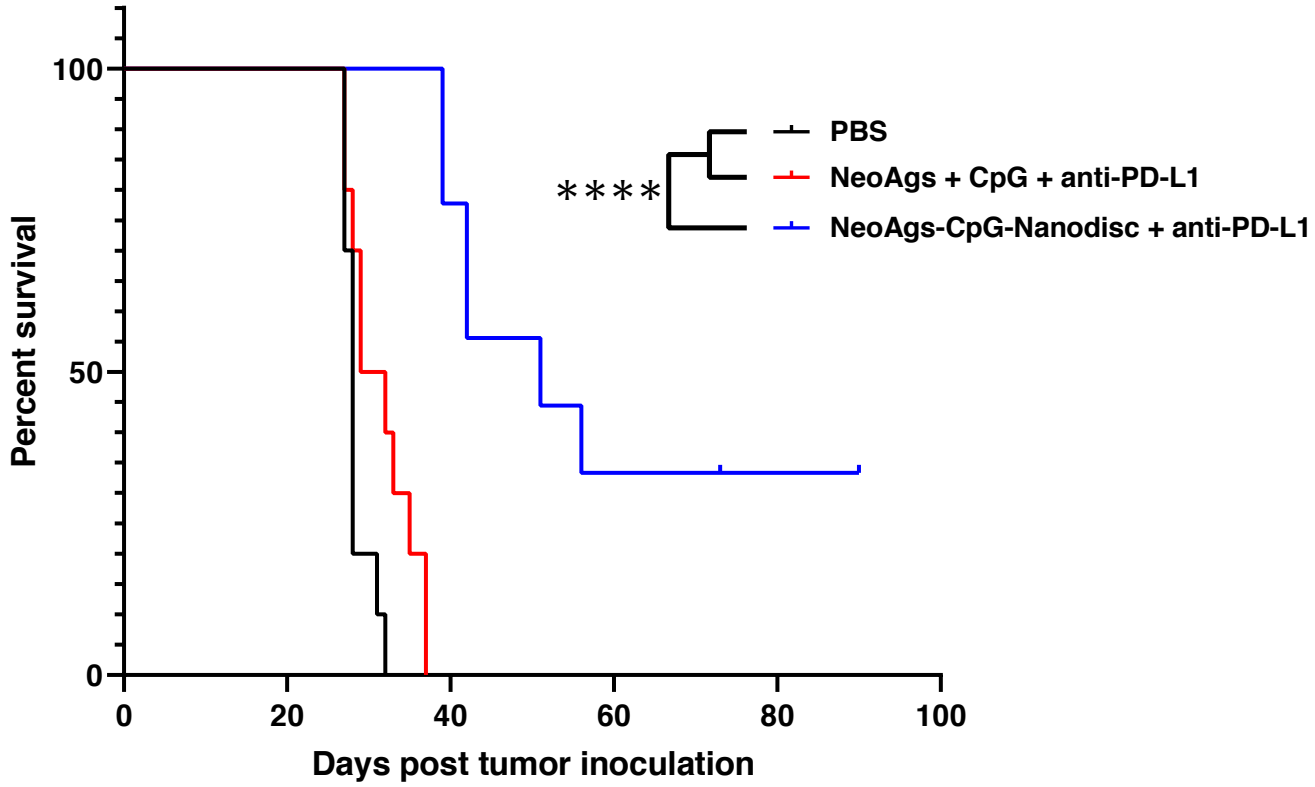

*Figure 2-18. Kaplan-Meier overall survival curve for all treatment groups in second therapeutic study. ****P<0.0001.*

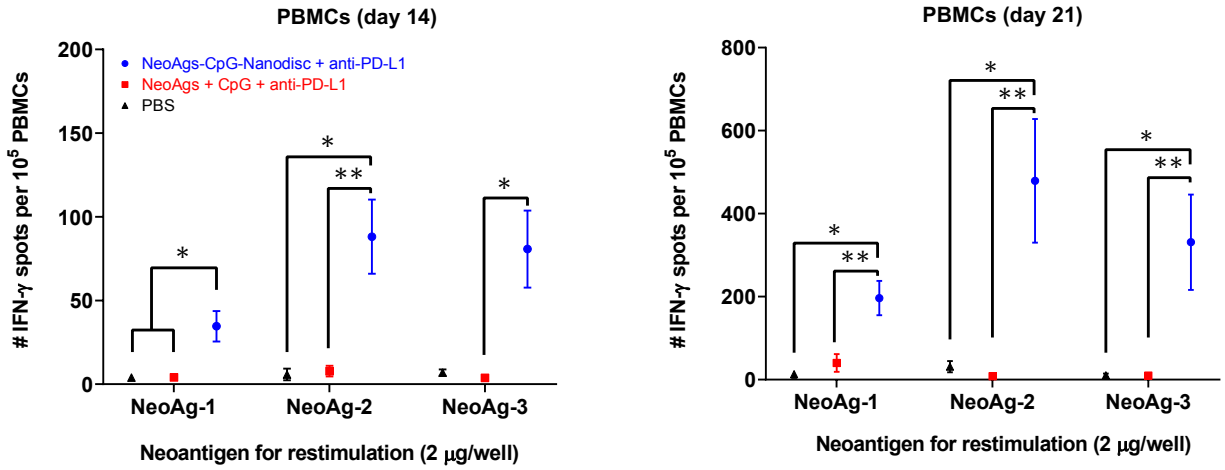

*Figure 2-19. IFN-γ ELISPOT of cells in the blood of GL261 brain tumor-bearing mice 6 days after the second and third vaccinations. *P<0.05, **P<0.01.*

2.4.6. Vaccination with a cocktail of GBM1, GBM2, and GBM3 NeoAgs-CpG-Nanodisc reverses immunosuppression in a GL261 orthotopic model

Analysis of the brain tumor microenvironments of mice vaccinated with NeoAgs-CpG-Nanodisc + anti-PD-L1 revealed significant increases in frequencies of CD8+ T cells ($p<0.0001$) and significant decreases in frequencies of Tregs ($p<0.001$), M1 ($p<0.001$) and M2 ($p<0.01$) macrophages, and PD1+ CD8+ T cells ($p<0.0001$) when compared to untreated controls (Figure 2-20). No differences in CD4+ T cell or activated DC frequencies were observed. Overall, these results were consistent with our tumor microenvironment analysis of subcutaneous flank tumors. The increase in CD8+ T cells and decreases in PD1+ CD8+ T cells and Tregs together indicated a reversal of immunosuppression within the brain tumors of mice treated with our nanovaccine + anti-PD-L1. Additionally, the decreased frequencies of macrophages within the tumors, also known as tumor-associated macrophages (TAMs), of the mice treated with our nanovaccine + anti-PD-L1 could also contribute to the reversal of immunosuppression that is typically induced by TAMs. In the future, more in-depth cytokine analysis of tumor tissue could be conducted to understand fully the mechanisms by which immunosuppression was reversed to improve overall survival of the mice treated with our nanovaccine + anti-PD-L1.

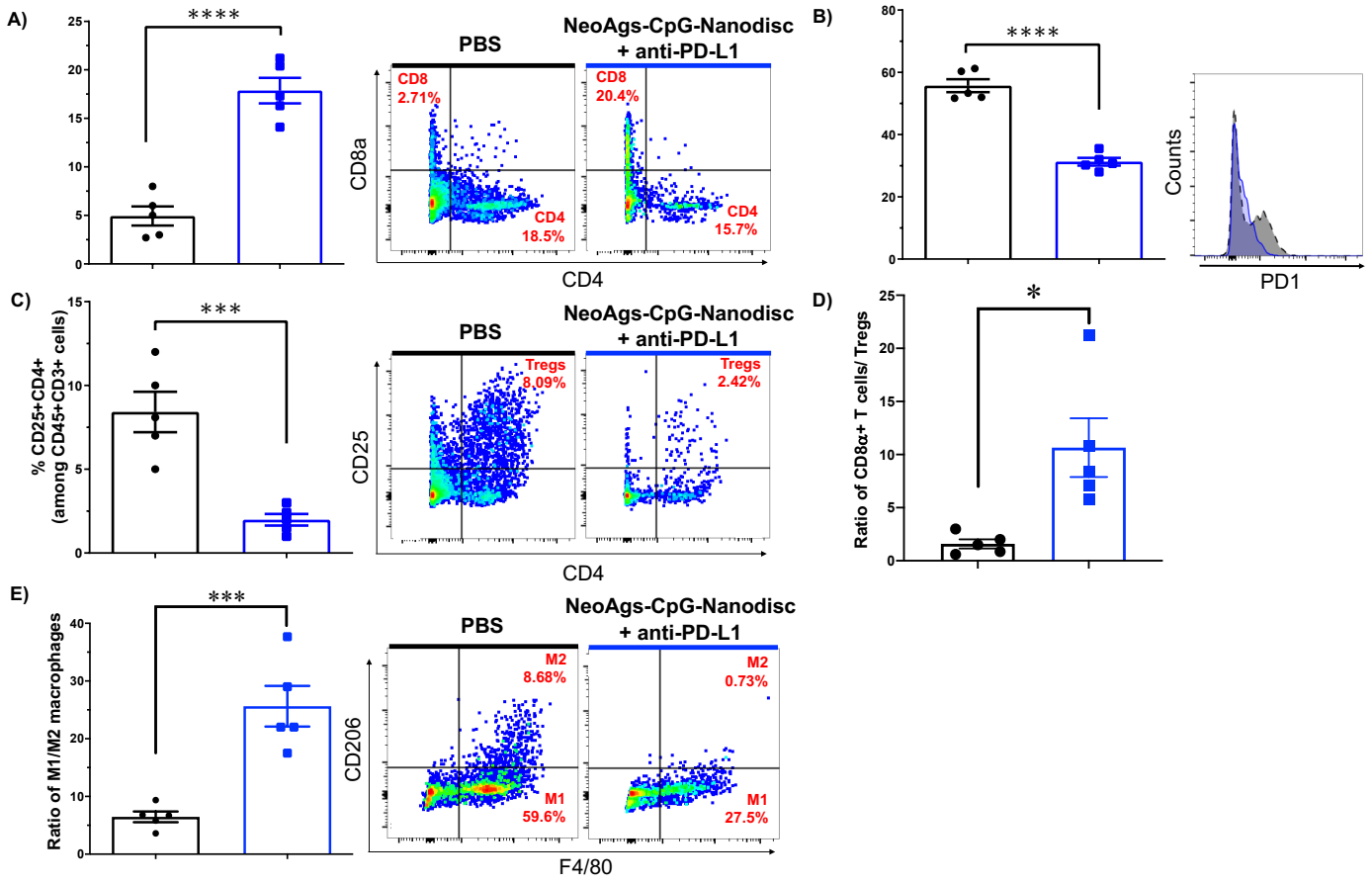

*Figure 2-20. Tumor microenvironment analysis of GBM tumors in CNS. A-E) C57BL/6 mice were inoculated with GL261 cells and treated, and GBM tumors were isolated and analyzed by flow cytometry. Shown are A) CD8a T cells among all T cells, B) PD-1 receptor expression on CD8a+ T cells, C) CD25+CD4+ regulatory T cells, D) ratio of CD8a+ T cells to regulatory T cells, and E) the ratio of M1 (CD206- F4/80+) to M2 (CD206+ F4/80+) macrophages. *P<0.05, ***P<0.001, ****P<0.0001.*

Chapter 3. Optimization of the formulation process for neoantigen-loaded sHDL nanodiscs through alteration of peptide physicochemical properties

3.1. Abstract

The current formulation process for neoantigen-loaded sHDL nanodiscs is complex, involving multiple lyophilization and pH adjustment steps that could result in material loss upon product transfer between vials and excessive titration time, respectively. A simpler formulation process is desirable for clinical translation of this neoantigen delivery platform (Figure 3-1). Methods that can be employed for such formulation simplification include directly conjugating lipid to neoantigen peptide in rehydration solvent to eliminate lyophilization, increasing neoantigen water solubility to reduce the use of organic solvents altogether, and exploiting electrostatic interactions between neoantigen peptides and adjuvant to eliminate the use of lipid anchor altogether.

In this chapter, we employed all of these methods separately to determine whether (1) formulation simplification is feasible and (2) immunogenicity of neoantigen loaded is retained for each method using model MC38 colon adenocarcinoma neoantigen Adpgk.

We found that two methods, directly conjugating lipid to neoantigen peptide in DMSO and increasing neoantigen solubility through PEGylation, worked well to reduce formulation process complexity and completion time while also retaining neoantigen immunogenicity as compared to the traditional formulation method. Proceeding with the PEGylation method, we compared the immunogenicity of second MC38 neoantigen Reps1 along with Adpgk between traditional and PEGylated formulation methods. Again, we found that PEGylated formulations were comparable to traditional formulations for both neoantigens with respect to the generation of neoantigen-specific CD8+ T cells. Taking formulation comparison a step further, we challenged all mice that had been prophylactically vaccinated with each of the formulations with MC38 tumor cells. Between traditional and PEGylated formulations, no significant differences in median survival were observed for either neoantigen, indicating similar anti-tumor protection between traditional and PEGylated formulations.

In full, these studies have revealed that the currently complex neoantigen-loaded sHDL formulation can be simplified by adding a small PEG chain to the end of the neoantigen peptide sequence and that such a modification has no effect on the immunogenicity of the neoantigen itself. The protective anti-tumor immunities of the PEGylated and traditional formulations were comparable for both neoantigens, supporting our hypothesis that simplifying the formulation could make the sHDL platform for neoantigen delivery more clinically translatable while retaining anti-tumor efficacy.

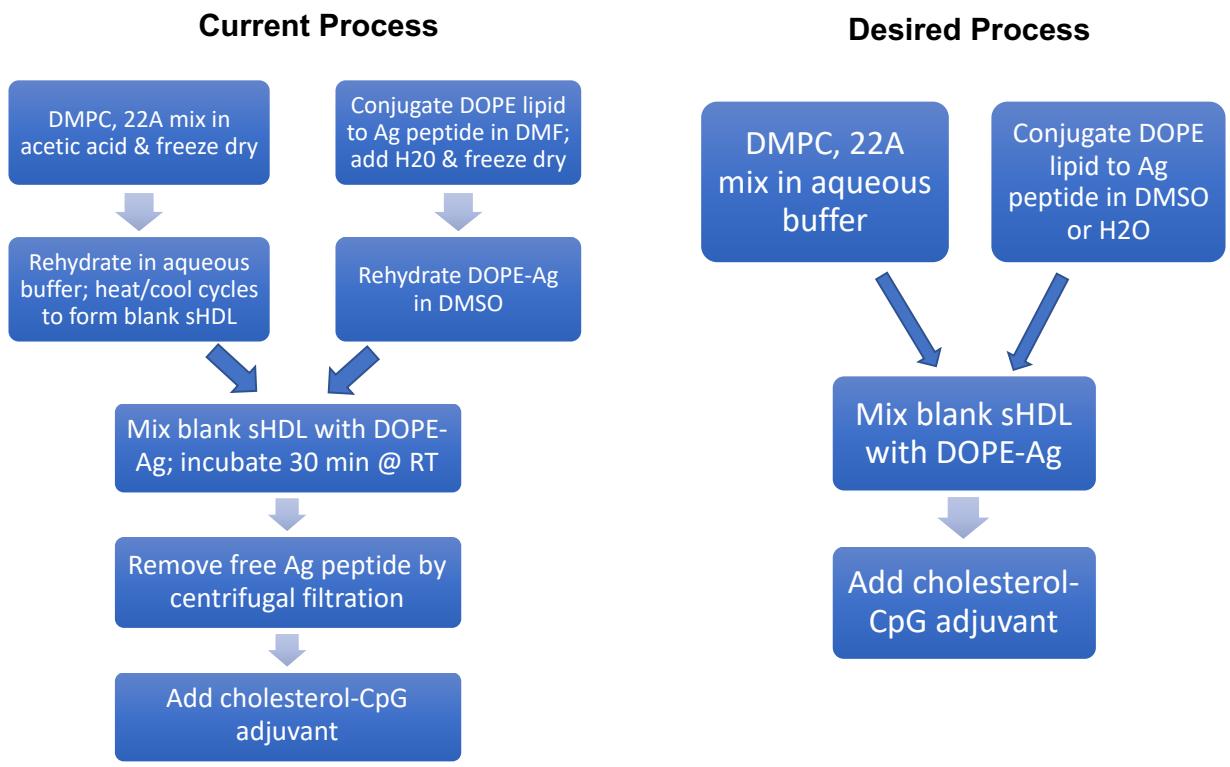

Figure 3-1. Comparative flow charts explaining the current and desired formulation processes for neoantigen-loaded sHDL nanodiscs.

3.2. Introduction

One of the major obstacles of delivering neoantigen peptides is the peptides' solubility, which directly affects the peptides' trafficking and lymphatic delivery. Water-soluble peptides, which have greater proportions of charged residues, are quite easy to deliver because they can be injected with just about any buffering solution that is currently used in clinical settings. Water-insoluble peptides, however, are more common and much more difficult to deliver due to their hydrophobicity and their potential to form micelles, a structure that cannot be incorporated into nanoparticle platforms such as our synthetic HDL nanovaccine platform, or aggregates.

This results in only a minor fraction of the peptide dose reaching the target lymphoid tissues, limiting overall vaccine efficacy. Knowing this, we have modified our process for

neoantigen peptide loading onto synthetic HDL nanoparticles to include lipid conjugation in organic solvents and pH adjustment of the particle solution prior to peptide addition to increase peptide solubility. The full neoantigen peptide-loaded synthetic HDL formulations can usually be worked back to a neutral pH following purification for safe administration of the nanovaccines, but some peptides are more stubborn and require maintenance in strongly acidic or basic conditions. Unfortunately, acidic conditions cause precipitation of our CpG oligonucleotide adjuvants, and basic conditions cause inflammation and abscess formation at the injection site. Moreover, removal of organic solvent from reaction mixtures and rehydration of reaction products combined with product transfer between vials results in some product loss. Taken together, we have learned that we cannot, at this time, classify peptides into categories of one formulation method versus another and need to find a simpler way to streamline the production of neoantigen peptide-loaded synthetic HDLs.

Fortunately, poly(ethylene glycol) has been demonstrated in many drug delivery applications, especially in cancer, to be a solubilizing polymer for hydrophobic drug molecules[125,126-129], likely due to PEG's rearrangement of water molecules through hydrogen bonding. Thus, we hypothesized that 1) functionalizing hydrophobic peptides would increase these peptides' hydrophilicity, enabling simpler loading onto our synthetic HDL nanoparticles in aqueous solutions for more efficient synthesis and reduced material loss. We also hypothesized that 2) the PEGylated peptides would have comparable, if not better, immunogenicity to the original peptide *in vivo*.

Table 3-1. CSS-modified Adpgk (ASMTNMELM) and Reps1 (AQLANDVVL) neoantigen peptide properties predicted by pepcalc.com.

Sequence	total # residues	#charged residues	#ionizable residues	# hydrophobic residues	% hydrophobic	MW	pI (estimated)
CSSASMTNMELM	12	1	2	5	41.67%	1304.54	1
CSSAQLANDVVL	12	1	2	6	50.00%	1219.4	0.69

3.3. Materials & Methods

3.3.1. Materials

HS-(PEG)8-KSSASMTNMELM (PEG8-Adpgk), HS-(PEG)8-KSSAQLANDVVL (PEG8-Reps1), HS-(PEG)4-KSSASMTNMELM (PEG4-Adpgk), and HS-(PEG)4-KSSAQLANDVVL (PEG4-Reps1) were synthesized by and purchased from Genemed Synthesis, Inc. CSSASMTNMELM (Adpgk) and CSSAQLANDVVL (Reps1)) were synthesized by and purchased from RS Synthesis. RRRRRRRRR-CSS-ASMTNMELM (R9-Adpgk) and CSS-ASMTNMELM-RRRRRRRRR (Adpgk-R9) were synthesized by and purchased from RS Synthesis. Apolipoprotein A1 mimetic peptide 22A was synthesized by GenScript. 1,2-Dimyristoyl-sn-glycero-3-phosphocholine (DMPC) was purchased from NOF America. 1,2-dioleoyl-sn-glycero-3-phosphoethanolamine-N-[3-(2-pyridyldithio)propionate] (DOPE-PDP) was purchased from Avanti Polar Lipids. Cholesterol-modified CpG1826 was synthesized by Integrated DNA Technologies.

C57BL/6 female mice, aged 5-6 weeks, were purchased from Jackson Laboratories. MC38 cells were purchased from Kerafast. HPLC was performed using a Thermo Scientific™ BioBasic™ Phenyl HPLC Column. UPLC/MS was performed using either an Acquity UPLC® BEH HILIC 1.7 μm 2.1 x 50 mm column or an Acquity UPLC® BEH300 C4 1.7 μm 2.1 x 150 mm column. GPC was performed using a TSKgel G3000SWxl column from Tosoh Bioscience. Adpgk tetramer was generously provided by NIH.

3.3.2. Formulation of Adpgk-sHDL using different simplification methods

In the traditional formulation, the lipid-peptide conjugate and sHDL were synthesized in parallel processes. DOPE-PDP lipid was reconstituted in DMF, added

directly to Adpgk peptide powder, and reacted for 3 hours at room temperature on an orbital shaker. The reaction mixture was then diluted with ultrapure water, flash frozen, and lyophilized overnight. While sHDL was reconstituted in 10 mM sodium phosphate buffer and thermocycled to form nanodiscs, the dried lipid-peptide conjugate was reconstituted in DMSO at a concentration equivalent to 2 mg/mL DOPE-PDP. Finally, the sHDL solution's pH was adjusted with ammonium hydroxide to a final concentration of 0.075 M ammonium hydroxide to facilitate peptide solubility, and the lipid-peptide DMSO solution was then added to the sHDL solution and allowed to incubate for at least 1 hour at room temperature on an orbital shaker. The final formulation was purified using 10 kDa MWCO centrifugal filters.

In the DMSO formulation, DMF was simply replaced with DMSO, the solvent used to reconstitute the lyophilized lipid-peptide conjugate, to allow for direct conjugation of lipid to peptide in DMSO followed by direct addition of the lipid-peptide solution to sHDL. The purification process remained the same for the DMSO formulation as for the traditional formulation.

In the PEGylated formulation, no organic solvents were used at all. This method could potentially go without purification if the lipid-peptide conjugation was efficient enough at lower peptide-to-lipid molar ratios. Nonetheless, we tested three different lipid-to-peptide molar ratios in the PEGylated formulation process to determine the optimal ratio (Figure 3-4, Figure 3-5, Figure 3-6). For this formulation, DMPC and DOPE-PDP were dissolved in chloroform and combined with 22A dissolved in methanol. The organic solvents in the mixture were evaporated under nitrogen gas, and the dried film was reconstituted in 5 mM sodium phosphate buffer to form sHDL-PDP.

Simultaneously, PEGylated Adpgk was reconstituted in ultrapure water at 2 mg/mL, subsequently added directly to sHDL-PDP, and left to incubate on an orbital shaker for 2 hours at room temperature. The purification process remained the same for the PEGylated formulation as for the traditional formulation.

In the Adpgk-R9 and R9-Adpgk formulations, blank sHDL was made in 10 mM sodium phosphate buffer, and cholesterol-modified CpG1826 (cho-CpG) was inserted into sHDL by simple mixing (CpG-sHDL). Either Adpgk-R9 and R9-Adpgk were then reconstituted in water and mixed with CpG-sHDL at 150 μg/mL peptide and 300 μg/mL cho-CpG, a mass ratio determined to be optimal based on DLS size analysis of particles formed (~10 nm being ideal) using several different mass ratios of peptide to cho-CpG (Figure 3-8, Table 3-2). The formulations were not purified.

Table 3-2. Summary of formulation details for testing different simplification methods for neoantigen-loaded sHDL.

Formulation ID	**Neoantigen modification**	**Simplification method**	**Lyophilization required?**
traditional	CSS	none	yes
DMSO	CSS	direct lipid-peptide conjugation in DMSO, direct addition of conjugate to sHDL	no
PEGylated	HS-PEG(4)-KSS	direct incorporation of peptide into sHDL by pre-inserting DOPE-PDP in sHDL, all aqueous conditions	no
Adpgk-R9	CSS-peptide-RRRRRRRRR	electrostatic complexation of modified peptide with pre-formed CpG-sHDL	no
R9-Adpgk	RRRRRRRRR-CSS-peptide	electrostatic complexation of modified peptide with pre-formed CpG-sHDL	no

3.3.3. Chromatographic analysis of different sHDL formulations

Three different chromatographic analyses were used: HPLC, UPLC/MS, and GPC. For HPLC analysis, samples were diluted in 50/50 methanol/acetonitrile + 0.1% trifluoroacetic acid (TFA) and filtered through PTFE syringe filters. Samples were run in 40 μL volumes on a reverse-phase BioBasic™ phenyl column for 100 minutes at 0.4 mL/min. Peak areas were analyzed at 220 nm. To determine neoantigen peptide-lipid conjugation efficiency, peak areas corresponding to DOPE-PDP (~83 min) were compared between DOPE-PDP alone or sHDL-PDP samples and neoantigen-DOPE or PEGylated neoantigen-sHDL samples. To determine neoantigen loading efficiency, peak areas corresponding to neoantigen-DOPE (various elution times ~78-81 min) were compared between pre-purified and purified samples.

For UPLC/MS analysis, conjugation efficiency was determined using a HILIC column. Samples were run in 5 μL volumes for 5 minutes, and peak areas at 941.81 Da corresponding to DOPE-PDP (MW DOPE-PDP – MW sodium ion + 1) were compared between DOPE-PDP alone and neoantigen-DOPE samples. Incorporation efficiency was determined using a C4 column on which samples were run in 5 μL volumes for 14 minutes. Peak areas corresponding to neoantigen-DOPE conjugates were compared between pre-purified and purified samples. Mass channels for conjugate detection were determined by different fractions of MW neoantigen + MW DOPE lipid + 1 (**Error! Reference source not found.**).

For GPC analysis, incorporation efficiency of cho-CpG or complexation of arginine-tagged neoantigen peptide with CpG was determined by running samples in 30 μL volumes for 20 minutes and comparing the peak areas of either neoantigen-loaded

sHDL samples before and after cho-CpG addition or sHDL/CpG samples before and after arginine-tagged neoantigen peptide. A leftward shift in retention time was also indicative of successful incorporation or complexation due to increased molecular weight.

3.3.4. Justification of model for testing PEGylated-NeoAg-sHDL

To test our hypotheses on PEGylating neoantigen peptides for the simplification of sHDL formulations, we thought it best to choose a well-established neoantigen model--MC38 colon adenocarcinoma. In 2014, Yadav et al. published their impressive findings on neoantigen identification in MC38 and TRAMP-C1 mouse tumors using next generation exome sequencing. MC38 tumors exhibited much greater mutational frequencies than did TRAMP-C1 tumors, and just seven neoepitopes in MC38 tumors were found to bind MHC-I while no TRAMP-C1 neoepitopes were found to do so. Therefore, the study proceeded with closer examination of the MC38 neoepitopes. Out of the seven MHC-I neoepitopes identified, five were predicted to have high MHC-I binding affinities, and two of these five--Adpgk and Reps1--possessed mutated residues between the 3rd and 7th amino acid in their peptide sequences, a location known to be of primary recognition by TCRs[38,130]. Since this publication, myriad research groups have been using Adpgk and Reps1 neoantigens to study and develop precision cancer immunotherapy methods and applications[131]. Moreover, our lab has published several works on cancer immunotherapy using the Adpgk neoantigen[16,90,132].

3.3.5. Prophylactic treatment regimen for comparison of immunogenicity between formulations

Female C57BL/6 mice were vaccinated with each of the formulations (n = 5) subcutaneously at the tail base on a biweekly basis with 15 μg peptide and 15 μg CpG per vaccination (Figure 3-11). Nanodisc formulations were diluted to 0.15 mg/mL NeoAg, including the volume of CpG added, for 100 μL s.c. injections. NeoAg peptides were dissolved in 10 mM sodium phosphate buffer and diluted to 0.15 mg/mL NeoAg, including the volume of CpG added, for 100 μL s.c. injections. Mice were challenged with 1.5 x 10^6 MC38 cells in the right flank 18 days after the last prophylactic vaccination to test the anti-tumor immunity established by prophylactic vaccination.

3.3.6. Statistical analysis

Analyses of ELISPOT, FACS, and tumor growth were executed using one-way ANOVA tests with Tukey's post-hoc analyses for multiple comparisons and two-tailed t-tests for individual group comparisons, all at an alpha level of 0.05. Analyses of survival differences were executed using Kaplan-Meier survival analyses with Log-rank Mantel-Cox tests at an alpha level of 0.05.

3.4. Results & Discussion

3.4.1. Analysis of formulations using multiple methods of simplification with Adpgk neoantigen

We used HPLC to analyze the traditional, DMSO, and PEGylated formulations for conjugation of peptide to lipid and incorporation of the peptide into sHDL (Figure 3-2, Figure 3-3, Figure 3-7). In the HPLC chromatograms, 22A is visible at 68 minutes,

DMPC at 76 minutes, and DOPE-PDP at 83 minutes. We used GPC to analyze the Adpgk-R9 and R9-Adpgk formulations for complexation of the peptides with CpG-sHDL (Figure 3-9, Figure 3-10). In the GPC chromatograms, CpG-sHDL is visible at 8 minutes. We achieved overall neoantigen incorporation efficiencies of 97% for the traditional formulation, 96% for the DMSO formulation, and 90% for the PEGylated formulation. These were calculated by multiplying the lipid-peptide conjugation efficiency, determined by the concentration of DOPE-PDP leftover, by the conjugate retention percentage after purification. We also achieved some successful complexation between Adpgk-R9 or R9-Adpgk and CpG-sHDL as indicated by the leftward shift in retention time of the sHDL nanodiscs following incubation with either one of the polyarginine-functionalized Adpgk peptides. The GPC charts shown are representative of 2 out of the 9 different mass ratios we tested to achieve maximum complexation. The final mass ratio chosen for both Adpgk-R9/CpG-sHDL and R9-Adpgk/CpG-sHDL was 150 μg/mL peptide and 300 μg/mL CpG based on both DLS results showing ~10 nm nanodisc formation and on GPC results showing a decrease in peak area for CpG-sHDL around 8 minutes and an increase in peak area for complexed Adpgk-R9/CpG-sHDL or R9-Adpgk/CpG-sHDL around 5.5 minutes.

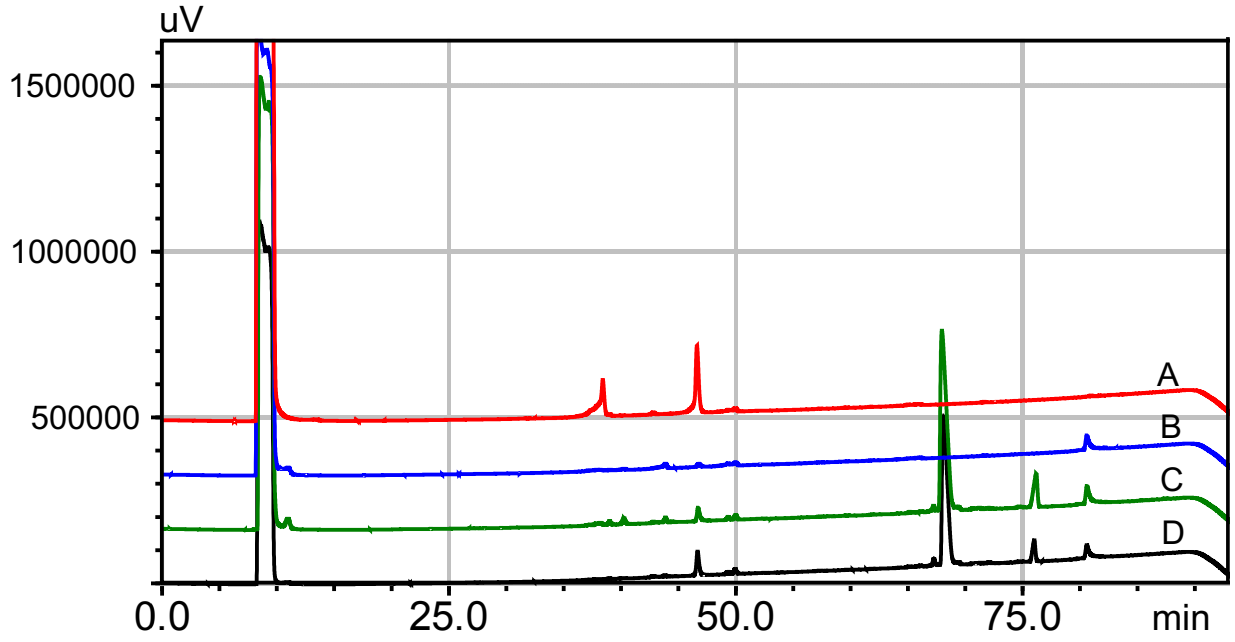

Figure 3-2. HPLC analysis of traditional formulation (λ = 220 nm). (A) free Adpgk peptide (B) DOPE-Adpgk conjugate (C) Adpgk-sHDL before purification (D) Adpgk-sHDL after purification.

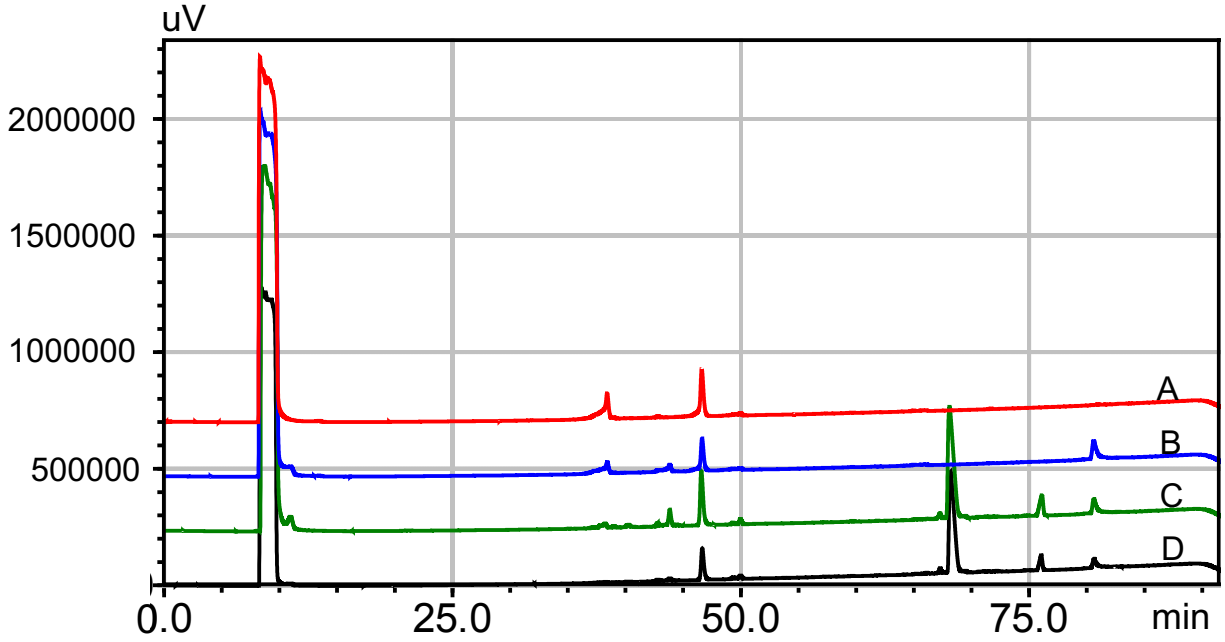

Figure 3-3. HPLC analysis of DMSO formulation (λ = 220 nm). (A) DOPE-PDP (B) free Adpgk peptide (C) Adpgk-sHDL before purification (D) Adpgk-DOPE conjugate.

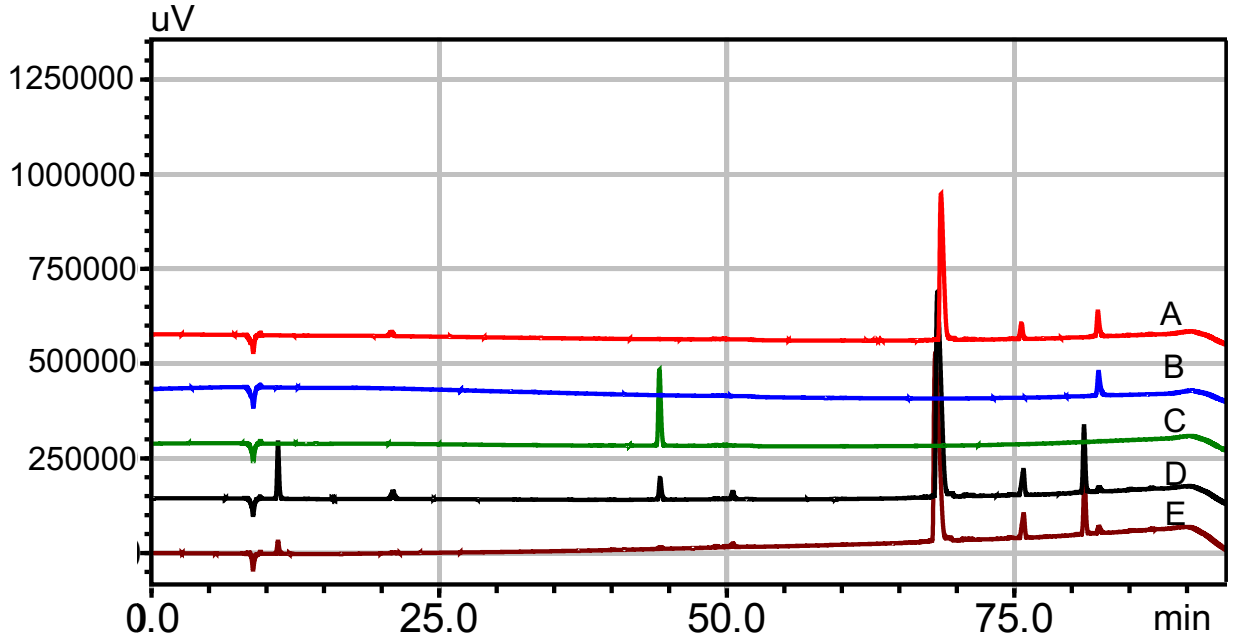

Figure 3-4. HPLC analysis of PEGylated formulation using low molar ratio (1.5:1) of PEG4-Adpgk peptide to DOPE-PDP lipid (λ = 220 nm). (A) sHDL-PDP (B) DOPE-PDP (C) free PEGylated Adpgk peptide (D) PEGylated Adpgk-sHDL before purification (E) PEGylated Adpgk-sHDL after purification.

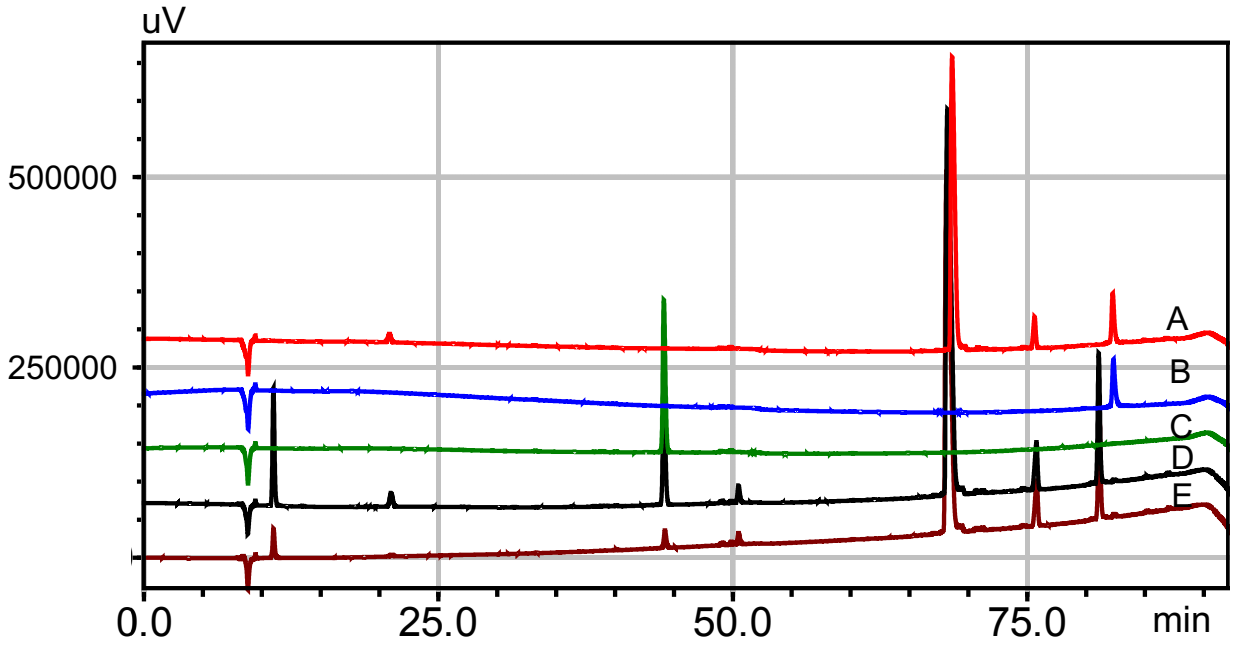

Figure 3-5. HPLC analysis of PEGylated formulation using medium molar ratio (2:1) of PEG4-Adpgk peptide to DOPE-PDP lipid (λ = 220 nm). (A) sHDL-PDP (B) DOPE-PDP (C) free PEGylated Adpgk peptide (D) PEGylated Adpgk-sHDL before purification (E) PEGylated Adpgk-sHDL after purification.

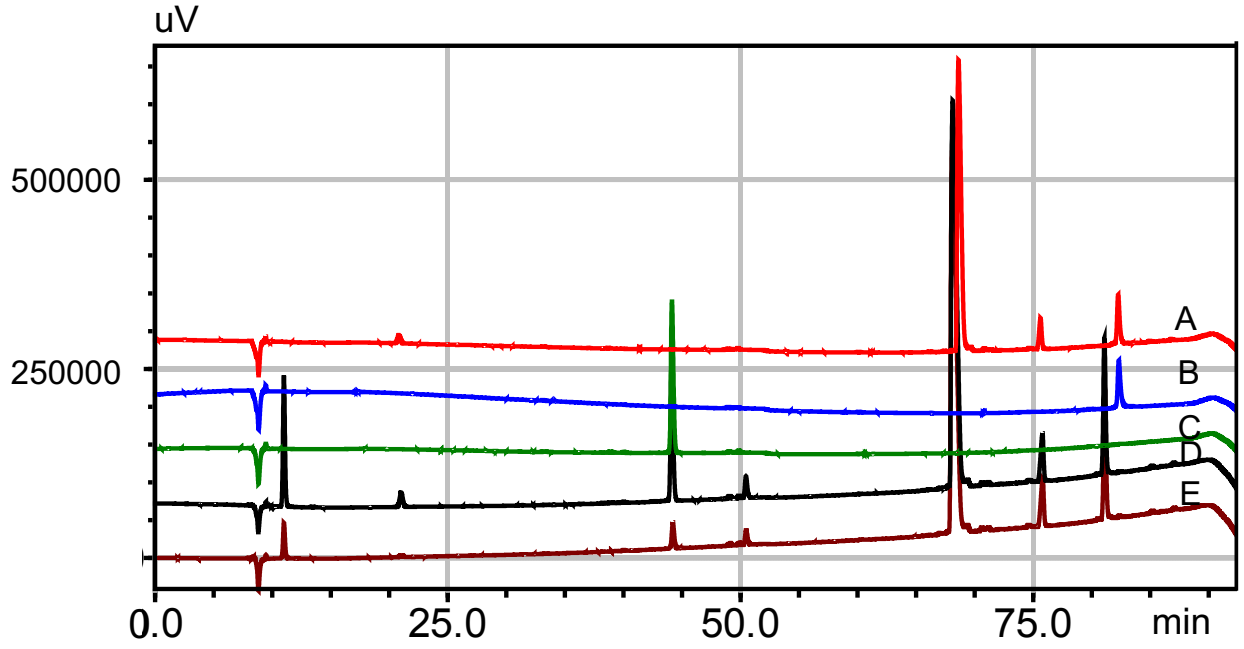

Figure 3-6. HPLC analysis of PEGylated formulation using high molar ratio (2.5:1) of PEG4-Adpgk peptide to DOPE-PDP lipid (λ = 220 nm). (A) sHDL-PDP (B) DOPE-PDP (C) free PEGylated Adpgk peptide (D) PEGylated Adpgk-sHDL before purification (E) PEGylated Adpgk-sHDL after purification.

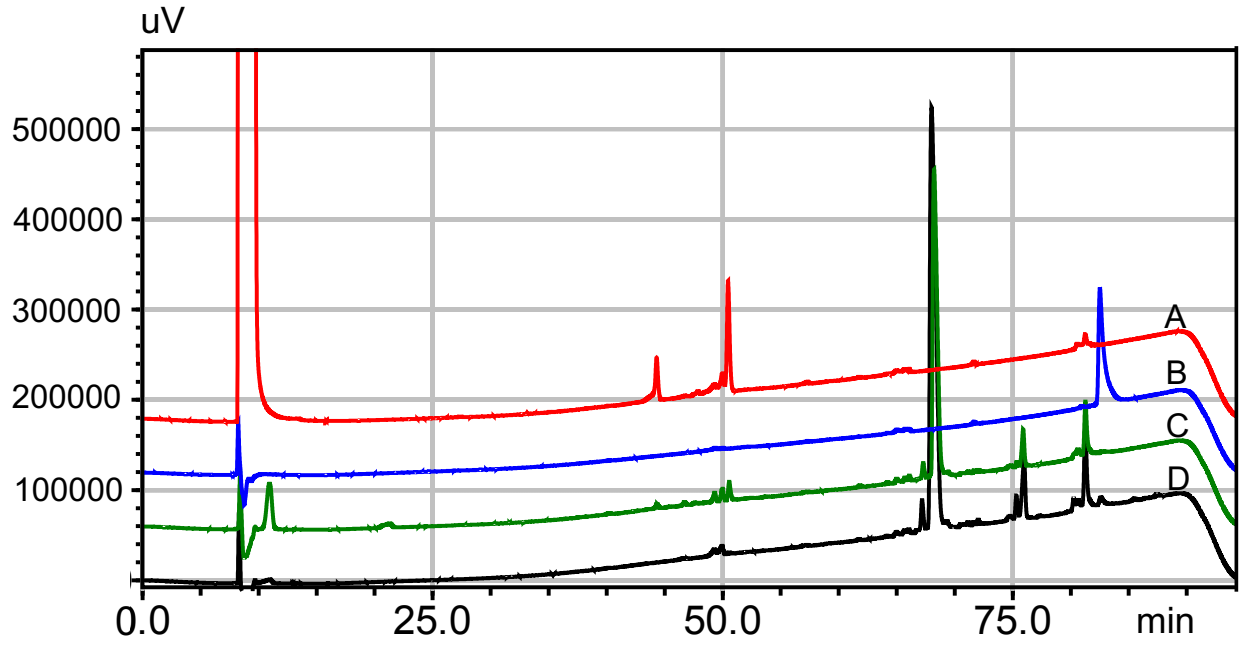

Figure 3-7. HPLC analysis of scaled-up large batch of PEGylated formulation using low molar ratio (1.5:1) of PEG4-Adpgk peptide to DOPE-PDP lipid (λ = 220 nm). (A) free PEGylated Adpgk peptide (B) DOPE-PDP (C) PEGylated Adpgk-sHDL before purification (D) PEGylated Adpgk-sHDL after purification.

Formulation 1: Adpgk-R9 300 μg/mL + CpG-sHDL 150 μg/mL

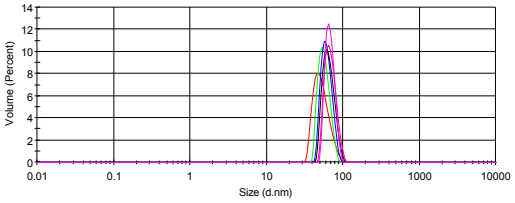

Formulation 2: R9- Adpgk 300 μg/mL + CpG-sHDL 150 μg/mL

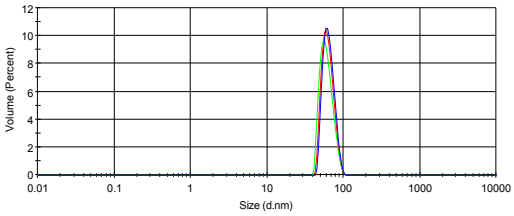

Formulation 3: Adpgk-R9 150 μg/mL + CpG-sHDL 150 μg/mL

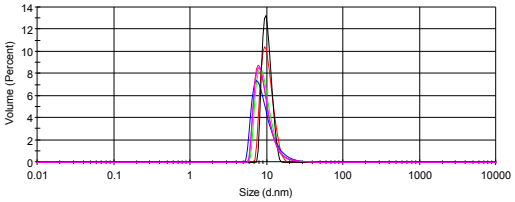

Formulation 4: R9- Adpgk 150 μg/mL + CpG-sHDL 150 μg/mL

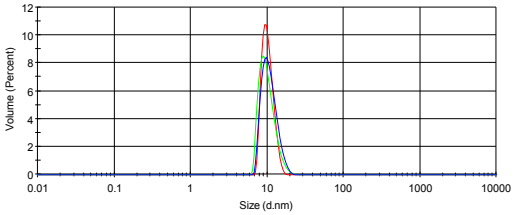

Formulation 5: Adpgk-R9 75 μg/mL + CpG-sHDL 150 μg/mL

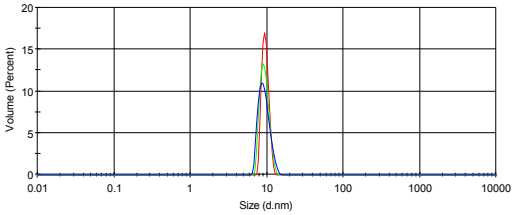

Formulation 6: R9- Adpgk 75 μg/mL + CpG-sHDL 150 μg/mL

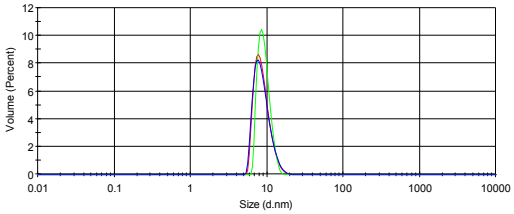

Formulation 7: Adpgk-R9 300 μg/mL + CpG-sHDL 300 μg/mL

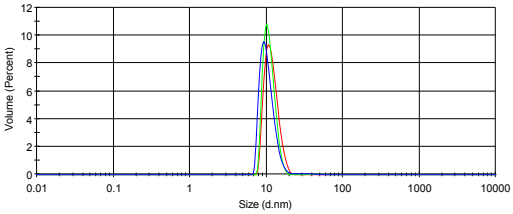

Formulation 8:R9- Adpgk 300 μg/mL + CpG-sHDL 300 μg/mL

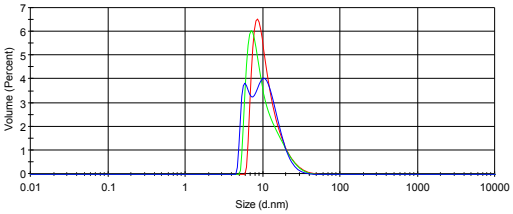

Formulation 9: Adpgk-R9 150 μg/mL + CpG-sHDL 300 μg/mL

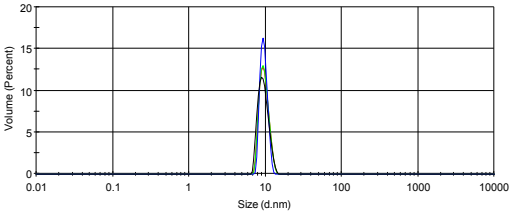

Formulation 10: R9- Adpgk 150 μg/mL + CpG-sHDL 300 μg/mL

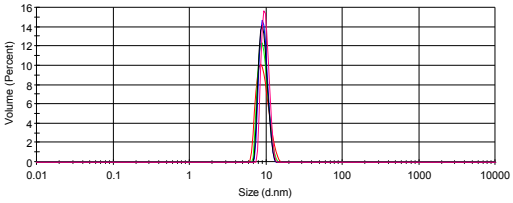

Formulation 11: Adpgk-R9 75 μg/mL + CpG-sHDL 300 μg/mL

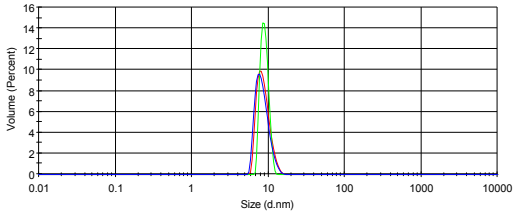

Formulation 12: R9- Adpgk 75 μg/mL + CpG-sHDL 300 μg/mL

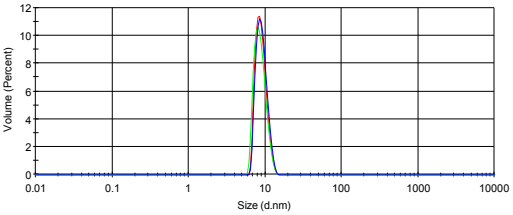

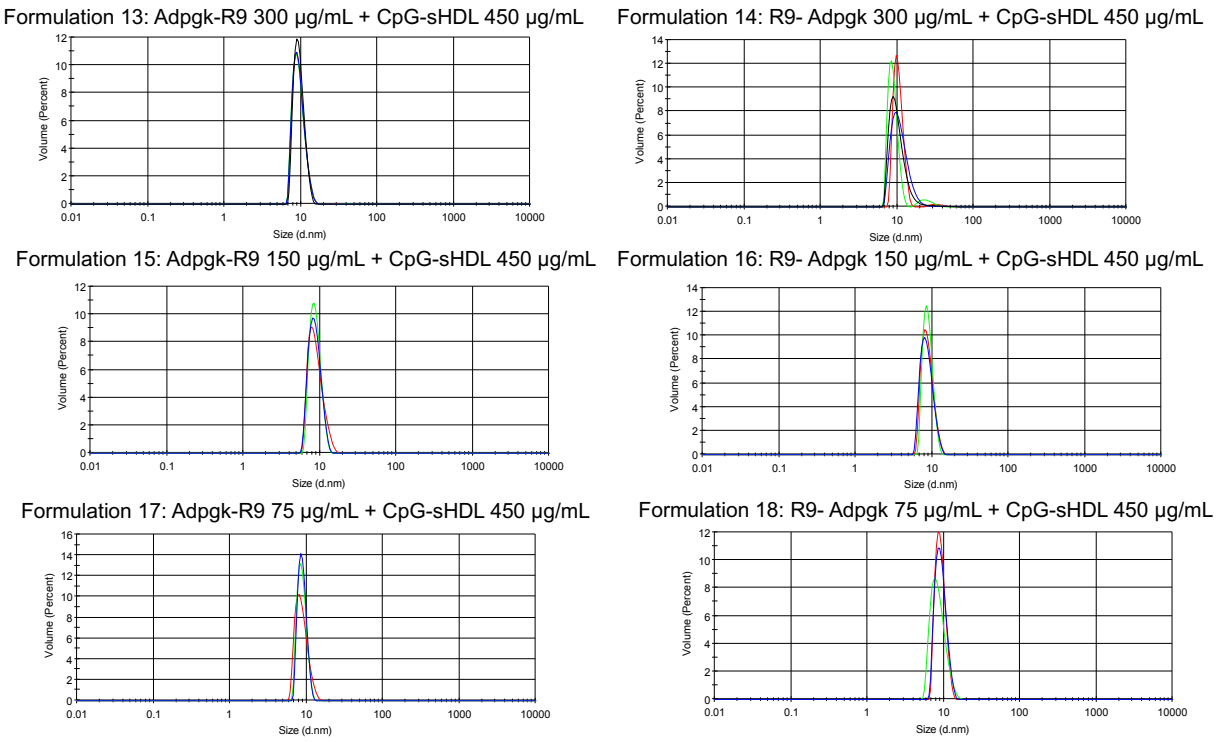

Figure 3-8. DLS size analysis of all attempted formulations using arginine-tagged Adpgk.

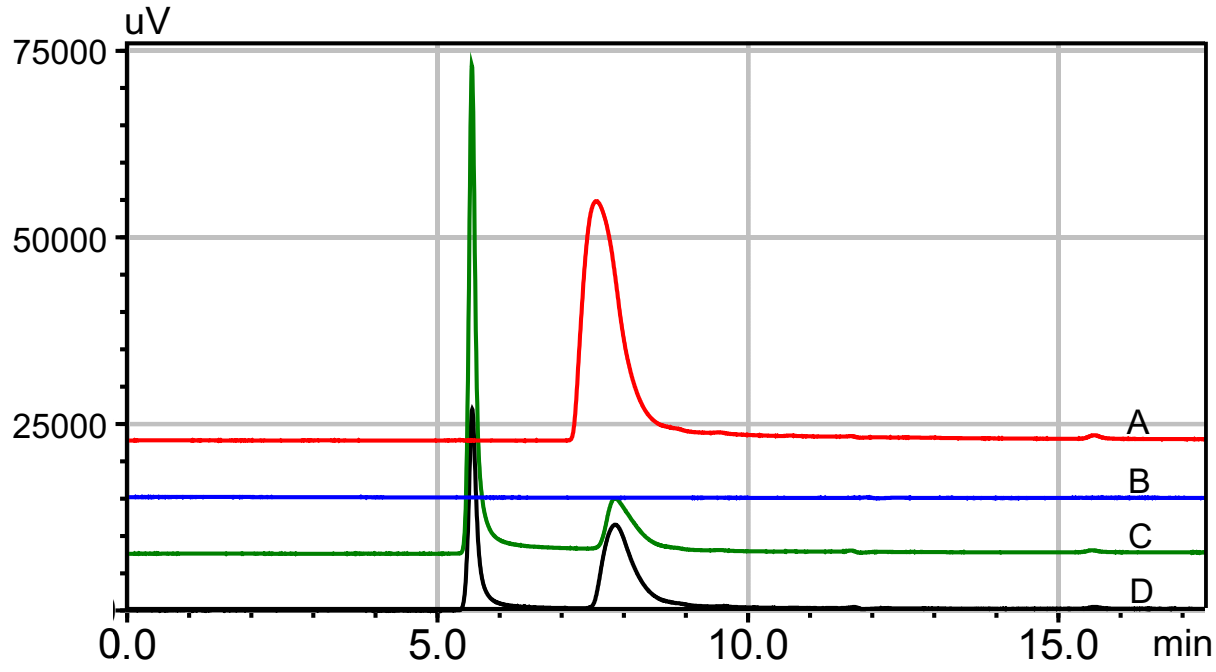

Figure 3-9. GPC analysis of Adpgk-R9 formulation (λ = 260 nm). (A) CpG-sHDL (B) free Adpgk-R9 peptide (C) Adpgk-R9/CpG-sHDL at 150 μg/mL peptide, 150 μg/mL CpG (D) Adpgk-R9/CpG-sHDL at 75 μg/mL peptide, 150 μg/mL CpG.

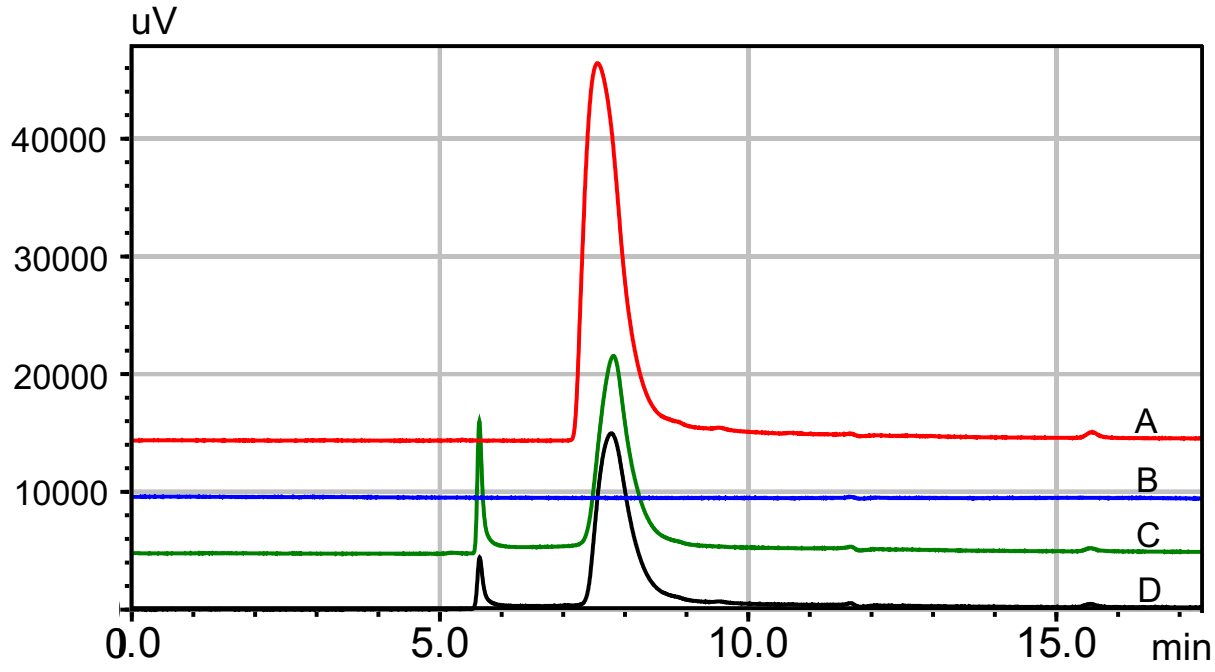

Figure 3-10. GPC analysis of R9-Adpgk formulation (λ = 260 nm). (A) CpG-sHDL (B) free R9-Adpgk peptide (C) R9-Adpgk/CpG-sHDL at 150 μg/mL peptide, 150 μg/mL CpG (D) R9-Adpgk/CpG-sHDL at 75 μg/mL peptide, 150 μg/mL CpG.

3.4.2. DMSO and PEGylated formulations exhibit immunogenicity similar to the traditional formulation in a prophylactic setting.

First, we decided to perform a prophylactic vaccination study to determine the immunogenic potential of each formulation relative to the traditional formulation, which our lab has previously demonstrated. We did this by comparing the frequency of Adpgk-positive CD8+ T cells among each group of female C57BL/6 mice vaccinated with each of the formulations subcutaneously at the tail base on a biweekly basis (Figure 3-11). We found that, after the second and third vaccinations, frequencies of Adpgk-positive CD8+ T cells in the peripheral blood of mice treated with either the DMSO or PEGylated formulations were comparable to those in the blood of mice treated with the traditional formulation. Mice treated with either the Adpgk-R9 or R9-Adpgk formulations, however,

did not demonstrate these similarities and instead showed 4-fold and 8-fold lower frequencies of Adpgk-positive CD8+ T cells after the second and third vaccinations compared to mice treated with the traditional formulation (Figure 3-12). In summary, the results indicated that the Adpgk-R9 and R9-Adpgk formulations were not worth pursuing as simplified formulation methods due to their diminished immunogenicity while the DMSO and PEGylated formulations showed promising immunogenic similarities to the traditional formulation. However, the mice treated with the DMSO formulation exhibited somewhat lower Adpgk-positive CD8+ T cells than did mice treated with the PEGylated formulation, and we also were concerned about oxidation of the Adpgk peptide during formulation with DMSO given the three oxidation-prone methionine residues on the peptide. Thus, we decided to proceed with the PEGylated formulation as a simplification solution. We also selected another MC38 neoantigen to test, Reps1, to validate the merit of our simplification solution. All further studies utilize both Adpgk and Reps1 in PEGylated and non-PEGylated forms.

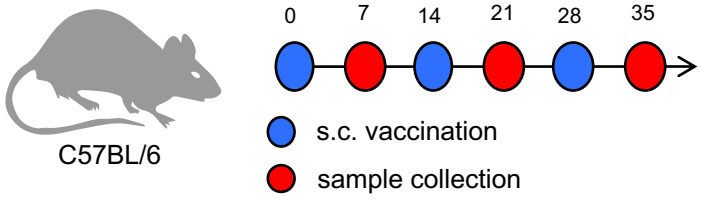

Figure 3-11. Treatment regimen and study timeline for prophylactic vaccination study using different formulation methods for Adpgk neoantigen-loaded sHDL.

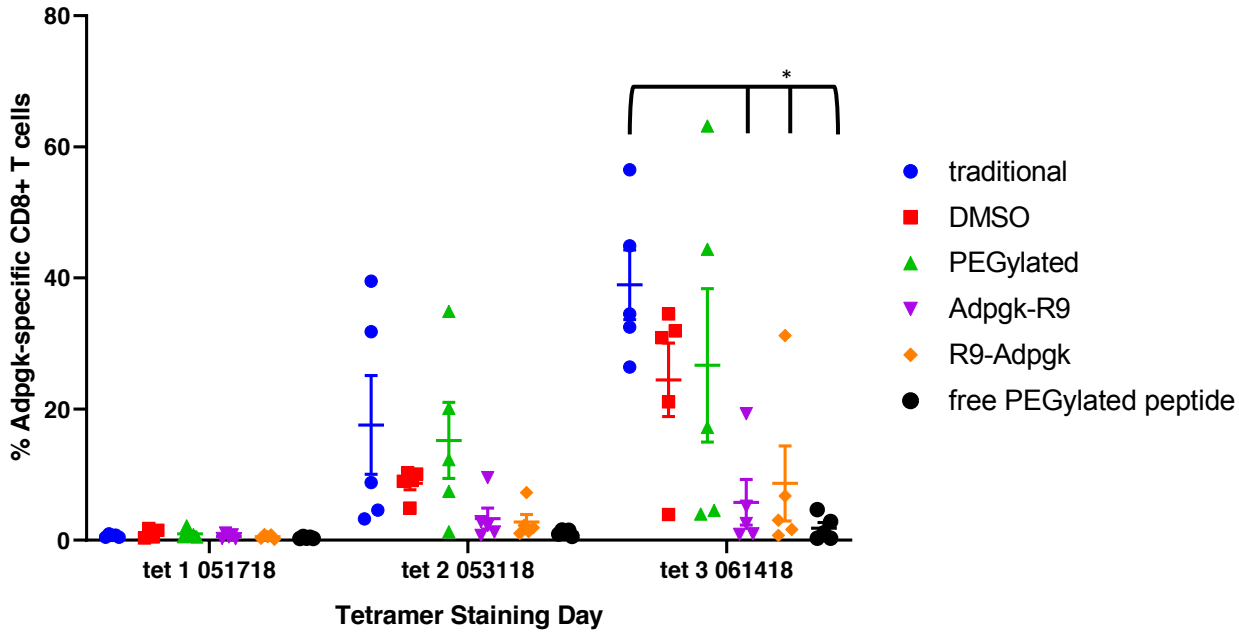

*Figure 3-12. FACS analysis of PBMCs showing frequencies of Adpgk-specific CD8+ T cells in systemic circulation 1 week after each vaccination. *P<0.05.*

3.4.3. Analysis of PEG4-Adpgk and PEG4-Reps1 nanodisc formulations

Formulations were quantified using HPLC, showing successful conjugation to DOPE and retention of the conjugate after purification. We achieved 84% conjugation efficiency and 75% conjugate retention after purification for a 63% overall incorporation efficiency in the PEG(4)-Reps1-sHDL formulation (Figure 3-13) and 98% conjugation efficiency and 84% conjugate retention after purification for an 82% overall incorporation efficiency in the PEG(4)-Adpgk-sHDL formulation (Figure 3-14). In the HPLC chromatograms, 22A is visible at 68 minutes, DMPC at 76 minutes, and DOPE-PDP at 83 minutes. Traditional formulations were analyzed by UPLC/MS (**Error! Reference source not found.**). We also used DLS to perform size analysis of our formulations and found that, after loading cho-CpG onto PEG(4)-Reps1-sHDL and PEG(4)-Adpgk-sHDL, the nanodiscs retained an ideal size of 8-12 nm for effective lymphatic drainage (Table 3-3).

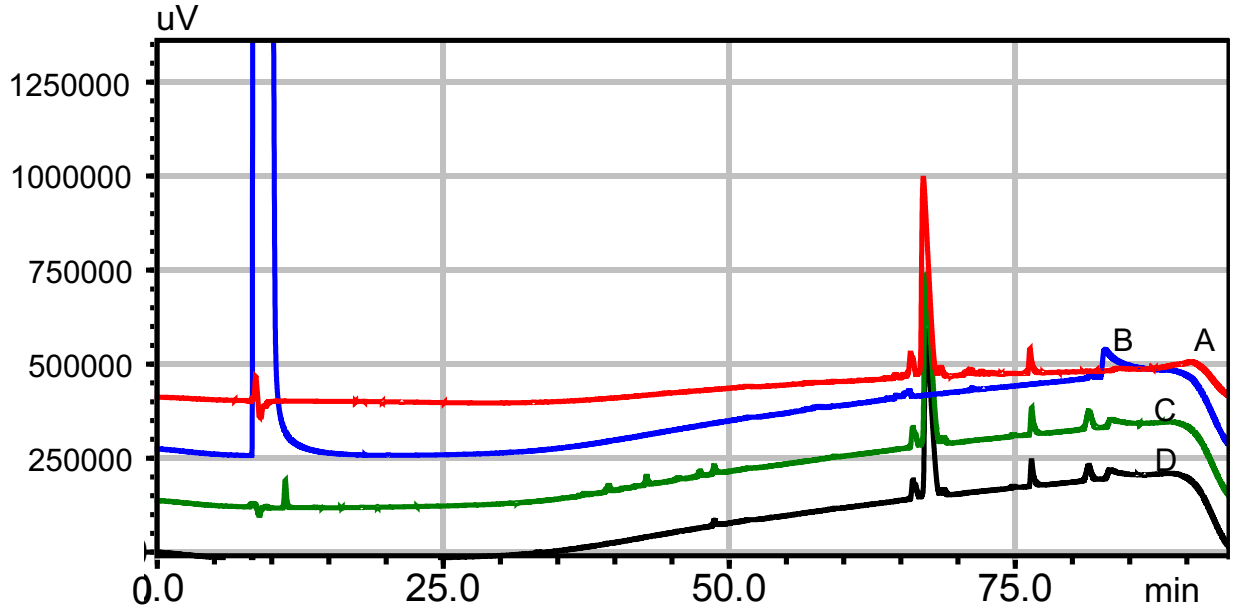

Figure 3-13. HPLC analysis of PEG4-Reps1 formulation (λ = 220 nm). (A) blank sHDL (B) DOPE-PDP (C) PEGylated Reps1-sHDL before purification (D) PEGylated Reps1-sHDL after purification.

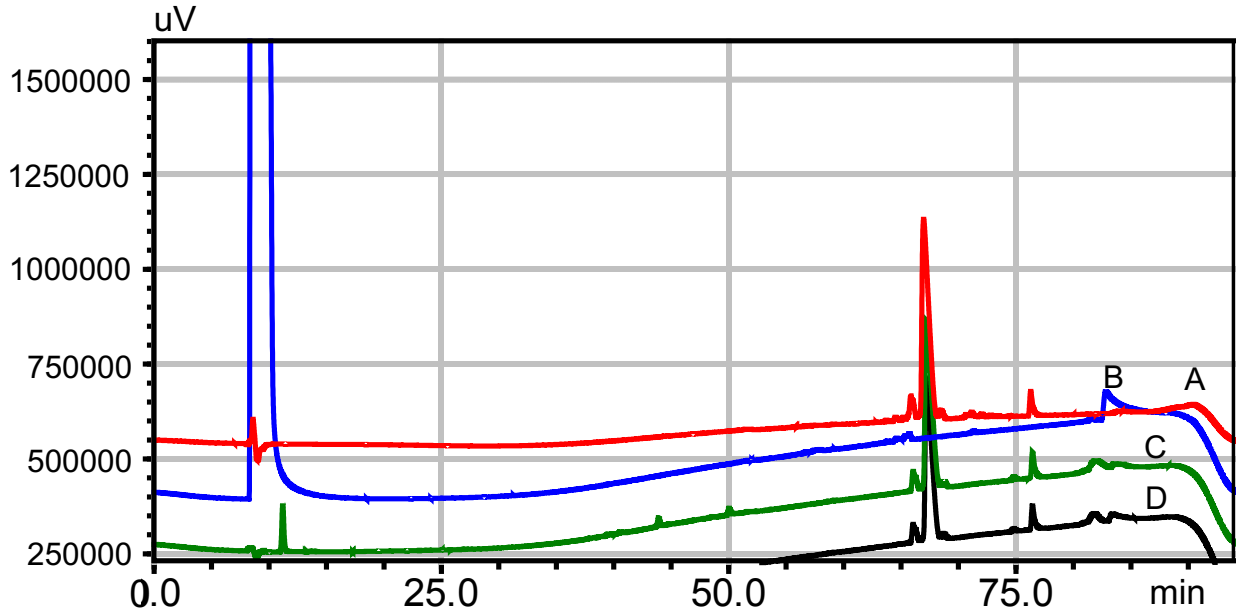

Figure 3-14. HPLC analysis of PEG4-Adpgk formulation (λ = 220 nm). (A) blank sHDL (B) DOPE-PDP (C) PEGylated Adpgk-sHDL before purification (D) PEGylated Adpgk-sHDL after purification.

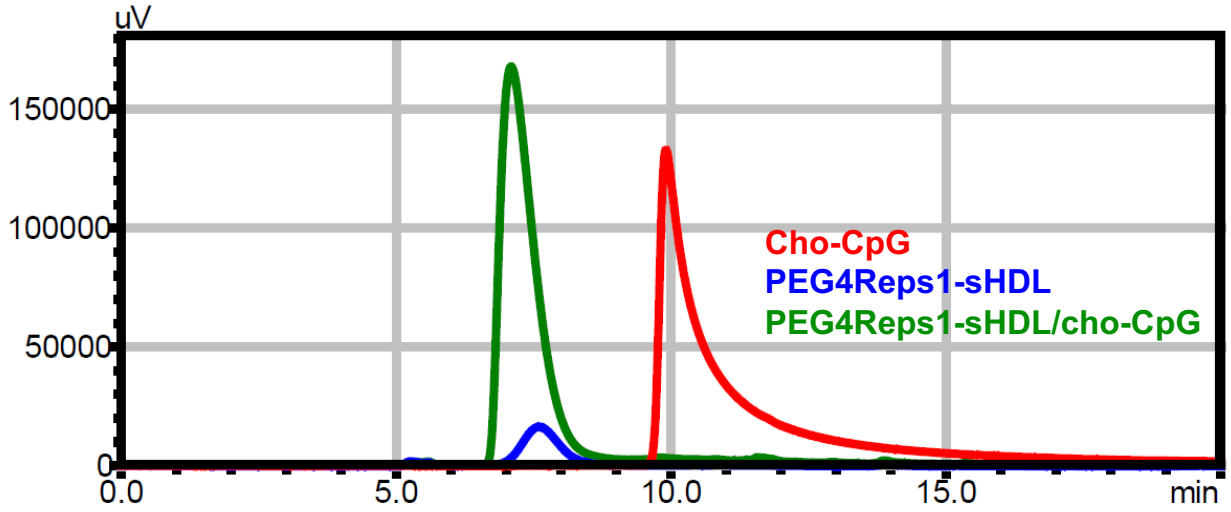

Figure 3-15. GPC analysis of PEG4-Reps1 formulation following cho-CpG loading. Free cho-CpG is shown in red, PEG4Reps1-sHDL before cho-CpG loading in shown in blue, PEG4Reps1-sHDL after cho-CpG loading is shown in green.

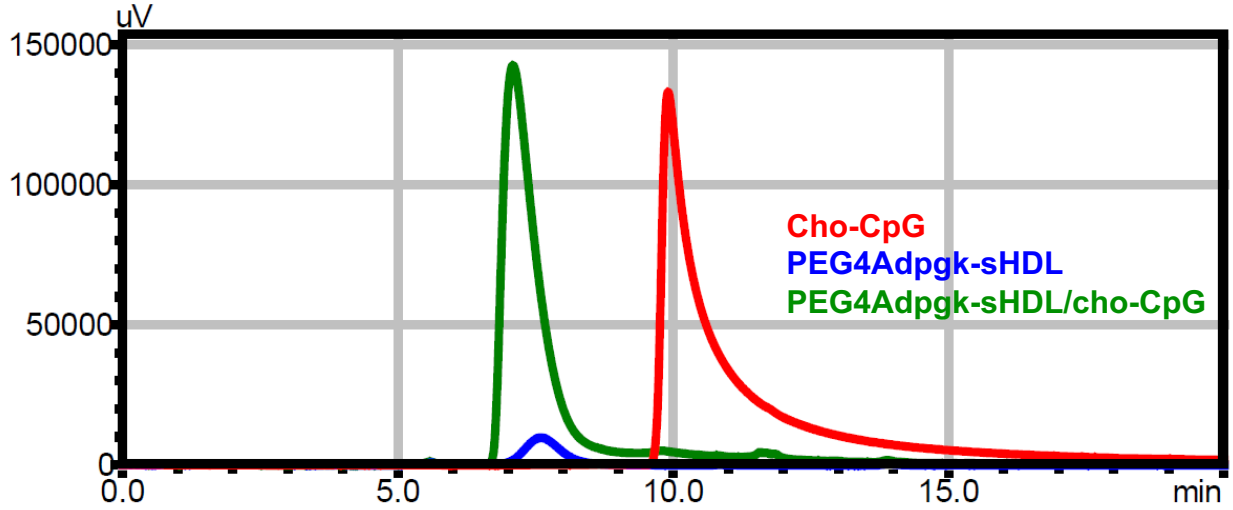

Figure 3-16. GPC analysis of PEG4-Adpgk formulation following cho-CpG loading. Free cho-CpG is shown in red, PEG4Adpgk-sHDL before cho-CpG loading in shown in blue, PEG4Adpgk-sHDL after cho-CpG loading is shown in green.

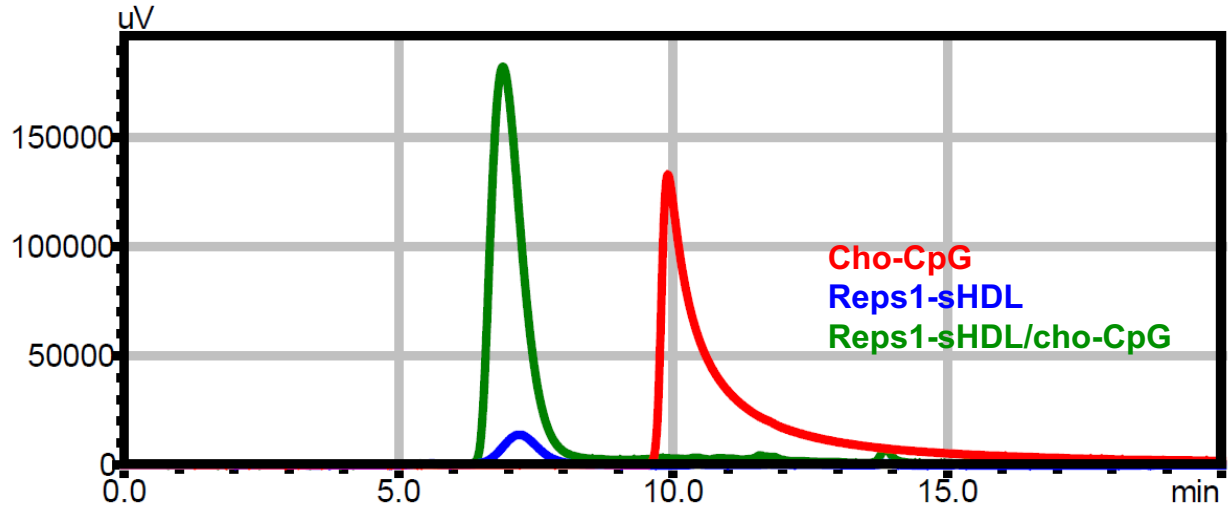

Figure 3-17. GPC analysis of Reps1 formulation following cho-CpG loading. Free cho-CpG is shown in red, Reps1-sHDL before cho-CpG loading in shown in blue, Reps1-sHDL after cho-CpG loading is shown in green.

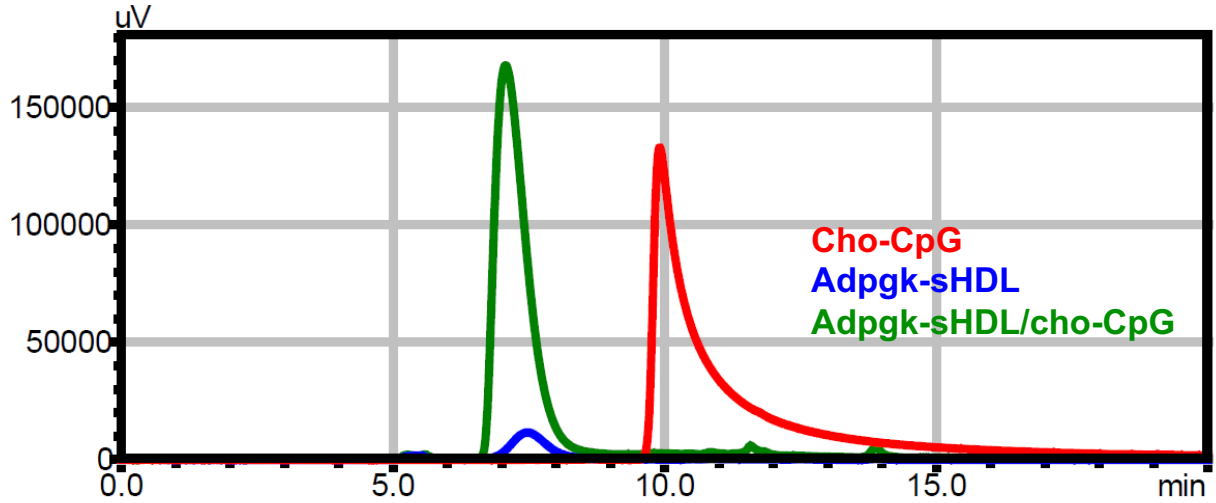

Figure 3-18. GPC analysis of Adpgk formulation following cho-CpG loading. Free cho-CpG is shown in red, Adpgk-sHDL before cho-CpG loading in shown in blue, Adpgk-sHDL after cho-CpG loading is shown in green.

Table 3-3. Summary of size and zeta potential of PEGylated and traditional Reps1 and Adpgk neoantigen-loaded sHDL formulations.

Formulation	Size +/- SD (nm)	Zeta Potential +/- SD (mV)
PEG(4)Reps1-sHDL/cho-CpG	9.384 +/- 2.349	-9.15 +/- 3.72
Reps1-sHDL/cho-CpG	11.23 +/- 2.527	-8.35 +/- 4.41
PEG(4)Adpgk-sHDL/cho-CpG	9.936 +/- 2.613	-5.87 +/- 6.32
Adpgk-sHDL/cho-CpG	9.831 +/- 2.856	-5.14 +/- 7.69

3.4.4. PEG4-Adpgk and PEG4-Reps1 are just as immunogenic as Adpgk and Reps1 when delivered on sHDL nanodiscs

We performed a prophylactic vaccination study to determine the immunogenic potential of PEGylated neoantigen formulations relative to the traditional formulation with free neoantigen peptide as a control. We compared the frequency of Reps1- or Adpgk-specific CD8+ T cells among each group using IFN-γ ELISPOT. We found that, for both Adpgk and Resp1 neoantigens, mice vaccinated with PEGylated and traditional formulations exhibited comparably strong neoantigen-specific CD8+ T cell responses after all three vaccinations ($p>0.05$). Both PEGylated and traditional formulations induced significantly greater neoantigen-specific CD8+ T cell responses than did soluble neoantigen for Adpgk and Reps1, which is consistent with previous results in this chapter and in Chapter 2 (Figure 3-19). Taken together, these results support our hypothesis that PEGylated neoantigen-loaded sHDL would maintain vaccine immunogenicity while simplifying the formulation process for the vaccine itself.

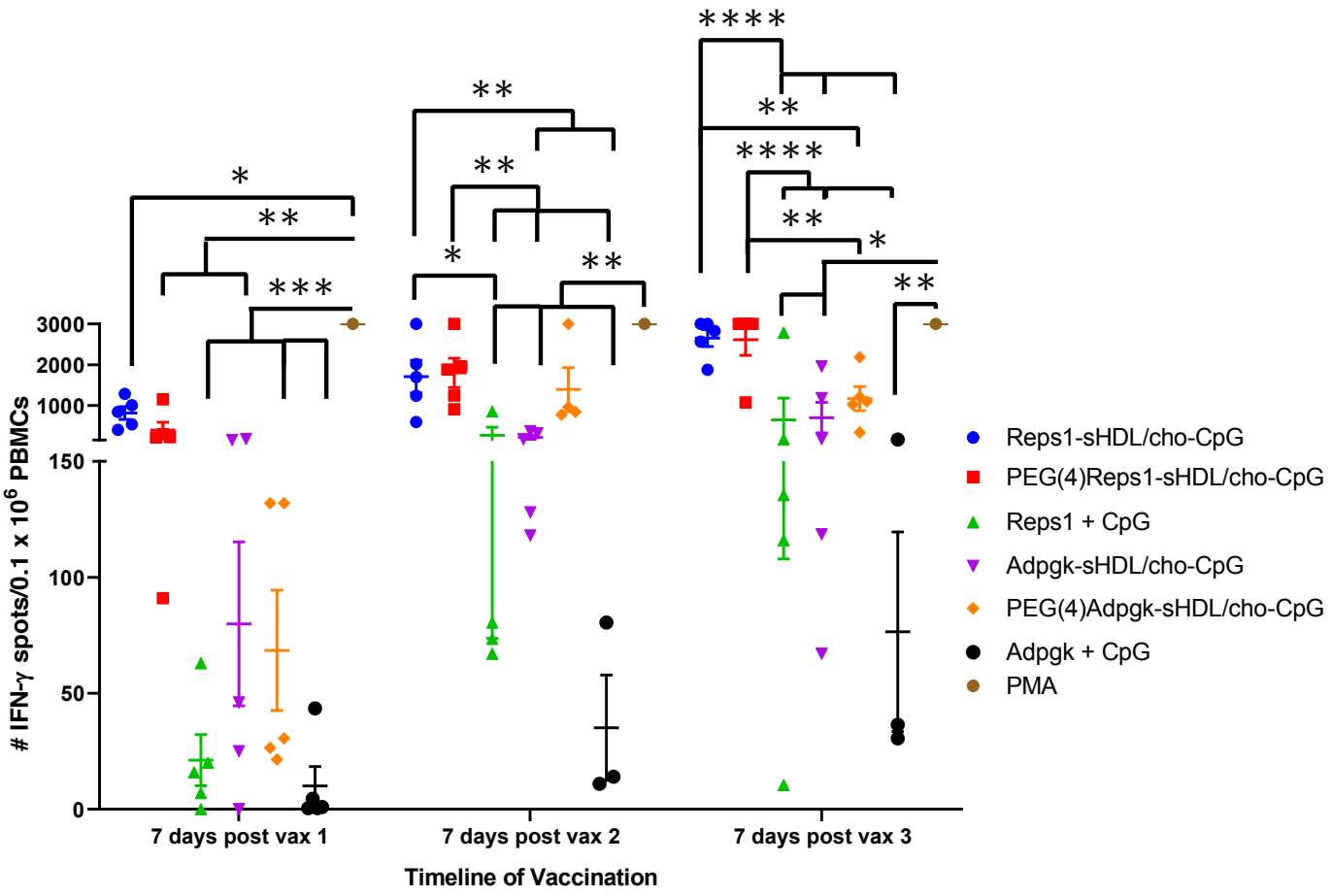

*Figure 3-19. IFN-γ ELISPOT of PBMCs showing frequencies of neoantigen-specific CD8+ T cells in systemic circulation 1 week after each vaccination. *P<0.05, **P<0.01, ***P<0.001, ****P<0.0001.*

3.4.5. PEGylated and traditional formulations exhibited comparable protective anti-tumor immunity

Taking formulation comparison a step further, we challenged all prophylactically vaccinated mice with MC38 tumor cells in the flank 11 days after the third vaccination. Between traditional and PEGylated formulations, significant differences in tumor growth were only observed with Adpgk neoantigen (day 20, $p<0.05$) (Figure 3-20). At earlier time points, prophylactic treatment with PEG4Adpgk-sHDL/CpG slowed tumor growth

more effectively than did Adpgk-sHDL/CpG, but this effect did not last past day 20. After day 20, mice began reaching tumor end points, rendering further tumor growth comparisons inaccurate. Median survival rates for each vaccination group were similar: PEG4Reps1-sHDL/CpG, 23 days; Reps1-sHDL/CpG, 22 days; free Reps1 + CpG, 23 days; PEG4Adpgk-sHDL/CpG, 30 days; Adpgk-sHDL/CpG, 26 days; free Adpgk + CpG, 31 days. No significant differences in median survival were observed between formulations for either neoantigen (Figure 3-21), indicating similar anti-tumor protection between traditional and PEGylated formulations. Age-matched naïve mice were also inoculated with MC38 tumor cells for comparative purposes, but mice in this group grew tumors slower than some mice in prophylactically vaccinated groups. Though interesting, this observation should not be one of concern because naïve control median survival was 26.5 days, which was similar to the rates of all other groups, and tumor challenge was initiated in a prophylactic setting, which is not clinically relevant in the context of our sHDL nanovaccine.

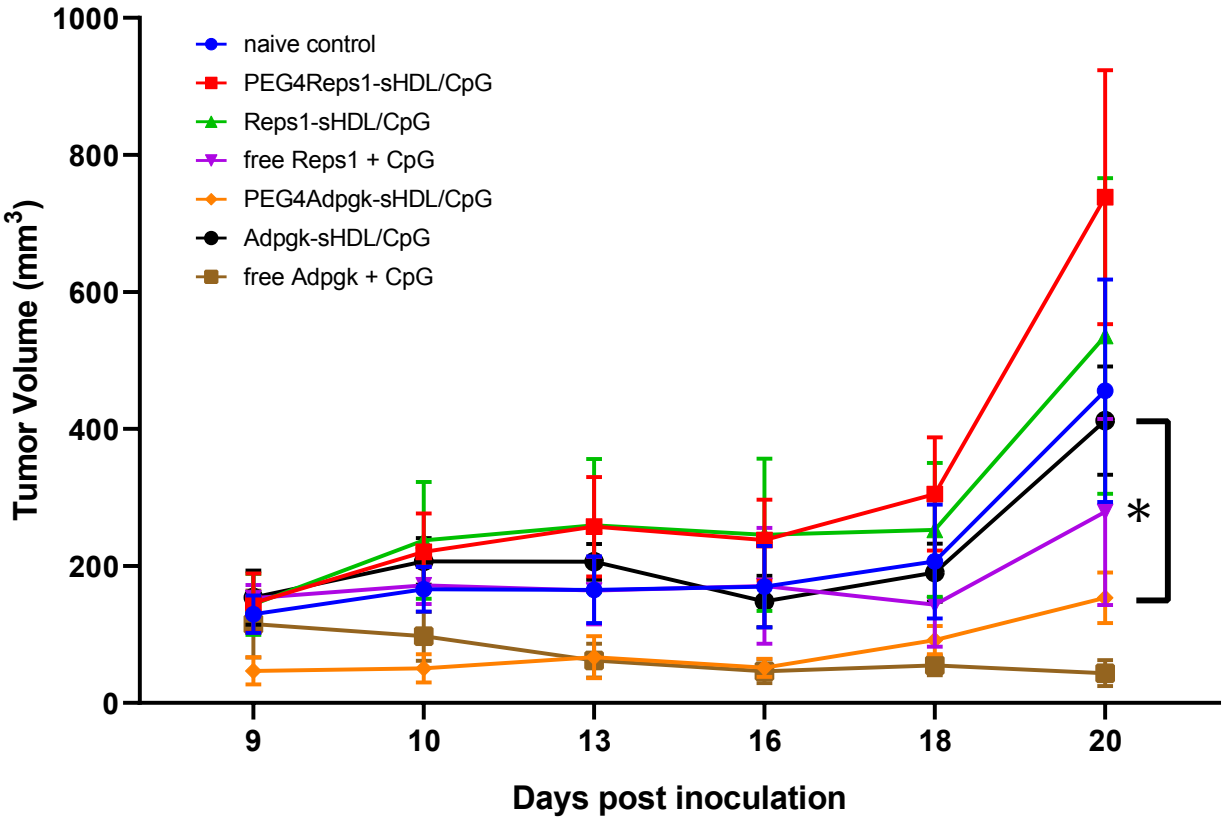

*Figure 3-20. Tumor growth summary for all treatment groups in prophylactic vaccination study through day 20 after tumor inoculation. *P<0.05.*

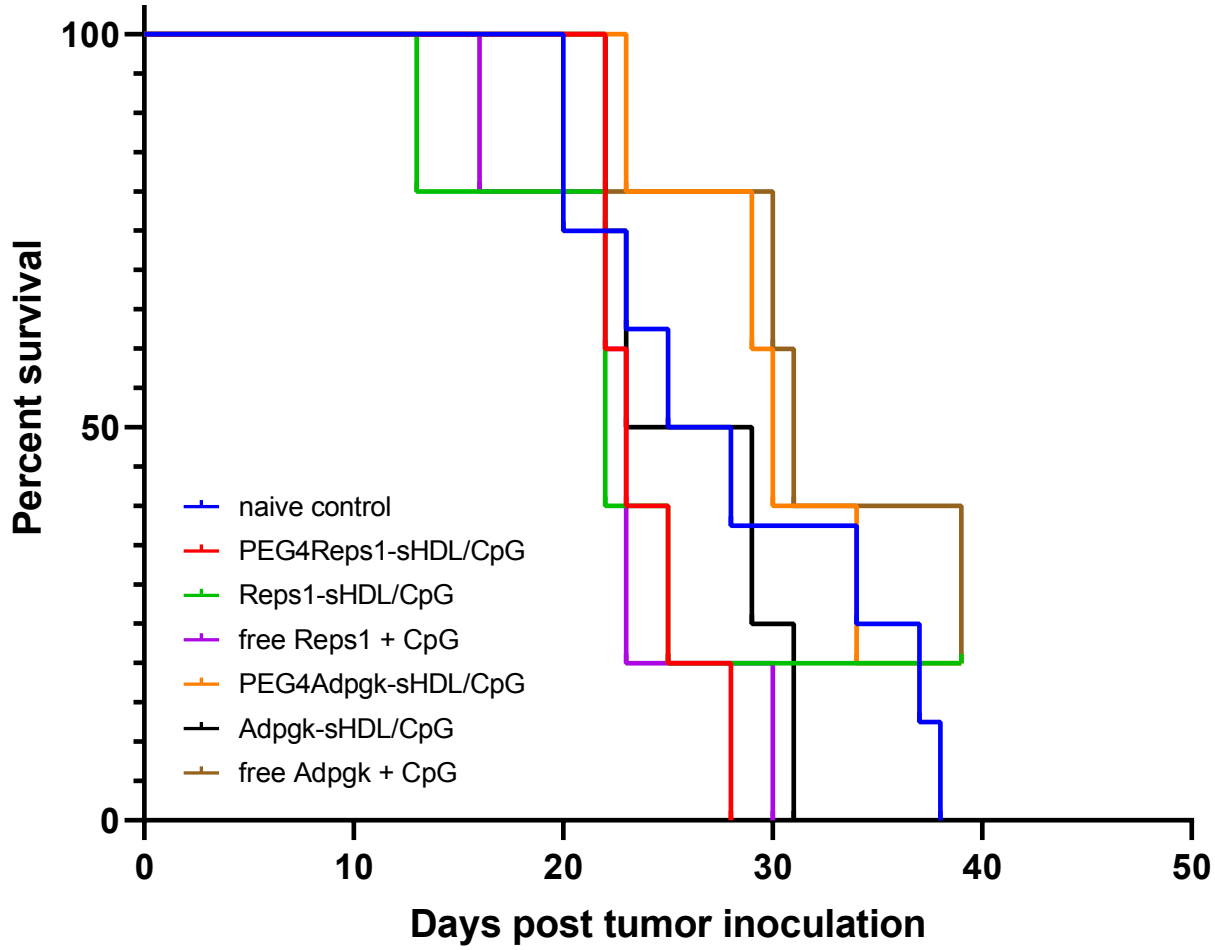

Figure 3-21. Kaplan-Meier overall survival curve for all treatment groups in prophylactic study. No significant differences in survival were observed.

Moving forward, future studies should explore the anti-tumor efficacy of these different formulations in a therapeutic setting through vaccination of tumor-bearing mice. This prophylactic study has shown us that the simplified, PEGylated neoantigen-sHDL formulations induce neoantigen-specific CD8+ T cells and elicit anti-tumor protective immunity similarly to traditional formulations, justifying peptide PEGylation as a viable method for streamlining nanovaccine formulation. However, prophylactic vaccination is not realistic in the context of most cancers and cannot accurately capture the interactions between vaccination-induced immune populations and the tumor itself. Thus, more meaningful comparisons between PEGylated and traditional formulations'

effects on tumor growth and survival of tumor-bearing mice may be made through execution of a therapeutic vaccination study. Additionally, neoantigens derived from different tumor models should be evaluated for immunogenicity and anti-tumor efficacy using the PEGylated formulation methodology to establish that the method is versatile and robust for clinical translation of a personalized cancer vaccination platform.

Chapter 4. Synthetic HDL nanoparticles delivering docetaxel and CpG for chemo-immuno-therapy of colon carcinoma

4.1. Abstract

Colon carcinomas themselves comprise over two-thirds of all colorectal cancers with an overall 5-year survival rate of 64%, which rapidly decreases to 14% when the cancer becomes distant or metastatic, usually progressing into the liver. Depending on the stage of colon carcinoma at diagnosis, patients can undergo surgery to attempt tumor resection or move directly to chemotherapy with one or a combination of drugs. As with most cancers, colon carcinomas do not always respond to chemotherapies, so targeted therapies and immunotherapies have been developed to aid chemotherapy.

Approved targeted therapies for colon carcinoma are limited to protein inhibitors that aim to prevent new blood vessel formation around the tumor or to interrupt tumor cell proliferation so that tumor growth can be slowed but do not directly induce tumor cell killing. Immunotherapies like anti-CTLA-4 and anti-PD-1 prevent T cell death, allowing for increased T cell activation and tumor recognition for indirect tumor cell killing[105]. Unfortunately, these targeted therapies and immunotherapies are associated with several adverse events due to their systemic or oral administration.

In this work, we have developed a localized combination therapy for colon carcinoma whereby chemo- and immuno-therapeutic entities are delivered to the tumor on the same delivery vehicle for maximal anti-tumor efficacy and minimal off-target effects. We first encapsulated chemotherapeutic docetaxel (DTX) into the hydrophobic core of synthetic HDL (sHDL) nanodiscs and then co-loaded cholesterol-modified Toll-like receptor 9 (TLR9) agonist CpG (cho-CpG) oligonucleotide onto the surface of sHDLs. DLS analysis showed that DTX-loaded sHDLs averaged a particle size of 11.1 nm, similar to that of blank sHDLs, and that insertion of cho-CpG slightly increased the particle size to 11.3 nm. An *in vitro* cytotoxicity assay showed that murine MC38 colon carcinoma cells incubated with free DTX or DTX-loaded sHDL (DTX-sHDL) for 48 hours experienced cell death at similar rates. *In vivo* survival analysis of MC38 tumor-bearing mice treated intratumorally with DTX-sHDL/CpG (median survival = 43 days) showed significant improvement in overall survival compared to mice treated with DTX (median survival = 23 days, $p < 0.0001$) or DTX-sHDL (median survival = 28 days, $p<0.0001$). Two of seven mice treated with DTX-sHDL/CpG experienced complete tumor regression. None of the mice experienced any systemic toxicity as indicated by body weight maintenance and normal serum enzyme and protein levels. In total, we have demonstrated that chemo- and immuno-therapies can be co-loaded into sHDLs, delivered locally to the tumor, and improve survival outcomes significantly compared to chemotherapy alone.

4.2. Introduction

Colon adenocarcinomas constitute the vast majority of all diagnosed colorectal cancer cases with an incidence rate of more than 140,000 people per year. Although

the average 5-year survival rate for patients diagnosed with colorectal cancer is greater than 60%, colorectal cancer remains the 2nd leading cause of death in the United States[133]. This is likely due to nearly half of treated patients developing recurrent disease. Currently, the standard-of-care for patients with colon adenocarcinoma is surgery, radiation, chemotherapy, and possibly immunotherapy via immune checkpoint blockade. Though effective, both chemotherapy and immune checkpoint blockade agents are administered systemically and are delivered to the tumor itself in a very limited amount. Moreover, neither chemotherapy nor immune checkpoint blockade directly elicits immune memory against the tumor, which is crucial for preventing tumor recurrence. Thus, combining chemotherapy with an immuno-stimulatory agent that promotes immune cell interaction with tumor antigens is an exciting strategy that is readily translational and beginning to be explored[134,135].

We hypothesize that sHDL encapsulating docetaxel chemotherapy and decorated with toll-like receptor 9 (TLR9) agonist CpG oligonucleotide delivery to colon adenocarcinoma tumors will effectively suppress tumor growth and result in long-term survival as compared to monotherapy delivery. TLR9 agonists interact with their receptors on a plethora of immune cells and are primarily involved in activation and maturation of dendritic cells and differentiation of B cells. These dendritic cells and B cells can then undergo cross-presentation of tumor-specific antigens and secretion of anti-tumor antibodies, respectively[136,137]. The source of these antigens often comes from apoptotic tumor cells, which can be directly produced by chemotherapeutic cytolysis (Figure 4-1). We have previously reported the combination of CpG with

chemotherapy for the treatment of glioblastoma and, given the promising results of this study, have decided to apply it to a different yet aggressive tumor model[137].

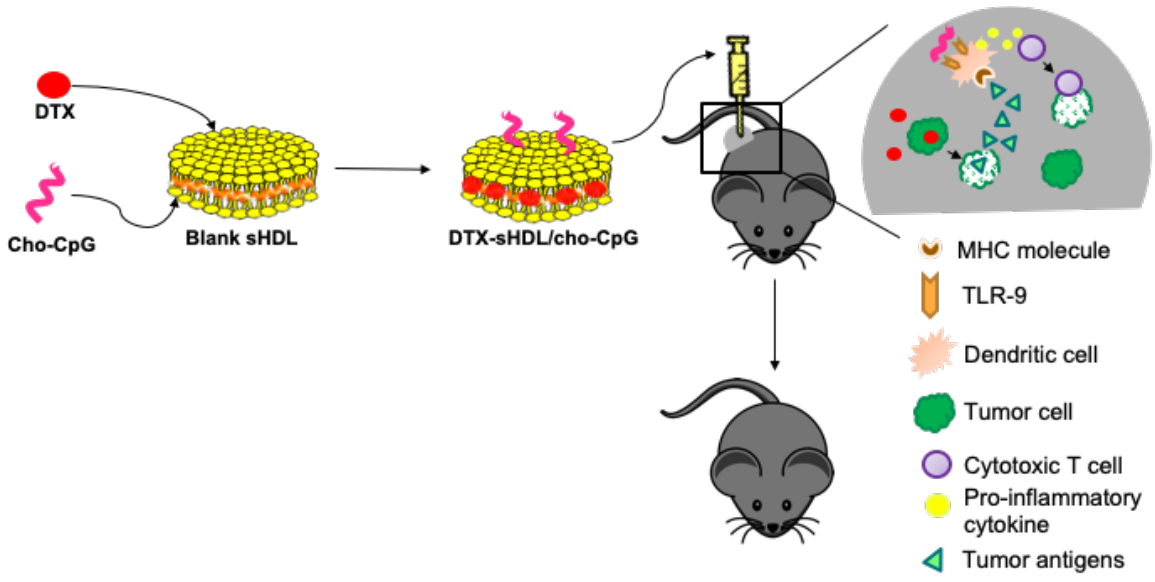

Figure 4-1. Graphical representation of hypothesis that co-delivery of chemo- and immuno-therapeutic entities will synergistically elicit anti-tumor efficacy.

Several nanoparticles have been used for co-delivery of these two moieties, but none of them have been approved for clinical use. In the early 2000s, Weigel et al. published data showing the enhanced antitumor effects of cyclophosphamide and topotecan when combined with CpG in mouse models of embryonal rhabdomyosarcoma. Almost a decade later, Buhtoiarov et al. demonstrated that co-delivery of CpG with vincristine, cyclophosphamide and doxorubicin in murine melanoma and neuroblastoma models significantly improved the antitumor effects of multidrug chemotherapy regimens alone. In 2015, Lollo et al. used lipid nanocapsules with a cationic chitosan shell to deliver paclitaxel and CpG simultaneously to glioblastoma tumors in mice through convection-enhanced delivery and showed that

this co-delivery significantly improved survival outcomes compared to Taxol® and separate injections of paclitaxel and CpG[138-140]. sHDL has already been demonstrated as safe and well-tolerated in high doses in the clinic, making it a readily translatable platform for co-delivered combination therapy for colon adenocarcinoma patients. Here, we describe the superior antitumor efficacy of co-delivering docetaxel chemotherapy and TLR9 agonist CpG on sHDL nanoparticles to tumors over docetaxel alone.

4.3. Materials & Methods

4.3.1. Materials

Egg sphingomyelin (eSM) was acquired from Avanti Polar Lipids. Apolipoprotein A-1 mimetic peptide 22A was acquired from GenScript Inc. Docetaxel (DTX) was acquired from Cayman Chemicals. MC38 cells were purchased from Kerafast, Inc. Cholesterol-modified CpG1826 was custom ordered from Integrated DNA Technologies.

4.3.2. Formulation and characterization of DTX-sHDL

The docetaxel-loaded sHDL (DTX-sHDL) was prepared as described previously[137]. Briefly, 22A, egg sphingomyelin (eSM) and DTX were dissolved in acetic acid. The acetic acid solutions of 22A, eSM and DTX were mixed and freeze-dried for 24 h (mass ratio of 22A: eSM: DTX = 1:2:0.05). The lyophilized powder was rehydrated by PBS (pH 7.4). 3 heat-cooling cycles (50°C 5 min followed by room temperature 5 min) were performed to form DTX-sHDL. DTX-sHDL/CpG particles were prepared by incubating DTX-sHDL with cholesterol-CpG in 10 mM phosphate buffer at the room temperature for 2 h. The particle size of DTX-sHDL was analyzed by dynamic laser scattering (DLS). The purity of the DTX-sHDL nanoparticles was evaluated by gel permeation

chromatography (GPC) at 220 nm using Tosoh TSK gel G3000SWx 7.8 mm× 30 cm column (Tosoh Bioscience, King of Prussia, PA).

4.3.3. *In vitro* uptake assays

MC38 cells were cultured in RPMI medium supplemented with 10% Fetal Bovine Serum and 1% Penicillin/Streptomycin antibiotics. When cells reached their exponential growth phase, they were trypsinized and plated on 12-well tissue culture plates at 50,000 cells per well to be incubated overnight at 37C to allow adherence. HDL was labeled with lipophilic dye DiD at a ratio of 2:1:0.01 eSM:22A:DiD. DiD-labeled sHDL was passed through a desalting column (MWCO 7kDa) to remove free dye molecules prior to use.

Cells were dosed with three different concentrations of DiD-sHDL normalized by 22A concentration to evaluate the effect of dose on cell uptake. Following dosing, cells were incubated at 37C for 3 hours and then washed with PBS before analysis by confocal microscopy on a Nikon A1si confocal microscope or by FACS on a CytoFlex cytometer. FlowJo and ImageJ were used for quantitative analysis.

For the Block lipid transport-1 (BLT-1) inhibition experiment, cells were pretreated with SR-B1 inhibitor BLT-1 with different concentrations for 1 h. Then, DiD-sHDL was added to each well (final 22A concentration = 10 μg/mL). The cells were further incubated for 3 hours followed by FACS analysis.

4.3.4. *In vitro* cytotoxicity assay

MC38 cells were cultured in RPMI medium supplemented with 10% Fetal Bovine Serum and 1% Penicillin/Streptomycin antibiotics. When cells reached their exponential growth phase, they were trypsinized and plated on 96-well tissue culture plates at

10,000 cells per well to be incubated overnight at 37C to allow adherence. Cells were dosed with six different doses of DTX in either free drug form or encapsulated in HDL to test the effect of increasing dose on cell death. Following dosing, cells were incubated at 37C for 48 hours before analysis using the CellTiter 96® Aqueous Non-Radioactive Cell Proliferation Assay (MTS) from Promega. Absorbance at 490 nm was quantified using a BioTek SynergyNEO spectrophotometer. Negative control wells (without treatment) were considered to have the maximum absorbance at 100% viability, and viability of other wells was calculated as the ratio of treated well absorbance to untreated well absorbance.

4.3.5. Western blot of SR-B1 expression on murine cancer cells

Four different murine cancer cell lines--MC38, B16-F10, CT-26, and 4T1--were cultured, trypsinized, and spun down so that cell pellets could be collected and flash frozen. Cell lysates were prepared and centrifuged at 16,000 x g for 20 minutes at 4C. Supernatant was collected and stored on ice to perform total protein quantification by BCA assay. Samples were normalized to 30 µg total protein for loading onto an SDS-PAGE gel. The gel was run, transferred, and incubated with SR-B1 and actin primary antibodies overnight at 4C followed by incubation with HRP-conjugated secondary antibody at room temperature. The gel was imaged using a BioRad chemiluminescent imager and analyzed with ImageJ.

4.3.6. *In vivo* treatment using combination chemotherapy and immunotherapy

Thirty-five female C57BL/6 mice aged 7-8 weeks (Charles River Laboratories) were inoculated with 1 million MC38 cells at a concentration of 10 million cells/mL subcutaneously superior to the right flank. On day 8 after tumor inoculation, mice were

split into four groups of seven for treatments. Mice were injected intratumorally with (1) PBS, (2) DTX, (3) DTX-HDL, or (4) DTX-HDL/CpG twice a week at 1 mg/kg DTX and 15 μg CpG for five treatments. Mice were euthanized when tumors surpassed 15 mm in one dimension or ulcerated extensively.

4.3.7. Systemic toxicity assessment of chemotherapy and immunotherapy

Mouse body weights were measured regularly to monitor toxicity-associated weight loss. Blood samples were taken four days after the final treatments were administered for serum isolation, and liver enzymes were measured by the In-Vivo Animal Core Animal Diagnostic Laboratory for further analysis. Livers were excised upon euthanization and cryopreserved for histological analysis. Livers were embedded in OCT compound, flash frozen, and cut into 8 micrometer sections at -10°C on a cryostat (ThermoFisher Scientific, Dr. Megan Weivoda lab).

4.3.8. Statistical analysis

Analyses of ELISPOT, FACS, and tumor growth were executed using one-way ANOVA tests with Tukey's post-hoc analyses for multiple comparisons and two-tailed t-tests for individual group comparisons, all at an alpha level of 0.05. Analyses of survival differences were executed using Kaplan-Meier survival analyses with Log-rank Mantel-Cox tests at an alpha level of 0.05.

4.4. Results

4.4.1. Drug and adjuvant loading into sHDL do not affect size or shape of sHDL.

DTX is loaded in sHDL particles using a simple co-lyophilization/rehydration method as described previously. DLS analysis showed that DTX-loaded sHDLs have an average particle size of 11.1 nm, which is similar to that of blank sHDL particles.

Insertion of cho-CpG slightly increased the particle size to 11.3 nm (Figure 4-2). All formulations demonstrated a high purity (> 90%) in GPC analysis (Figure 4-3). The consistent size of DTX-loaded sHDL both before and after loading of DTX and cho-CpG in conjunction with high formulation purity were satisfactory, allowing us to proceed with *in vitro* and *in vivo* studies.

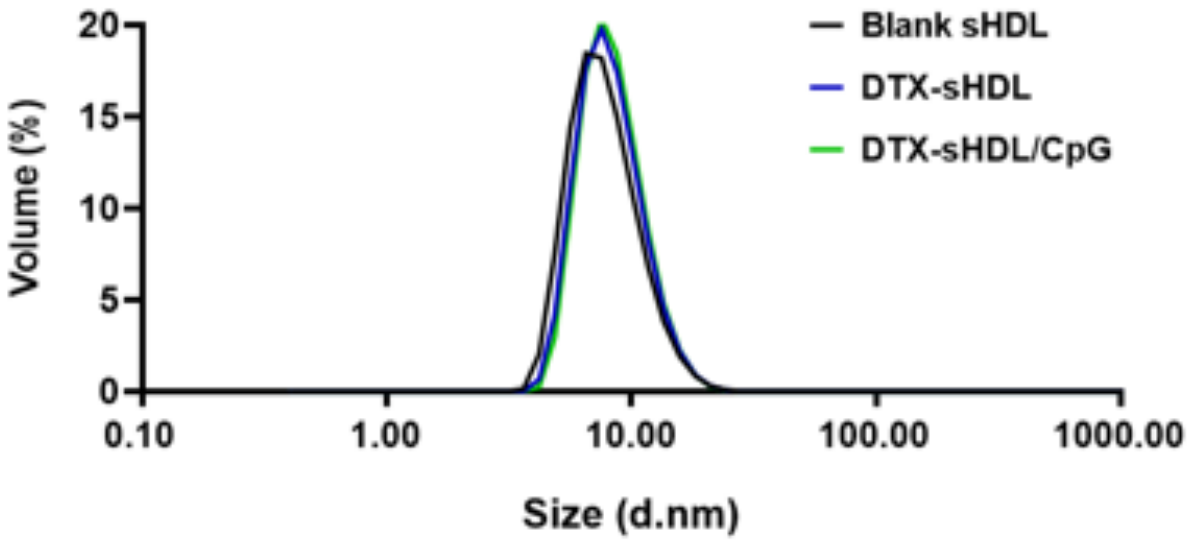

Figure 4-2. Dynamic light scattering (DLS) analysis of blank sHDL (black curve), DTX-sHDL (blue curve), DTX-sHDL/CpG (green curve).

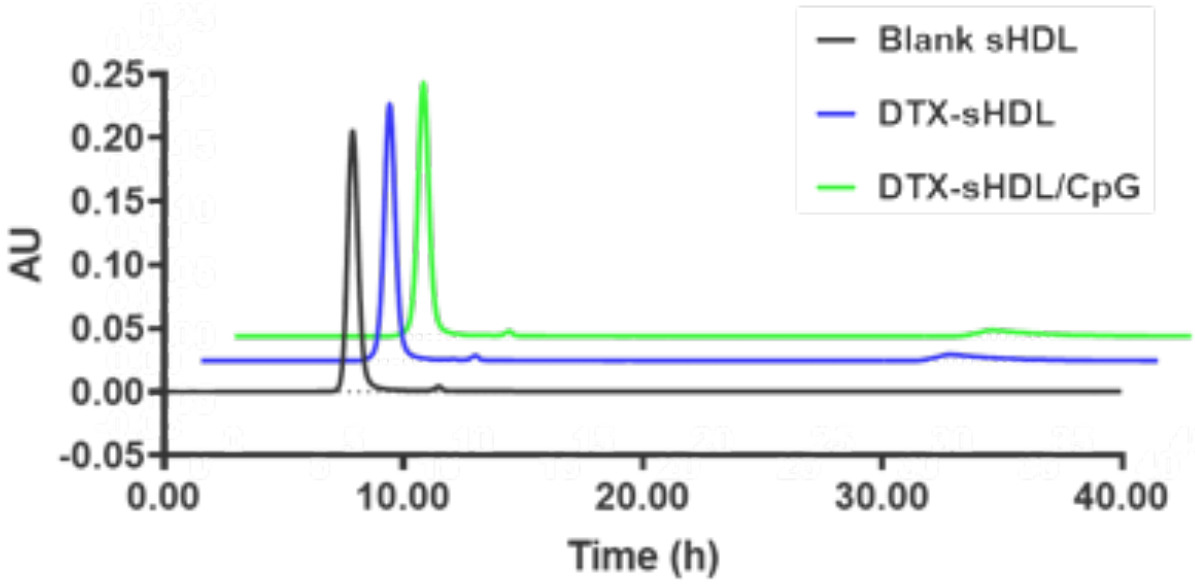

Figure 4-3. Gel permeation chromatography (GPC) analysis of blank sHDL (black curve), DTX-sHDL (blue curve), DTX-sHDL/CpG (green curve).

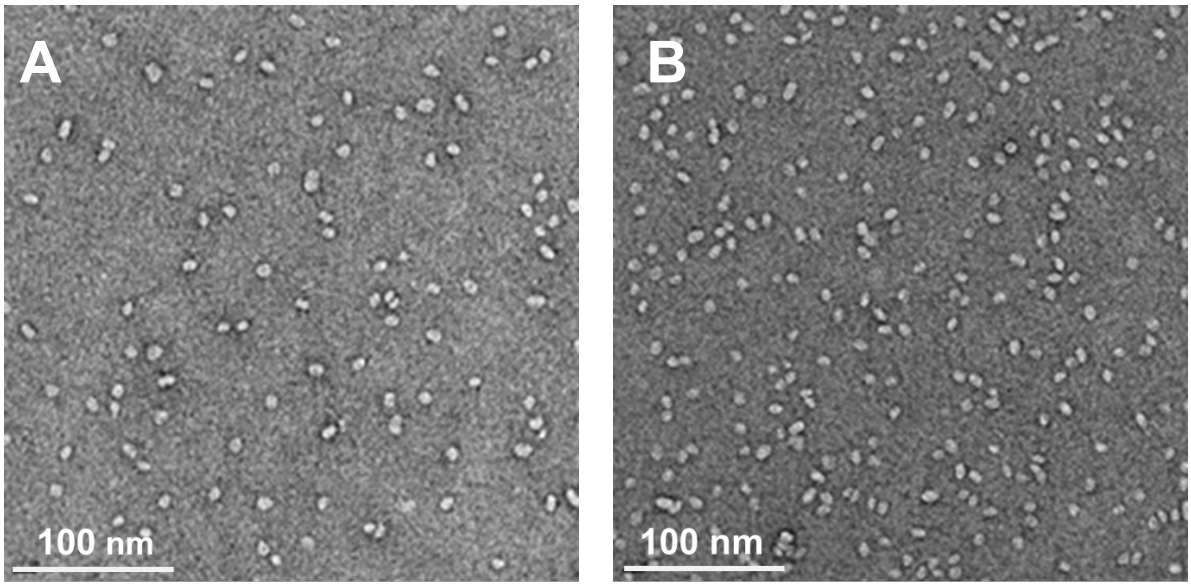

Figure 4-4. Transmission electron microscopy (TEM) images of DTX-sHDL (A) and DTX-sHDL/CpG (B) particles.

4.4.2. SR-B1 is highly expressed by MC38 cells and plays a role in cellular uptake of sHDL.

To validate our choice of colon cancer model for evaluating our DTX-loaded sHDL formulations, we looked at MC38 cells' SR-B1 expression level to verify that sHDL could be recognized and endocytosed by MC38 cells. Western blot analysis of MC38 cell lysate showed high expression of SR-B1 relative to actin band density. This SR-B1 expression level was comparable to that of other tumor cell lines with known increased expression of SR-B1[141] (Figure 4-5A). We then looked at sHDL uptake by MC38 cells *in vitro* to gather quantitative evidence that MC38 cells will readily scavenge sHDL in real time. When cultured with DiD-labeled sHDL for three hours, MC38 cells exhibited dose-dependent uptake of sHDL (Figure 4-5B, Figure 4-6A). To confirm that SR-B1 played a role in this uptake, we inhibited the SR-B1 on MC38 cells by adding Block lipid transporter 1 (BLT-1) to cell cultures for 1 hour before treatment with DiD-sHDL again

for 3 hours. Indeed, we observed a marked decrease in cellular uptake of sHDL with increasing pretreatment doses of BLT-1 ($p < 0.01$) (Figure 4-6B). Together, these results support our choice of an MC38 cancer model because of high cellular SR-B1 expression and efficient cellular uptake of sHDL.

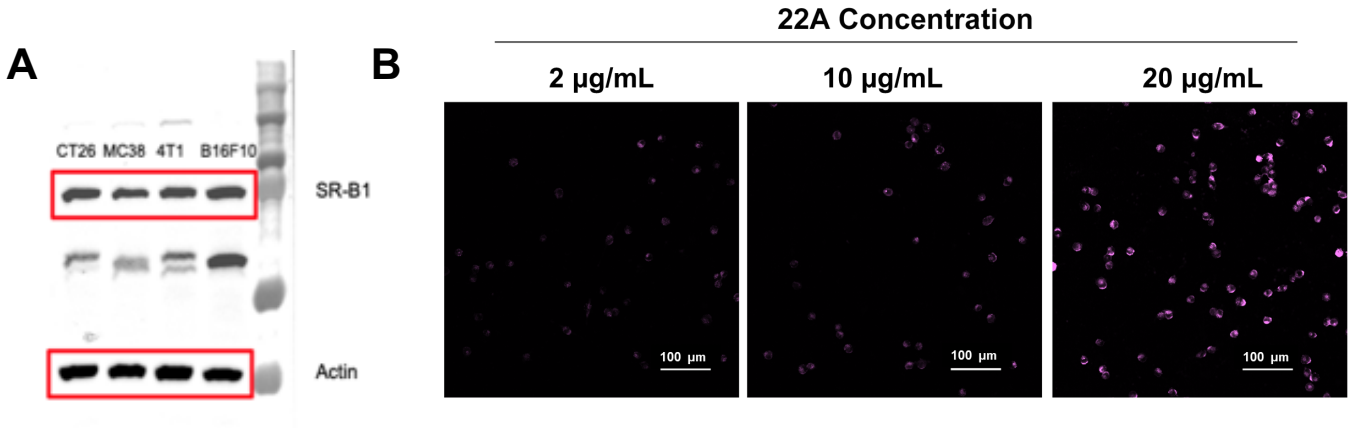

Figure 4-5. Cell uptake of sHDL by MC38 cells. (A) Western blot analysis of SR-B1 expression by four cancer cell lines: CT26, MC38, 4T1, B16F10. (B) Confocal microscope images of DiD-labeled sHDL by MC38 cells at three different concentrations.

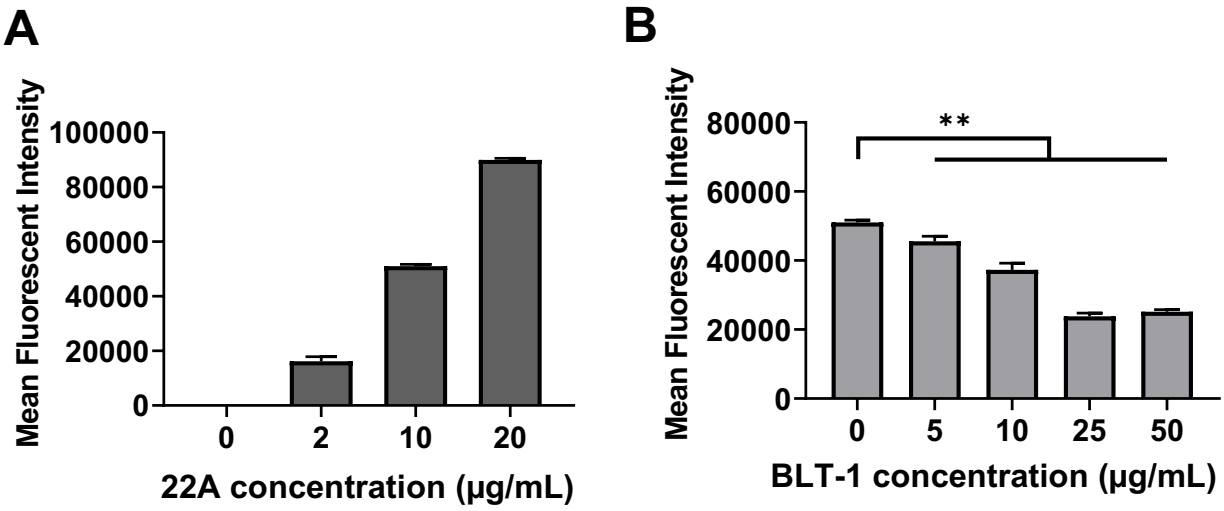

Figure 4-6. (A) Quantitative analysis of DiD-labeled sHDL uptake by MC38 cells. (B) Quantitative analysis of DiD-labeled sHDL uptake by MC38 cells when pre-incubated with SR-B1 blocking molecule BLT-1.

4.4.3. Delivery of DTX by sHDL maintains the cytotoxic effect of DTX on MC38 cells.

Now that we validated the sHDL scavenging potential of MC38 cells, we tested the cytotoxic potential of DTX-loaded sHDL on MC38 cells *in vitro*. After 48 hours of incubation with free DTX or DTX-loaded sHDL (DTX-sHDL), MC38 cells were analyzed by MTT assay using a UV spectrophotometer. We observed no significant differences in cytotoxicity at higher doses of DTX between the two treatment groups. DTX-sHDL induced cell death at a similar rate to DTX alone after just 48 hours in doses of 16 and 24 micrograms per ~50,000 cells (Figure 4-7).

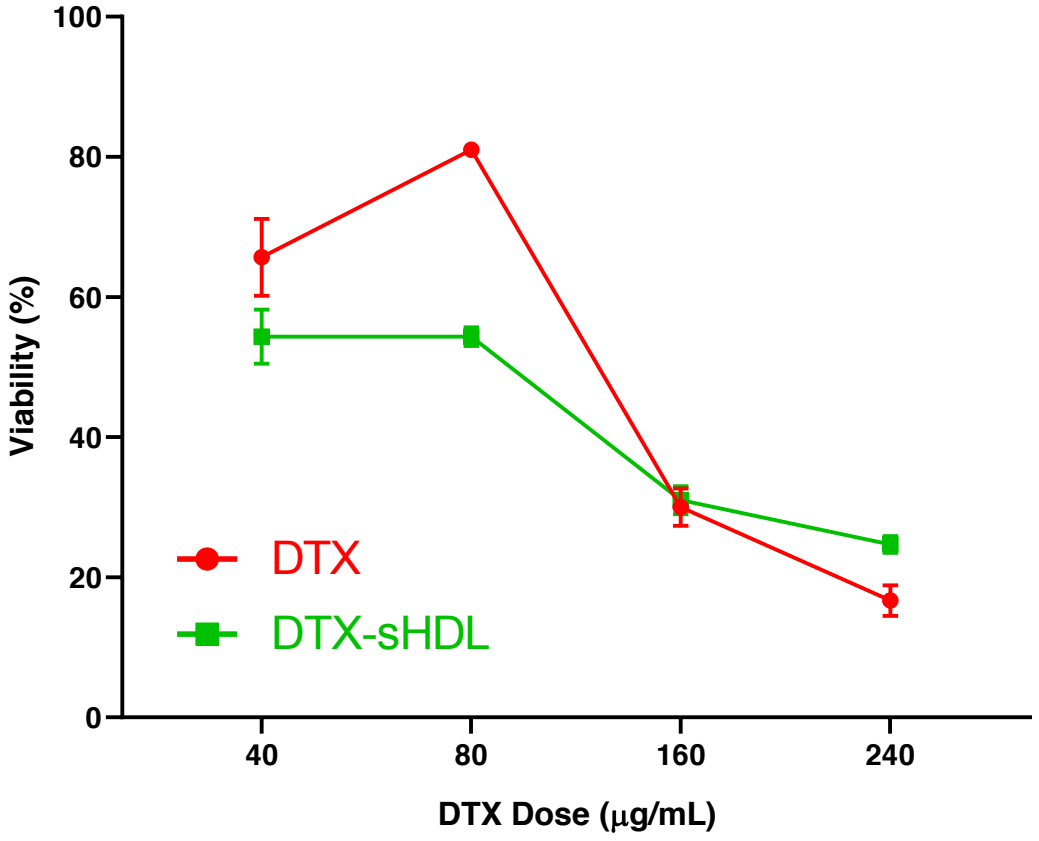

Figure 4-7. Cytotoxicity analysis of MC38 cells incubated for 48 hours in a 96-well plate with either free DTX or DTX-sHDL at different drug molecule concentrations.

4.4.4. Combination of immuno-stimulatory agent with DTX increases antitumor effects and prolongs survival.

While we have demonstrated that sHDL enhances the delivery of DTX *in vitro*, single-agent therapy is often insufficient for total eradication of the tumor, especially in colon adenocarcinoma. Thus, we decided to incorporate immunostimulatory agent CpG1826 into our DTX-sHDL formulation to test the efficacy of combination therapy relative to single-agent chemotherapy and to determine whether this additional component would augment sHDL's delivery enhancement of DTX *in vivo*. We observed significantly reduced tumor growth in mice treated with DTX-sHDL/CpG compared to DTX-sHDL and DTX alone with no differences between DTX and DTX-sHDL groups themselves, indicating the enhanced antitumor effect of combination therapy (Figure 4-9A). We also saw that mice treated with DTX-sHDL/CpG survived significantly longer (median survival = 43 days) ($p < 0.0001$) than mice treated with DTX-sHDL (median survival = 28 days) and DTX alone (median survival = 23 days) (Figure 4-9B). Two of seven mice treated with DTX-sHDL/CpG experienced complete tumor regression. None of the mice experienced any systemic toxicity as indicated by body weight maintenance, normal serum enzyme and protein levels, and consistent liver morphology with control (Figure 4-10). Overall, we learned that combining immunostimulatory agent CpG1826 with DTX-sHDL significantly improved survival as compared to single agent chemotherapy via DTX-sHDL.

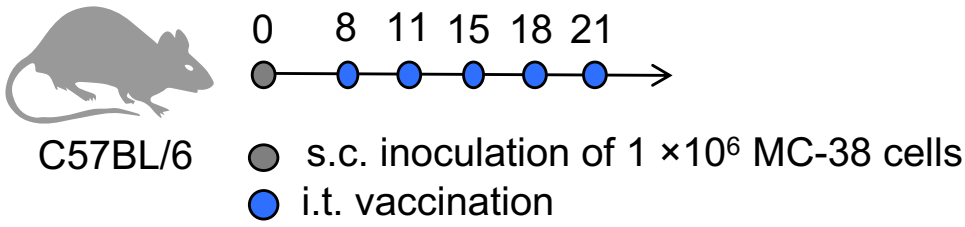

Figure 4-8. Treatment regimen and timeline of therapeutic animal study.

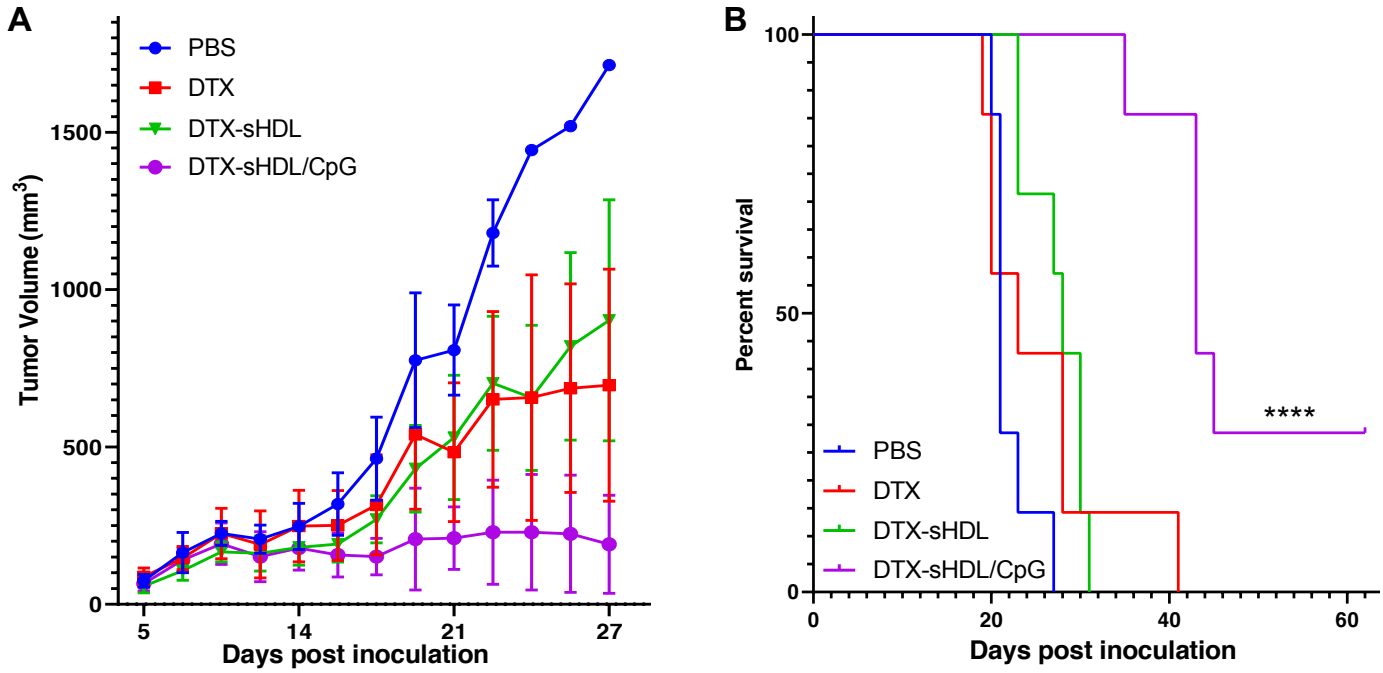

*Figure 4-9.(A) Average tumor growth curves for mice treated with PBS (blue), DTX (red), DTX-sHDL (green), and DTX-sHDL/CpG (purple). Error bars represent SEM. (B) Kaplan-Meier survival curves for mice treated with PBS (blue), DTX (red), DTX-sHDL (green), and DTX-sHDL/CpG (purple). ****P<0.0001.*

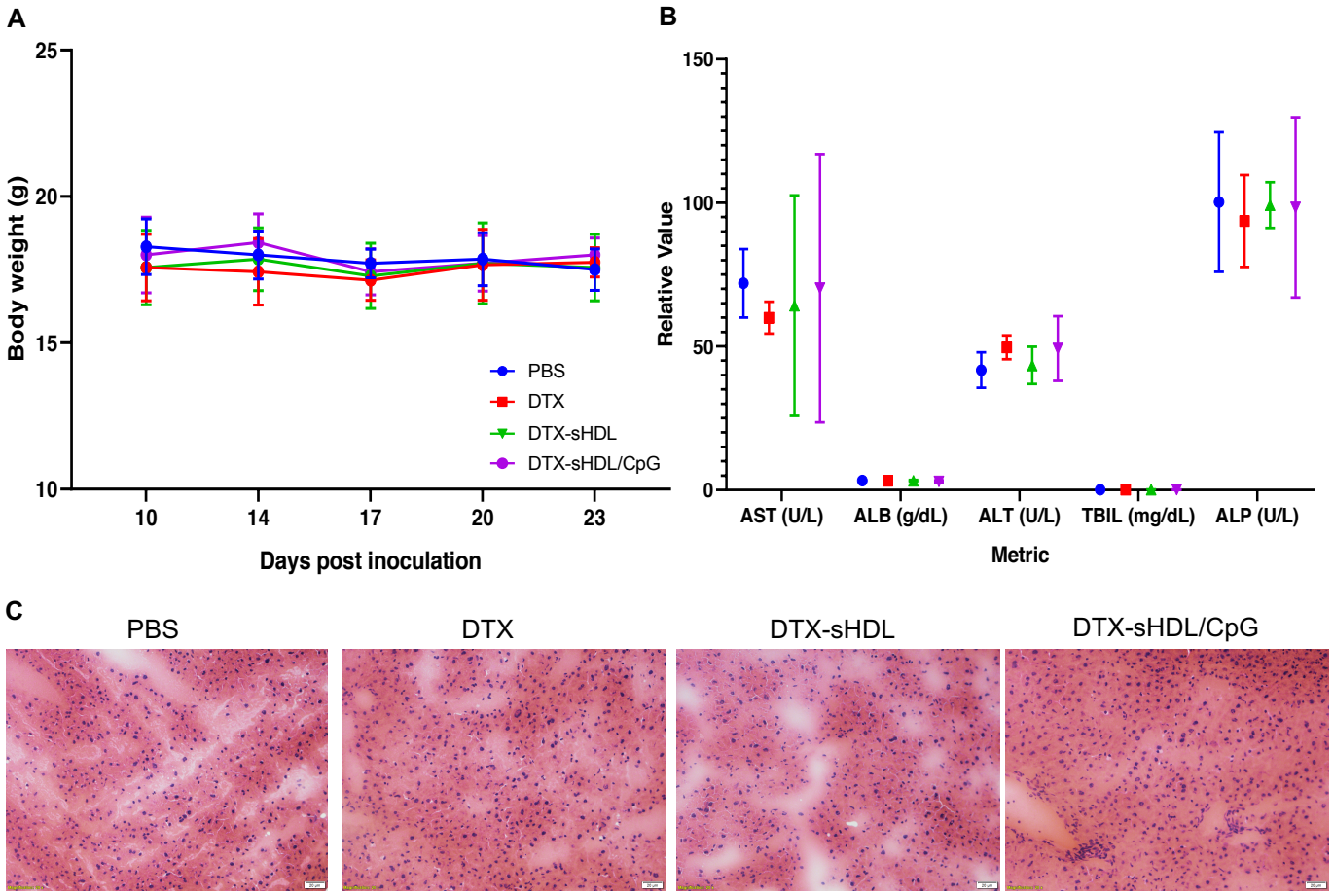

Figure 4-10. (A) Body weight measurements for study duration. (B) Liver panel toxicity analysis of aspartate aminotransferase (AST), albumin (ALB), alanine aminotransferase (ALT), total bilirubin (TBIL), and alkaline phosphatase (ALP). (C) H&E staining of liver sections from mice treated with each of the four treatments used in this study. Scale bars represent 20 microns.

4.5. Discussion

In this work, we hypothesized 1) that sHDL encapsulating docetaxel chemotherapy would enhance the delivery of docetaxel to target colon adenocarcinoma cells and 2) that combining this single-agent therapy with TLR9 agonist CpG would augment the antitumor efficacy of the monotherapy, suppressing tumor growth and prolonging survival. Through several *in vitro* experiments, we showed that sHDL uptake by MC38 cells is indeed mediated by SR-B1, which is highly expressed on these cells. MC38 cells exhibited a large capacity for sHDLs as evidenced by quantitative FACS

identification of sHDL-positive cells and qualitative confocal microscopy images. These findings agree with the current literature that has shown high SR-B1 expression allows for greater accumulation of cholesterol in tumor cells via HDL uptake to prolong tumor cell survival[33,141]. Following incubation of MC38 cells with either free DTX or DTX-sHDL, we observed that DTX-sHDL induced cell death at a similar rate to DTX at multiple dose levels. This result supports the hypothesis that sHDL can delivery DTX to tumor cells without compromising the cytotoxic activity of DTX, which potentiates the clinical translation of sHDL nanoparticles as drug delivery vehicles for hydrophobic chemotherapeutic molecules. We tested our formulation *in vivo* with an additional immunostimulatory component, CpG oligonucleotide. Indeed, CpG significantly improved the antitumor efficacy of DTX, suppressing tumor growth and prolonging survival in mice treated with DTX-sHDL/CpG as compared to mice treated with DTX-sHDL or DTX alone. Complete responses were achieved in two of the seven mice treated with DTX-sHDL/CpG, supporting the hypothesis that combination therapy with an immuno-stimulatory component would augment the antitumor efficacy of DTX alone. Interestingly, there were no significant differences in tumor growth or survival between the DTX-sHDL and DTX treatment groups. DTX-sHDL treatment marginally improved survival rates as compared to DTX treatment, but no differences whatsoever were observed in tumor growth rates. These findings disagree with other studies that have shown nanoparticle delivery significantly increases delivery of drug molecules to the target site. These findings are likely due to the intratumoral route of administration of DTX and DTX-sHDL, which does not showcase the tumor targeting abilities of sHDL nanoparticles as seen after the intravenous administration [132,137,142]. Larger differences

in treatment efficacy between free DTX and DTX-sHDL groups may be better observed if the treatments were given intravenously or subcutaneously, both of which could demonstrate the superior trafficking abilities of sHDL and its cargo as has been demonstrated in the literature[90,137,142]. Moreover, we only tested one dose of DTX, and it is possible that DTX-sHDL may be more effective than free DTX at lower doses. Additionally, a deeper mechanistic understanding of this combination therapy is needed through delineating the individual therapeutic contributions of free DTX versus free CpG and by testing this platform in an orthotopic mouse model.

Nonetheless, we have described the superior antitumor efficacy of co-delivering docetaxel chemotherapy and TLR9 agonist CpG on sHDL nanoparticles to MC-38 colon adenocarcinoma tumors when compared to docetaxel alone. Our findings are significant because sHDL has already been demonstrated to be safe and well-tolerated in high doses in the clinic, making it a readily translatable platform for co-delivered combination therapy for colon adenocarcinoma patients. Indeed, no systemic toxicity was elicited by the sHDL-DTX-CpG treatment. We have also shown that this platform is translatable to other cancers as it has been previously effective in a glioblastoma model[137]. Our results give promise to the evolution of highly effective, minimally invasive, and non-toxic multi-functional cancer therapies for colon adenocarcinoma.

Chapter 5. Conclusions & Perspectives

Within this dissertation, we have explored (1) the therapeutic ability of sHDL nanodiscs to deliver neoantigens for glioblastoma multiforme to exert robust anti-tumor effects, (2) the retention of immunogenicity of colon adenocarcinoma neoantigen-loaded sHDL nanodiscs following formulation simplification, and (3) the ability of sHDL nanodiscs to co-deliver chemo- and immuno-therapeutic entities to colon adenocarcinoma tumors.

In the first project, we found that delivery of neoantigens by sHDL nanodisc was significantly more effective compared to delivery of soluble neoantigens in neoantigen-specific CD8+ T cell production, tumor growth reduction, and survival prolongation in murine glioblastoma multiforme models. Interestingly, while NeoAg-3-specific CD8+ T cell frequencies were not significantly different between mice treated with nanovaccine +/- anti-PD-L1 and mice treated with soluble NeoAgs +/- anti-PD-L1, possibly due to competitive binding to MHC-I between NeoAg-1 and NeoAg-3. Future investigation of this hypothesis should be considered to determine whether inclusion of NeoAg-3 in the nanovaccine is substantiated. Anti-tumor effects were augmented by the addition of immune checkpoint blockade using anti-PD-L1, supporting the current opinion surrounding cancer treatment that combination therapy, namely immunotherapy, will be the most effective approach to reducing patient tumor burden and prolonging survival

moving forward. Moreover, treating glioblastoma tumor-bearing mice with our neoantigen-loaded sHDL nanovaccine in combination with anti-PD-L1 was able to reverse immunosuppression within the tumor microenvironment as indicated by significant increases in CD8+ T cells and concomitant decreases in PD-1 expression on CD8+ T cells and Treg frequencies within the tumor. Long-term survivors that were rechallenged with tumor cells in the opposite flank or hemisphere did not experience tumor recurrence, evidencing establishment of anti-tumor immune memory. Future studies on this work should investigate the cytokine profiles within the tumor microenvironment to support reversal of immunosuppression, evaluate immune memory cell characteristics to determine whether memory is generated by all three neoantigens equally and when it is generated, and to test the nanovaccine in combination with other immune checkpoint blockades in the orthotopic model. The hypothesis proposed regarding immune tolerance induction by soluble neoantigens would also be interesting to test to support further the use of sHDL as a delivery vehicle for antigens and adjuvants.

In the second project, we showed that we were able to simplify our formulation process for neoantigen-loaded sHDL through chemical modification of two neoantigen peptides using short chain PEG and pre-made lipoprotein films. We verified that the simplified PEGylated formulations induced neoantigen-specific CD8+ T cell expansion similar to our traditional formulations, substantiating the overarching goal of the project to streamline personalized vaccination formulations for clinical translation. Although prophylactic vaccination did not slow MC38 tumor growth equally between the two neoantigens Reps1 and Adpgk, we did see that PEGylated formulations and traditional

formulations exhibited anti-tumor efficacy similar to each other. Adpgk formulations were better able to slow tumor growth and prolong overall survival of tumor-challenged mice than were Reps1 formulations, which indicates that our MC38 cell line expressed Reps1 at much lower levels than Adpgk. Future studies on this work should include tumor challenge of prophylactically Reps1-vaccinated mice with MC38 cells expressing higher levels of Reps1, therapeutic vaccination of tumor-bearing mice with PEGylated formulations, and evaluation of different tumor models using nanovaccine formulations of other PEGylated neoantigens. The data from these studies will tell us whether PEGylating neoantigen peptides for aqueous sHDL nanodisc loading will improve process efficiency for multiple cancers while retaining nanovaccine anti-tumor activity. Scalability of PEGylated peptide and conjugate lipid synthesis should also be tested as large-scale manufacturing of sHDL has already been done successfully.

In the third project, we demonstrated the superior anti-tumor efficacy of co-delivering chemo- and immune-therapeutic entities on sHDL nanodiscs in a murine colon carcinoma model. *In vitro* cytotoxicity assays of MC38 cells incubated with either free DTX or DTX-sHDL revealed that DTX-sHDL induced cell death at a similar rate to DTX at multiple dose levels, supporting the hypothesis that sHDL can delivery DTX to tumor cells without compromising the cytotoxic activity of DTX and potentiating the clinical translation of sHDLs as drug delivery vehicles for chemotherapeutic molecules. *In vivo* evaluation of DTX-sHDL co-loaded with CpG oligonucleotide revealed that CpG significantly improved the antitumor efficacy of DTX, suppressing tumor growth and prolonging survival in mice treated with DTX-sHDL/CpG as compared to mice treated with DTX-sHDL or DTX alone. Complete responses were achieved in two of the seven

mice treated with DTX-sHDL/CpG, supporting the hypothesis that combination therapy with an immuno-stimulatory component would augment the antitumor efficacy of chemotherapy alone. Future studies on this work should include exploration of different routes of administration, as the intratumoral route is not realistic in all cases and types of cancer, in a variety of tumor models and also evaluation of different chemotherapeutic and immunotherapeutic entities because patient responses to specific drugs are quite heterogenous. Evaluation of the tumor microenvironment would also be interesting to determine whether the combination of chemo- and immuno-therapies alters the immune cell population within the tumor significantly compared to single therapeutic agents.

In full, this dissertation has (1) exposed a highly efficacious, tumor-specific, and personalized nanovaccine design for improving treatment of patients with GBM, (2) streamlined the neoantigen-sHDL nanovaccine formulation process for clinical translation, and (3) proposed an efficient method for co-delivery of chemo- and immuno-therapeutic entities for site-specific, non-toxic cancer treatment using sHDL nanodiscs. We believe that sHDL nanodiscs are versatile drug delivery vehicles and could set the stage for personalized and combinatorial cancer nanovaccine design.

References

1 Pardoll, D. The blockade of immune checkpoints in cancer immunotherapy. *Nature Reviews Cancer* **12**, 252-264, doi:10.1038/nrc3239 (2012).

2 Hodi, F. S. *et al.* Improved survival with ipilimumab in patients with metastatic melanoma. *New England Journal of Medicine* **363**, 711-723 (2010).

3 Robert, C. *et al.* Pembrolizumab versus ipilimumab in advanced melanoma. *The New England journal of medicine* **372**, 2521-2532, doi:10.1056/NEJMoa1503093 (2015).

4 Garon, E. B. *et al.* Pembrolizumab for the treatment of non-small-cell lung cancer. *The New England journal of medicine* **372**, 2018-2028, doi:10.1056/NEJMoa1501824 (2015).

5 Rosenberg, J. E. *et al.* Atezolizumab in patients with locally advanced and metastatic urothelial carcinoma who have progressed following treatment with platinum-based chemotherapy: a single-arm, multicentre, phase 2 trial. *Lancet* **387**, 1909-1920, doi:10.1016/S0140-6736(16)00561-4 (2016).

6 Topalian, S. L. *et al.* Safety, activity, and immune correlates of anti-PD-1 antibody in cancer. *The New England journal of medicine* **366**, 2443-2454, doi:10.1056/NEJMoa1200690 (2012).

7 Wolchok, J. D. *et al.* Nivolumab plus ipilimumab in advanced melanoma. *New England Journal of Medicine* **369**, 122-133 (2013).

8 Demaria, S. *et al.* Immune-mediated inhibition of metastases after treatment with local radiation and CTLA-4 blockade in a mouse model of breast cancer. *Clin Cancer Res* **11**, 728-734 (2005).

9 Vanneman, M. & Dranoff, G. Combining immunotherapy and targeted therapies in cancer treatment. *Nat Rev Cancer* **12**, 237-251, doi:10.1038/nrc3237 (2012).

10 Cho, H. I., Barrios, K., Lee, Y. R., Linowski, A. K. & Celis, E. BiVax: a peptide/poly-IC subunit vaccine that mimics an acute infection elicits vast and effective anti-tumor CD8 T-cell responses. *Cancer Immunol Immunother* **62**, 787-799, doi:10.1007/s00262-012-1382-6 (2013).

11 Duraiswamy, J., Kaluza, K. M., Freeman, G. J. & Coukos, G. Dual blockade of PD-1 and CTLA-4 combined with tumor vaccine effectively restores T-cell rejection function in tumors. *Cancer Res* **73**, 3591-3603, doi:10.1158/0008-5472.CAN-12-4100 (2013).

12 Belcaid, Z. *et al.* Focal radiation therapy combined with 4-1BB activation and CTLA-4 blockade yields long-term survival and a protective antigen-specific memory response in a murine glioma model. *PLoS One* **9**, e101764, doi:10.1371/journal.pone.0101764 (2014).

13 Twyman-Saint Victor, C. *et al.* Radiation and dual checkpoint blockade activate non-redundant immune mechanisms in cancer. *Nature* **520**, 373-377, doi:10.1038/nature14292 (2015).
14 Chen, Q. *et al.* Photothermal therapy with immune-adjuvant nanoparticles together with checkpoint blockade for effective cancer immunotherapy. *Nature Communications* **7**, 13193, doi:10.1038/ncomms13193 (2016).
15 Bethune, M. & Joglekar, A. Personalized T cell-mediated cancer immunotherapy: progress and challenges. *Current Opinion in Biotechnology* **48**, 142-152, doi:10.1016/j.copbio.2017.03.024 (2017).
16 Kuai, R., Ochyl, L. J., Bahjat, K. S., Schwendeman, A. & Moon, J. J. Designer vaccine nanodiscs for personalized cancer immunotherapy. *Nature materials* **16**, 489-496, doi:10.1038/nmat4822 (2017).
17 Nam, J. *et al.* Chemo-photothermal therapy combination elicits anti-tumor immunity against advanced metastatic cancer. *Nat Commun* **9**, 1-13, doi:10.1038/s41467-018-03473-9 (2018).
18 Kugler, A. *et al.* Regression of human metastatic renal cell carcinoma after vaccination with tumor cell–dendritic cell hybrids. *Nature medicine* **6**, 332-336 (2000).
19 Panelli, M. C. *et al.* Phase 1 study in patients with metastatic melanoma of immunization with dendritic cells presenting epitopes derived from the melanoma-associated antigens MART-1 and gp100. *Journal of Immunotherapy* **23**, 487-498 (2000).
20 Heath, W. & Carbone, F. Cross-presentation in viral immunity and self-tolerance. *Nature Reviews Immunology*, doi:10.1038/35100512 (2001).
21 Restifo, N. P., Dudley, M. E. & Rosenberg, S. A. Adoptive immunotherapy for cancer: harnessing the T cell response. *Nat Rev Immunol* **12**, 269-281, doi:nri3191 [pii]
10.1038/nri3191 (2012).
22 Tang, J., Shalabi, A. & Hubbard-Lucey, V. M. Comprehensive analysis of the clinical immuno-oncology landscape. *Ann Oncol* **29**, 84-91, doi:10.1093/annonc/mdx755 (2018).
23 Lauss, M. *et al.* Mutational and putative neoantigen load predict clinical benefit of adoptive T cell therapy in melanoma. *Nature Communications* **8**, 1-11, doi:10.1038/s41467-017-01460-0 (2017).
24 Chheda, Z. *et al.* Novel and shared neoantigen derived from histone 3 variant H3.3K27M mutation for glioma T cell therapy. *Journal of Experimental Medicine* **215**, 141-157, doi:10.1084/jem.20171046 (2018).
25 Smith, T. T. *et al.* In situ programming of leukaemia-specific T cells using synthetic DNA nanocarriers. *Nat Nanotechnol* **12**, 813-820, doi:10.1038/nnano.2017.57 (2017).
26 Kosmides, A. K., Necochea, K., Hickey, J. W. & Schneck, J. P. Separating T Cell Targeting Components onto Magnetically Clustered Nanoparticles Boosts Activation. *Nano Lett* **18**, 1916-1924, doi:10.1021/acs.nanolett.7b05284 (2018).
27 Fadel, T. R. *et al.* A carbon nanotube-polymer composite for T-cell therapy. *Nat Nanotechnol* **9**, 639-647, doi:10.1038/nnano.2014.154 (2014).

28 Cheung, A. S., Zhang, D. K. Y., Koshy, S. T. & Mooney, D. J. Scaffolds that mimic antigen-presenting cells enable ex vivo expansion of primary T cells. *Nat Biotechnol* **36**, 160-169, doi:10.1038/nbt.4047 (2018).
29 Fadul, C. E. *et al.* Immune Response in Patients With Newly Diagnosed Glioblastoma Multiforme Treated With Intranodal Autologous Tumor Lysate-dendritic Cell Vaccination After Radiation Chemotherapy. *Journal of immunotherapy (Hagerstown, Md. : 1997)* **34**, 382-389, doi:10.1097/CJI.0b013e318215e300 (2011).
30 Stephan, M., Moon, J., Um, S., Bershteyn, A. & Irvine, D. Therapeutic cell engineering with surface-conjugated synthetic nanoparticles. *Nature Medicine* **16**, 1035-1041, doi:10.1038/nm.2198 (2010).
31 Huang, B. *et al.* Active targeting of chemotherapy to disseminated tumors using nanoparticle-carrying T cells. *Science Translational Medicine* **7**, 1-21, doi:10.1126/scitranslmed.aaa5447 (2015).
32 Zheng, Y. *et al.* In vivo targeting of adoptively transferred T-cells with antibody- and cytokine-conjugated liposomes. *Journal of Controlled Release* **172**, 426-435, doi:10.1016/j.jconrel.2013.05.037 (2013).
33 Zheng, Y., Tang, L., Mabardi, L., Kumari, S. & Irvine, D. Enhancing Adoptive Cell Therapy of Cancer through Targeted Delivery of Small-Molecule Immunomodulators to Internalizing or Noninternalizing Receptors. *Acs Nano* **11**, 3089-3100, doi:10.1021/acsnano.7b00078 (2017).
34 Schumacher, T. N. & Schreiber, R. D. Neoantigens in cancer immunotherapy. *Science* **348**, 69-74, doi:10.1126/science.aaa4971 (2015).
35 Hu, Z., Ott, P. A. & Wu, C. J. Towards personalized, tumour-specific, therapeutic vaccines for cancer. *Nat Rev Immunol* **18**, 168-182, doi:10.1038/nri.2017.131 (2018).
36 Sahin, U. & Tureci, O. Personalized vaccines for cancer immunotherapy. *Science* **359**, 1355-1360, doi:10.1126/science.aar7112 (2018).
37 Castle, J. C. *et al.* Exploiting the Mutanome for Tumor Vaccination. *Cancer Research* **72**, 1081-1091, doi:10.1158/0008-5472.can-11-3722 (2012).
38 Yadav, M. *et al.* Predicting immunogenic tumour mutations by combining mass spectrometry and exome sequencing. *Nature* **515**, 572, doi:10.1038/nature14001 https://www.nature.com/articles/nature14001#supplementary-information (2014).
39 Gubin, M. M. *et al.* Checkpoint blockade cancer immunotherapy targets tumour-specific mutant antigens. *Nature* **515**, 577-581, doi:10.1038/nature13988 (2014).
40 Kreiter, S. *et al.* Mutant MHC class II epitopes drive therapeutic immune responses to cancer. *Nature* **520**, 692-696, doi:10.1038/nature14426 (2015).
41 Ott, P. A. *et al.* An immunogenic personal neoantigen vaccine for patients with melanoma. *Nature* **547**, 217-221, doi:10.1038/nature22991 (2017).
42 Sahin, U. *et al.* Personalized RNA mutanome vaccines mobilize poly-specific therapeutic immunity against cancer. *Nature* **547**, 222 (2017).
43 Bijker, M. S. *et al.* CD8+ CTL priming by exact peptide epitopes in incomplete Freund's adjuvant induces a vanishing CTL response, whereas long peptides induce sustained CTL reactivity. *The Journal of Immunology* **179**, 5033-5040 (2007).

44 Kakimi, K. *et al.* A phase I study of vaccination with NY-ESO-1f peptide mixed with Picibanil OK-432 and Montanide ISA-51 in patients with cancers expressing the NY-ESO-1 antigen. *International journal of cancer* **129**, 2836-2846 (2011).
45 van Hall, T. & van der Burg, S. H. in *Advances in immunology* Vol. 114 51-76 (Elsevier, 2012).
46 Hailemichael, Y. *et al.* Persistent antigen at vaccination sites induces tumor-specific CD8(+) T cell sequestration, dysfunction and deletion. *Nat Med* **19**, 465-472, doi:10.1038/nm.3105 (2013).
47 Di Stasi, A., Jimenez, A. M., Minagawa, K., Al-Obaidi, M. & Rezvani, K. Review of the results of WT1 peptide vaccination strategies for myelodysplastic syndromes and acute myeloid leukemia from nine different studies. *Frontiers in immunology* **6**, 36 (2015).
48 Blander, J. M. & Medzhitov, R. Toll-dependent selection of microbial antigens for presentation by dendritic cells. *Nature* **440**, 808-812, doi:10.1038/nature04596 (2006).
49 Iwasaki, A. & Medzhitov, R. Regulation of adaptive immunity by the innate immune system. *Science* **327**, 291-295, doi:10.1126/science.1183021 (2010).
50 Jiang, H., Wang, Q. & Sun, X. Lymph node targeting strategies to improve vaccination efficacy. *Journal of Controlled Release* **267**, 47-56 (2017).
51 Fan, Y. C. & Moon, J. J. Nanoparticle drug delivery systems designed to improve cancer vaccines and immunotherapy. *Vaccines* **3**, 662-685, doi:10.3390/vaccines3030662 (2015).
52 Reddy, S. T. *et al.* Exploiting lymphatic transport and complement activation in nanoparticle vaccines. *Nat Biotechnol* **25**, 1159-1164 (2007).
53 Liu, H. *et al.* Structure-based programming of lymph-node targeting in molecular vaccines. *Nature* **507**, 519-522, doi:10.1038/nature12978 http://www.nature.com/nature/journal/v507/n7493/abs/nature12978.html#supplementary-information (2014).
54 Zhu, G. *et al.* Albumin/vaccine nanocomplexes that assemble in vivo for combination cancer immunotherapy. *Nature communications* **8**, 1954 (2017).
55 Dawidczyk, C. M. *et al.* State-of-the-art in design rules for drug delivery platforms: lessons learned from FDA-approved nanomedicines. *J Control Release* **187**, 133-144, doi:10.1016/j.jconrel.2014.05.036 (2014).
56 Zhu, G. *et al.* Intertwining DNA-RNA nanocapsules loaded with tumor neoantigens as synergistic nanovaccines for cancer immunotherapy. *Nature Communications* **8**, 1482, doi:10.1038/s41467-017-01386-7 (2017).
57 Luo, M. *et al.* A STING-activating nanovaccine for cancer immunotherapy. *Nat Nanotechnol* **12**, 648-654, doi:10.1038/nnano.2017.52 (2017).
58 Li, A. W. *et al.* A facile approach to enhance antigen response for personalized cancer vaccination. *Nature materials*, 1 (2018).
59 Gras Navarro, A., Björklund, A. T. & Chekenya, M. Therapeutic potential and challenges of natural killer cells in treatment of solid tumors. *Frontiers in immunology* **6**, 202 (2015).
60 Chen, G. *et al.* MRI-visible polymeric vector bearing CD3 single chain antibody for gene delivery to T cells for immunosuppression. *Biomaterials* **30**, 1962-1970 (2009).

61 Fan, Z., Chen, D. & Deng, C. Improving ultrasound gene transfection efficiency by controlling ultrasound excitation of microbubbles. *Journal of Controlled Release* **170**, 401-413 (2013).
62 Weber-Adrian, D. *et al.* Gene delivery to the spinal cord using MRI-guided focused ultrasound. *Gene therapy* **22**, 568 (2015).
63 Chertok, B., Langer, R. & Anderson, D. G. Spatial Control of Gene Expression by Nanocarriers Using Heparin Masking and Ultrasound-Targeted Microbubble Destruction. *ACS Nano*, doi:10.1021/acsnano.6b01199 (2016).
64 Mead, B. P. *et al.* Targeted gene transfer to the brain via the delivery of brain-penetrating DNA nanoparticles with focused ultrasound. *Journal of Controlled Release* **223**, 109-117 (2016).
65 Fan, C.-H. *et al.* Folate-conjugated gene-carrying microbubbles with focused ultrasound for concurrent blood-brain barrier opening and local gene delivery. *Biomaterials* **106**, 46-57 (2016).
66 Ling, D. *et al.* Multifunctional Tumor pH-Sensitive Self-Assembled Nanoparticles for Bimodal Imaging and Treatment of Resistant Heterogeneous Tumors. *Journal of the American Chemical Society* **136**, 5647-5655, doi:10.1021/ja4108287 (2014).
67 Yang, K. *et al.* Multimodal imaging guided photothermal therapy using functionalized graphene nanosheets anchored with magnetic nanoparticles. *Advanced materials* **24**, 1868-1872 (2012).
68 Lee, J.-H. *et al.* Exchange-coupled magnetic nanoparticles for efficient heat induction. *Nature nanotechnology* **6**, 418-422 (2011).
69 Riedinger, A. *et al.* Subnanometer local temperature probing and remotely controlled drug release based on azo-functionalized iron oxide nanoparticles. *Nano letters* **13**, 2399-2406 (2013).
70 Hayashi, K. *et al.* Superparamagnetic nanoparticle clusters for cancer theranostics combining magnetic resonance imaging and hyperthermia treatment. *Theranostics* **3**, 366 (2013).
71 Dames, P. *et al.* Targeted delivery of magnetic aerosol droplets to the lung. *Nature nanotechnology* **2**, 495-499 (2007).
72 Amirfazli, A. Nanomedicine: magnetic nanoparticles hit the target. *Nature nanotechnology* **2**, 467-468 (2007).
73 Galanzha, E. I. *et al.* In vivo magnetic enrichment and multiplex photoacoustic detection of circulating tumour cells. *Nature nanotechnology* **4**, 855-860 (2009).
74 Shevtsov, M. A. *et al.* 70-kDa heat shock protein coated magnetic nanocarriers as a nanovaccine for induction of anti-tumor immune response in experimental glioma. *Journal of Controlled Release* **220**, 329-340, doi:https://doi.org/10.1016/j.jconrel.2015.10.051 (2015).
75 Sirsi, S. & Borden, M. Microbubble Compositions, Properties and Biomedical Applications. *Bubble science engineering and technology* **1**, 3-17, doi:10.1179/175889709X446507 (2009).
76 Treat, L. H. *et al.* Targeted delivery of doxorubicin to the rat brain at therapeutic levels using MRI-guided focused ultrasound. *International journal of cancer* **121**, 901-907 (2007).

77 Burke, C. W., Alexander, E., Timbie, K., Kilbanov, A. L. & Price, R. J. Ultrasound-activated agents comprised of 5FU-bearing nanoparticles bonded to microbubbles inhibit solid tumor growth and improve survival. *Molecular Therapy* **22**, 321-328 (2014).
78 Chen, P.-Y. *et al.* Focused ultrasound-induced blood–brain barrier opening to enhance interleukin-12 delivery for brain tumor immunotherapy: a preclinical feasibility study. *Journal of translational medicine* **13**, 1 (2015).
79 Timbie, K. F. *et al.* MR image-guided delivery of cisplatin-loaded brain-penetrating nanoparticles to invasive glioma with focused ultrasound. *Journal of Controlled Release* (2017).
80 Suzuki, R. *et al.* A novel strategy utilizing ultrasound for antigen delivery in dendritic cell-based cancer immunotherapy. *Journal of Controlled Release* **133**, 198-205, doi:https://doi.org/10.1016/j.jconrel.2008.10.015 (2009).
81 Zhou, S. *et al.* Ultrasound-targeted microbubble destruction mediated herpes simplex virus-thymidine kinase gene treats hepatoma in mice. *Journal of Experimental & Clinical Cancer Research* **29**, 1 (2010).
82 Unga, J. & Hashida, M. Ultrasound induced cancer immunotherapy. *Advanced Drug Delivery Reviews* **72**, 144-153, doi:https://doi.org/10.1016/j.addr.2014.03.004 (2014).
83 Shi, J., Kantoff, P. W., Wooster, R. & Farokhzad, O. C. Cancer nanomedicine: progress, challenges and opportunities. *Nat Rev Cancer* **17**, 20-37, doi:10.1038/nrc.2016.108 (2017).
84 Kuai, R., Li, D., Chen, Y. E., Moon, J. J. & Schwendeman, A. High-density lipoproteins: nature's multifunctional nanoparticles. *ACS Nano* **10**, 3015-3041, doi:10.1021/acsnano.5b07522 (2016).
85 Morin, E. E., Li, X.-A. & Schwendeman, A. HDL in Endocrine Carcinomas: Biomarker, Drug Carrier, and Potential Therapeutic. *Frontiers in endocrinology* **9**, 715-715, doi:10.3389/fendo.2018.00715 (2018).
86 Cruz, P. M., Mo, H., McConathy, W. J., Sabnis, N. & Lacko, A. G. The role of cholesterol metabolism and cholesterol transport in carcinogenesis: a review of scientific findings, relevant to future cancer therapeutics. *Frontiers in pharmacology* **4** (2013).
87 Zheng, Y. *et al.* Scavenger receptor B1 is a potential biomarker of human nasopharyngeal carcinoma and its growth is inhibited by HDL-mimetic nanoparticles. *Theranostics* **3**, 477 (2013).
88 Shahzad, M. M. K. *et al.* Targeted delivery of small interfering RNA using reconstituted high-density lipoprotein nanoparticles. *Neoplasia (New York, N.Y.)* **13**, 309-319 (2011).
89 Qian, Y. *et al.* Targeting dendritic cells in lymph node with an antigen peptide-based nanovaccine for cancer immunotherapy. *Biomaterials* **98**, 171-183 (2016).
90 Kuai, R. *et al.* Subcutaneous nanodisc vaccination with neoantigens for combination cancer immunotherapy. *Bioconjugate chemistry* **29**, 771-775 (2018).
91 Irvine, D. Material aid for vaccines. *Nat Mater* **17**, 472-473, doi:10.1038/s41563-018-0089-2 (2018).

92 Tyagi, P. & Santos, J. L. Macromolecule nanotherapeutics: approaches and challenges. *Drug Discov Today* **23**, 1053-1061, doi:10.1016/j.drudis.2018.01.017 (2018).
93 Bhatnagar, B. S., Bogner, R. H. & Pikal, M. J. Protein Stability During Freezing: Separation of Stresses and Mechanisms of Protein Stabilization. *Pharmaceutical Development and Technology* **12**, 505-523, doi:10.1080/10837450701481157 (2007).
94 Association, A. B. T. *Brain Tumor Statistics*, <http://www.abta.org/about-us/news/brain-tumor-statistics/> (2015).
95 Society, A. C. *Brain and Spinal Cord Tumors in Adults*, <http://www.cancer.org/cancer/braincnstumorsinadults/> (2016).
96 Arbor Pharmaceuticals, L. *Gliadel*, <http://gliadel.com/hcp/> (2014).
97 Wang, D.-D., Yang, M., Zhu, Y. & Mao, C. Reiterated Targeting Peptides on the Nanoparticle Surface Significantly Promote Targeted Vascular Endothelial Growth Factor Gene Delivery to Stem Cells. *Biomacromolecules* **16**, 3897-3903, doi:10.1021/acs.biomac.5b01226 (2015).
98 Dong, H. *et al.* Tumor-associated B7-H1 promotes T-cell apoptosis: a potential mechanism of immune evasion. *Nature medicine* **8**, 793-800 (2002).
99 Parsa, A. T. *et al.* Loss of tumor suppressor PTEN function increases B7-H1 expression and immunoresistance in glioma. *Nat Med* **13**, 84-88, doi:http://www.nature.com/nm/journal/v13/n1/suppinfo/nm1517_S1.html (2007).
100 Prins, R. M. *et al.* Gene Expression Profile Correlates with T-Cell Infiltration and Relative Survival in Glioblastoma Patients Vaccinated with Dendritic Cell Immunotherapy. *Clinical Cancer Research* **17**, 1603-1615, doi:10.1158/1078-0432.ccr-10-2563 (2011).
101 Liau, L. M. *et al.* First results on survival from a large Phase 3 clinical trial of an autologous dendritic cell vaccine in newly diagnosed glioblastoma. *Journal of Translational Medicine* **16**, 142, doi:10.1186/s12967-018-1507-6 (2018).
102 Malkki, H. Trial Watch: Glioblastoma vaccine therapy disappointment in Phase III trial. *Nature reviews Neurology* **12**, 190 (2016).
103 Engelhardt, B. T cell migration into the central nervous system during health and disease: Different molecular keys allow access to different central nervous system compartments. *Clinical and Experimental Neuroimmunology* **1**, 79-93, doi:10.1111/j.1759-1961.2010.009.x (2010).
104 Johanns, T. M. *et al.* Endogenous Neoantigen-Specific CD8 T Cells Identified in Two Glioblastoma Models Using a Cancer Immunogenomics Approach. *Cancer Immunology Research*, doi:10.1158/2326-6066.cir-16-0156 (2016).
105 Society, T. A. C. *Colorectal Cancer*, 2018).
106 Kalyan, A., Kircher, S., Shah, H., Mulcahy, M. & Benson, A. Updates on immunotherapy for colorectal cancer. *Journal of gastrointestinal oncology* **9**, 160-169, doi:10.21037/jgo.2018.01.17 (2018).
107 Hazama, S. *et al.* A phase II study of five peptides combination with oxaliplatin-based chemotherapy as a first-line therapy for advanced colorectal cancer (FXV study). *Journal of translational medicine* **12**, 108 (2014).

108 Okuno, K., Sugiura, F., Inoue, K. & Sukegawa, Y. Clinical trial of a 7-peptide cocktail vaccine with oral chemotherapy for patients with metastatic colorectal cancer. *Anticancer research* **34**, 3045-3052 (2014).
109 Toubaji, A. *et al.* Pilot study of mutant ras peptide-based vaccine as an adjuvant treatment in pancreatic and colorectal cancers. *Cancer Immunology, Immunotherapy* **57**, 1413-1420 (2008).
110 Rahma, O. E. *et al.* The immunological and clinical effects of mutated ras peptide vaccine in combination with IL-2, GM-CSF, or both in patients with solid tumors. *Journal of translational medicine* **12**, 55 (2014).
111 Huang, H., Cruz, W., Chen, J. & Zheng, G. Learning from biology: synthetic lipoproteins for drug delivery. *Wiley Interdisciplinary Reviews: Nanomedicine and Nanobiotechnology* **7**, 298-314 (2015).
112 Hanif, F., Muzaffar, K., Perveen, K., Malhi, S. M. & Simjee, S. U. Glioblastoma Multiforme: A Review of its Epidemiology and Pathogenesis through Clinical Presentation and Treatment. *Asian Pacific journal of cancer prevention : APJCP* **18**, 3-9, doi:10.22034/APJCP.2017.18.1.3.
113 Huang, J. *et al.* Immune Checkpoint in Glioblastoma: Promising and Challenging. *Frontiers in pharmacology* **8**, 242-242, doi:10.3389/fphar.2017.00242 (2017).
114 Hashem, A. M. *et al.* CD40 Ligand Preferentially Modulates Immune Response and Enhances Protection against Influenza Virus. *The Journal of Immunology* **193**, 722-734, doi:10.4049/jimmunol.1300093 (2014).
115 Reardon, D. A. *et al.* Glioblastoma Eradication Following Immune Checkpoint Blockade in an Orthotopic, Immunocompetent Model. *Cancer immunology research*, canimm. 0151.2015 (2015).
116 Candolfi, M. *et al.* Intracranial glioblastoma models in preclinical neuro-oncology: neuropathological characterization and tumor progression. *Journal of Neuro-Oncology* **85**, 133-148, doi:10.1007/s11060-007-9400-9 (2007).
117 Johanns, T. M. *et al.* Endogenous neoantigen-specific CD8 T cells identified in two glioblastoma models using a cancer immunogenomics approach. *Cancer immunology research* **4**, 1007-1015 (2016).
118 Innovagen. *PepCalc.com*.
119 Apostolopoulos, V., Chelvanayagam, G., Xing, P.-X. & McKenzie, I. F. Anti-MUC1 antibodies react directly with MUC1 peptides presented by class I H2 and HLA molecules. *The Journal of Immunology* **161**, 767-775 (1998).
120 Jenkins, M., Pardoll, D., Mizuguchi, J., Quill, H. & Schwartz, R. T-Cell Unresponsiveness in vivo and in vitro: Fine Specificity of Induction and Molecular Characterization of the Unresponsive State. *Immunological Reviews* **95**, 113-135, doi:10.1111/j.1600-065X.1987.tb00502.x (1987).
121 Briner, T. J., Kuo, M. C., Keating, K. M., Rogers, B. L. & Greenstein, J. L. Peripheral T-cell tolerance induced in naive and primed mice by subcutaneous injection of peptides from the major cat allergen Fel d I. *Proceedings of the National Academy of Sciences* **90**, 7608-7612, doi:10.1073/pnas.90.16.7608 (1993).
122 Redmond, W. L. & Sherman, L. A. Peripheral Tolerance of CD8 T Lymphocytes. *Immunity* **22**, 275-284, doi:https://doi.org/10.1016/j.immuni.2005.01.010 (2005).

123 van Duikeren, S. *et al.* Vaccine-Induced Effector-Memory CD8⁺ T Cell Responses Predict Therapeutic Efficacy against Tumors. *The Journal of Immunology* **189**, 3397-3403, doi:10.4049/jimmunol.1201540 (2012).
124 Kaech, S. M., Wherry, E. J. & Ahmed, R. Effector and memory T-cell differentiation: implications for vaccine development. *Nature Reviews Immunology* **2**, 251+ (2002).
125 Pasut, G. *et al.* Polyethylene glycol (PEG)-dendron phospholipids as innovative constructs for the preparation of super stealth liposomes for anticancer therapy. *Journal of Controlled Release* **199**, 106-113, doi:http://dx.doi.org/10.1016/j.jconrel.2014.12.008 (2015).
126 Sezgin, Z., Yüksel, N. & Baykara, T. Preparation and characterization of polymeric micelles for solubilization of poorly soluble anticancer drugs. *European Journal of Pharmaceutics and Biopharmaceutics* **64**, 261-268, doi:https://doi.org/10.1016/j.ejpb.2006.06.003 (2006).
127 Shao, K. *et al.* Angiopep-2 modified PE-PEG based polymeric micelles for amphotericin B delivery targeted to the brain. *Journal of Controlled Release* **147**, 118-126 (2010).
128 Ooya, T., Lee, J. & Park, K. Effects of ethylene glycol-based graft, star-shaped, and dendritic polymers on solubilization and controlled release of paclitaxel. *Journal of controlled release* **93**, 121-127 (2003).
129 Nandi, I., Bateson, M., Bari, M. & Joshi, H. N. Synergistic effect of PEG-400 and cyclodextrin to enhance solubility of progesterone. *AAPS PharmSciTech* **4**, 1 (2003).
130 Rudolph, M. G., Stanfield, R. L. & Wilson, I. A. How TCRs bind MHCs, peptides, and coreceptors. *Annu. Rev. Immunol.* **24**, 419-466 (2006).
131 Aurisicchio, L. *et al.* Poly-specific neoantigen-targeted cancer vaccines delay patient derived tumor growth. *Journal of experimental & clinical cancer research : CR* **38**, 78-78, doi:10.1186/s13046-019-1084-4 (2019).
132 Kuai, R. *et al.* Elimination of established tumors with nanodisc-based combination chemoimmunotherapy. *Sci Adv* **4**, eaao1736, doi:10.1126/sciadv.aao1736 (2018).
133 Cancer, F. C. *Facts and Stats about Colorectal Cancer*, 2019).
134 McConathy, W. J., Nair, M. P., Paranjape, S., Mooberry, L. & Lacko, A. G. Evaluation of synthetic/reconstituted high-density lipoproteins as delivery vehicles for paclitaxel. *Anti-cancer drugs* **19**, 183-188 (2008).
135 Lacko, A. G., Nair, M., Paranjape, S., Johnson, S. & McConathy, W. J. High density lipoprotein complexes as delivery vehicles for anticancer drugs. *Anticancer research* **22**, 2045-2050 (2002).
136 Krieg, A. M. Toll-like receptor 9 (TLR9) agonists in the treatment of cancer. *Oncogene* **27**, 161 (2008).
137 Kadiyala, P. *et al.* High-Density Lipoprotein-Mimicking Nanodiscs for Chemo-immunotherapy against Glioblastoma Multiforme. *ACS nano* **13**, 1365-1384 (2019).
138 Buhtoiarov, I. N. *et al.* Anti-tumour synergy of cytotoxic chemotherapy and anti-CD40 plus CpG-ODN immunotherapy through repolarization of tumour-associated macrophages. *Immunology* **132**, 226-239 (2011).

139 Lollo, G. *et al.* Development of multifunctional lipid nanocapsules for the co-delivery of paclitaxel and CpG-ODN in the treatment of glioblastoma. *International journal of pharmaceutics* **495**, 972-980 (2015).
140 Weigel, B. J., Rodeberg, D. A., Krieg, A. M. & Blazar, B. R. CpG oligodeoxynucleotides potentiate the antitumor effects of chemotherapy or tumor resection in an orthotopic murine model of rhabdomyosarcoma. *Clinical Cancer Research* **9**, 3105-3114 (2003).
141 Zamanian-Daryoush, M. *et al.* Myeloid-specific genetic ablation of ATP-binding cassette transporter ABCA1 is protective against cancer. *Oncotarget* **8**, 71965-71980, doi:10.18632/oncotarget.18666 (2017).
142 Kuai, R., Li, D., Chen, Y. E., Moon, J. J. & Schwendeman, A. High-density lipoproteins: nature's multifunctional nanoparticles. *ACS nano* **10**, 3015-3041 (2016).